Resolution of Signal Components of a Resultant Electromagnetic Wave Received in a Multipath Field of Microwave Frequencies

Jürgen Richter

A thesis submitted in partial fulfilment of the requirements of the University of Glamorgan for the degree of a Doctor of Philosophy

May 1998

University of Glamorgan

DECLARATION

I declare that this thesis has not been, nor currently being, submitted for award of any other degree or similar qualification

signed 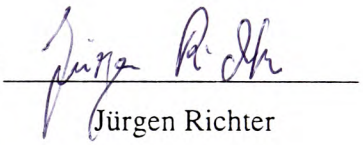

Jürgen Richter

ACKNOWLEDGMENTS

I wish to thank my director of studies, Professor Miqdad Al-Nuaimi for his guidance and thorough support throughout the research and his whole-hearted efforts in providing the necessary resources for the research project. With gratitude I would especially acknowledge Dr. Christopher Haslett, for his many valuable discussion and his supportive input into the theoretical and practical aspects of the project.

I am especially indebted to my colleagues of the radio propagation research group Dr. Ming Sheng Ding, Mr. Richard Stephens and Dr. Akram Hammoudeh for their invaluable assistance in the measurements.

Finally I would like to thank Prof. Dr. Heinecke and Prof. Dr. Lechner from the Fachhochschule Hannover for initiating and maintaining the collaboration between the German academic institute and their British counterpart, the University of Glamorgan, which enabled German students to study at British universities.

ABSTRACT

The growing use and demand for microwave communication systems has led to an increase in system density, particularly in urban areas. Consequently this rise has increased the risk of interference. Especially in urban areas the abundant presence of potential obstacles increase the risk of multipath propagation. Multipath propagation on radio links is associated with signal delays and signal level fades on which adversely influences the system performance.

For efficient frequency planning the knowledge of the multipath geometries involved is required. This knowledge can be obtained by resolving the experienced multipath field into its constituent components yielding their amplitudes and angles of arrivals at a receiver terminal.

Some previous investigations into the resolution of multipath generated height gain curves are documented in the literature. These generally however concentrate on resolving the two predominant signal components. In an urban environment the number of expected constituent signal components exceed the number of two. Resolution of more than two components requires considerably more effort than this relatively simple case.

This thesis provides a component resolution procedure which determines the individual amplitudes and angles of arrival of constituent multipath components. The procedure is applied to the spatial amplitude envelope observed when displacing a receiver incrementally over a distance of a few wavelength through a multipath field. The presented solution can be applied with inexpensive measurement and computational means. For the resolution process it is only required to record the envelope pattern amplitude values without any phase information being required. The use of a single standard antenna as receiver is also sufficient. The procedure does not require data of an array of antenna elements. The performance of the resolution procedure has been tested and validated in an extensive experimental programme which was part of this research.

Preliminary results of this project are published in the report of the European COST 235 project.

TABLE OF CONTENTS

CHAPTER 1 INTRODUCTION

1.1 Introduction

In microwave communications a dramatic development has taken place in recent years. In the past a typical microwave communications system consisted of two tall masts placed probably 50 km apart with open country in between. The recent developments in micro-electronics and information technology have had their impact on microwave communications leading to a widespread use of both fixed and mobile radio systems. Today there can be found terrestrial as well as satellite links used in rural and also in urban environments with fixed and mobile installations. Satellite television has become common and widely received by many households. Fixed terrestrial microwave links are increasing in numbers as are the services they carry, due to the expansion in telephony channels, analogue as well as in future digital high definition TV signals. Furthermore the needs of commerce, business and also domestic users increasingly require the availability of interactive communications.

According to a report by the Radiocommunications Agency of the Department of Trade and Industry (DTI)(1988), there will be an expected move away from copper cable traditionally used by telephone companies to radio waves. These can cater for local access links for the delivery of advanced data to mobile terminals, and there are suggestions for the implementation of a Microwave Video Distribution System (MVDS). Since the publication of the above mentioned DTI report MVDS components have be made available by many companies. Companies such as Phillips or Dudley Lab advertise their MVDS products in online catalogues (Phillips and Dudley Lab internet-site, 1998). A recent search by the author showed an existing system supplied by Dudley Lab in operation in Venezuela.It operates at 28 GHz, other systems at 23 GHz are also advertised. Phillips offers similar systems for a range of frequencies extending as high as 40 GHz. Some of the advertised systems operate bidirectionally and are therefore designed to accommodate new interactive digital TV

channels. They are also capable of supporting Local Multipoint Communications Systems (LMCS) for local area computer networks. A rise in applications and increase in the number of such systems in operation is therefore to be expected in the near future. Many of these services share the same frequency bands as the satellite services with obvious interference risks.

This rapid increase in applications gives rise to the problem of trying to accommodate the radio links in a relatively small geographical area. For example especially in terms of the mutual interference between co-and adjacent channel links. Hitherto simple geometrical separation techniques are employed which aim to control the level of this interference by maintaining sufficient separation between the growing number of systems catering for the consumer requirements. Furthermore it will not be satisfactory to seek solutions by moving to higher frequency bands. From an engineering and a business point of view it is much more desirable to use each available frequency band more efficiently since there is only a limited number of frequency bands available. Also very high frequencies radio links are more expensive and more difficult to operate using more advanced technology. They are also more likely to be influenced by factors like rain, snow and hail. In future there will be a growing demand to share radio frequencies amongst several users.

With an ever increasing number of services operating in the same frequency bands the problem of mutual interference becomes more and more significant. This also applies to the rapidly increasing use of mobile communication systems (e.g. cellular mobile telephone services) and the expansion of these services into higher frequency bands.

1.2 The Interference Problem

For system planners the two most important factors are the reliability and the possible co-channel interference experienced on a certain link. The interference may arise because a number of different factors which include the prevailing climate, length and topography of

the radio path and the presence of neighbouring co-channel transmitters. All combine to make it possible for a spurious transmission to be received by the radio terminal.

In the not too distant past the main objective for radio system planning engineers was to try and achieve sufficient service coverage of the area served by the link. This meant that the minimum signal level obtainable at most receiver locations for most of the time was sufficient to ensure a good quality of service. As far as taking into account basic terrain data and basic propagation mechanisms these were valuable and guaranteed a high quality service. However with the rapid increase in radio links the interference problems has become more and more important. This has led to the necessity of having to assess more accurately the level of interference experienced on the link and experienced as a function of time percentage (Hall and Barclay, 1989). The likelihood of interference increases immensely in densely populated areas where it maybe necessary to share frequencies among a number of users. Buildings, which are available abundantly in these areas may contribute to the amount of interference because of reflections and scatter from them. But they also offer the prospect of being used as shields to protect radio terminals against interference. For this purpose detailed knowledge about the behaviour of microwave signals in the shadow region of buildings is needed as well as knowledge about the possible paths in such a situation.

1.3 European initiatives for effective interference reduction

With increasing political and cultural integration in Europe plus the fact that radiowaves are not constrained by political boundaries it was necessary to set up Europe-wide programmes to perform effective methods of interference reduction especially in Western Europe.

Therefore initiatives were set up to co-ordinate radio transmissions across Europe and also provide both a more detailed understanding of the propagation mechanisms and data for an interference reduction on a European basis. The programmes supported by the ITU-R (International Telecommunications Union - Radio Communications Section) include various COST-programmes (European Collaboration in the field of Science and Technology). The

University of Glamorgan has collaborated in a number of research activities and contributed widely to two COST programmes over recent years, namely COST 210 and 235. The results of COST 210 were published in 1991 (Cost 210, 1991). Its primary objective was to recommend improved procedures for the prediction of statistics of signals likely to cause co-channel interference, to minimise the Co-ordination distance between radio systems in Europe.

One of the three main areas of research in this project dealt with interference reduction and site-shielding, named as one potentially useful method. This work was intensified in Working Group 3 in the COST 235 project which started in 1992 entitled "Radio wave propagation effects on the next-generation fixed service terrestrial telecommunications systems". The aim of this working group was to focus on developing new, accurate site shielding methods and eventually the formulation of a generalized site shielding procedure. Under those COST projects the University of Glamorgan in collaboration with the Radiocommunication Agency, Rutherford Appleton Laboratory and British Telecom Laboratories has investigated this useful interference reduction technique as part of their collaborative measurement and modelling programme.

1.4 Influence of buildings and site-shielding

Site-Shielding is an interference reduction technique which utilises obstacles to shield a radio terminal from an interfering signal. The shielding obstacle can be either natural or man-made, including the following: hills, vegetation, buildings, pits and embankments, fences and screens.

These techniques and their effectiveness have been subject to many investigations by previous researchers, signal reduction due to terrain was investigated by Boithias (1973), Lucia (1972) investigated the possibility of placing a receiving earth station in a pit.
Lucia (1970), Gould and Schmitt (1977) and Scheeren (1988) investigated the use of artificial site-shielding measures such as conducting solid or small meshed fences. A combination of

measures is documented by Bratnik (1983) for the Federal Express Corporations earth station on Somerset, New Jersey, where both a reinforced concrete wall and an artificial pit are use for shielding.

With microwave communication links increasingly being used in urban areas right into the heavily built up city centres as opposed to being confined to rural areas a few years ago, the prospect of using existing buildings to shield radio terminals from unwanted interference becomes more pressing. Research in order to provide system planners with data evaluating the amount of shielding provided has been conducted over recent years. Van Dooren (1994) carried out scale model investigations on the problem, whereas Haslett (1991) investigated actual buildings. Also theoretical investigations have been published by Haslett (1991), Levy (1993) and van Dooren (1993). These references investigate the diffraction mechanisms involved since it is the primary propagation mechanism utilised in site shielding.

Over a number of years as part of the site-shielding research at the University of Glamorgan the influence of buildings on microwaves has been investigated. Haslett (1993) modelled and measured the diffraction of microwaves cause by buildings and Ding (1994) carried out similar investigations on the scatter of radiowaves by buildings.

The prediction of the signal strength in the proximity of a building, which may be utilised for the purpose of site-shielding, in general has to take into consideration the possibility of multipath propagation of the signal. The receiving antenna could be subjected to the following modes of electromagnetic wave propagation:

1) Diffraction from two or more edges of the building.
2) Diffraction and specular reflection caused by edges and sides of adjacent buildings.
3) Scatter from an adjacent building or buildings.
4) Transmission through the shielding building.
5) Scatter from trees and other vegetation in the vicinity of radio terminal.

This leads to a situation where the receiving antenna in the proximity of buildings will always be subjected to the resultant of all the contributions travelling on the above mentioned signal paths.

This means that in investigating the propagation properties of buildings in an urban environment the probability of multipath propagation becomes significant, due to the fact that buildings will create a number of paths for the signal. A single isolated building can according to Haslett's (Haslett, 1993) investigations easily provide 35 dB of protection, the so called site-shielding factor (SSF). The site-shielding factor (SSF) is defined as the ratio of the received interference signal power in the absence of an obstacle to the received in the presence of the obstacle. This will normally be different from the diffraction loss (Haslett, 1993).

However in urban areas it is highly unlikely to find isolated buildings which could be utilised to protect a proposed receiver. In the presence of other buildings, and structures such as lamp-posts, roof-top antennas, metal banisters, fences and vegetation the scatter and reflections from those structures will lead to the forming of a multipath situation at this receiver location in the shadow of the shielding building. It was encountered during earlier measurements by Haslett, that the numerous contributions received in the shadow region of a building would when progressing further into the shadow make it impossible to distinguish the diffracted signal from the reflections and scatter from adjacent surfaces. This meant that the dynamic range of the measurements in the diffracted field was limited, because only the sum of the individual contributions could be measured and not only the diffracted signal. So to increase the dynamic range of the equipment a way of isolating the lateral contributions was needed. The problem experienced here is of course a general one affecting any radio wave link in terrain that contains a number of obstacles, and especially urban built up areas again. Whenever a receiver in these areas is placed in the shadow region of a shielding building or other structure it is very likely to receive unwanted contributions of the signal from reflections and scatter from adjacent structures. To distinguish, locate and evaluate the different contributions of this resulting multipath field a highly directive antenna would be needed to measure these individual components. And even with a very directive antenna

strong signal components may still 'leak' through side lobes of the antenna. Also a highly directive antenna would be very bulky and hence hard to handle and align and because a large antenna also means that it is very likely to be in its near field when measuring close to buildings, which effectively means a widening of the pattern again (Ding, 1994). For system planners in any situation where multipath propagation is experienced it will be of great interest to resolve this multipath into its constituent components to asses whether a proposed receiver location is suitable or whether countermeasures have to be taken. A detailed knowledge of both the angle under which the interfering component (of the same signal) arrives at the antenna and its magnitude is required to define the multipath field at that point.

1.5 Signal Separation

As mentioned in the previous paragraph in urban situations in many cases the receiving antenna is subject to a multipath field which results from the interaction of the component waves, which may be assumed to be plane, propagating past the antenna. The resultant field and the direction of the propagation of the various components constituting this multipath field together determine the level of the signal received by the antenna. A simple example is the classic interference pattern created when two waves travelling in opposite directions interact.

From a radio system planner point of view it is highly desirable to understand the propagation mechanisms affecting a planned or given link to find optimal solutions. It is of great value to be able to locate the position of an interfering source, which when done with respect to a planned or given receiver location may be described by the angle of arrival relative to a reference direction. Also the relative amplitude of this interference with respect to the wanted signal at the receiver is of great interest to asses the likely effect of the interfering signal.

For this purpose a procedure to resolve the combined multipath field observed at the receiver terminal into its constituent components is needed.

1.6 Objectives of the Research

In the light of the problems encountered in the previously mentioned research programme and the knowledge that multipath propagation is an ever present phenomenon in urban radio wave propagation, an investigation was carried out on how to resolve a multipath field into its constituent components. The main aim is to formulate a procedure, which will enable system planners to resolve a given multipath field from knowledge of its spatial variability over an appropriate distance. The resolution process consists of determining the relative magnitude of the constituent signal components and their angles of arrival at the receiver, relative to a reference direction.

The main objectives are listed below:

- Describing theoretically the received interference pattern in a multipath field consisting of 2 or more components accompanied by suitable simulations of multipath field patterns typically arising;
- Investigating the feasibility of analyzing the real part of the resulting interference pattern with suitable signal processing techniques, to gain information on the constituent components leading to the multipath field under consideration;
- Searching for the occurrence of similar or related problems in the published literature and investigating how their relationship with this project;
- Establishing a theoretical framework in which the problem of separating the multipath field into its components can be formulated for an arbitrary arrangement of sources;
- Considering a generalization of this theory to continuous signal source distributions in addition to discrete signal source contributions;
- Considering methods of finding solutions to specific cases which are likely to arise in practice. This involves analytical as well as computer simulation and practical measurements;

- Finally the formulation of a resolution procedure which yields accurate information on the relative magnitudes of the constituent signal components, their angles of arrival and an estimation of their accuracy.

1.7 Outline of the Thesis

Chapter 2 summarizes the relevant literature for this research project, which includes published material in books and articles on a range of subjects and related aspects of the work. This includes microwave propagation, site-shielding, multipath interference and optics. The latter was investigated because light waves behave in very similar fashion to microwaves, since they both are forms of electromagnetic waves.

Chapter 3 describes the theory of multipath interference outlining how the multipath field can be described mathematically. A simulation for received amplitude envelopes or interference pattern in a multipath geometry is given. Two main cases corresponding to discrete sources (reflections, diffraction etc), and continually distributed sources (scattered signals) are described.

Chapter 4 describes the use of the Fourier transform as a signal processing technique to analyze the interference pattern of a multipath field. This spatial pattern is received in a multipath field and can be detected by linearly displacing the receiving antenna in small displacement relative to the wavelength recording the signal amplitude at each step. The Fourier transform analysis, it is shown, can be usefully applied to the resolution of the multipath field.

Chapter 5 describes the development of a multipath resolution procedure using the discrete Fourier transform (DFT). Properties of the DFT relevant to the resolution procedure are discussed. Methods of improving the accuracy of the procedure results are presented. Also results of the application of the resolution procedure to simulated multipath geometries are given.

Chapter 6 describes an experimental programme carried out to test and validate the developed component resolution procedure. Experiments were carried out in three different environments.

i) Multipath geometries using specially set up multipath fields utilising reflector boards,
ii) multipath geometries arising from building formations,
iii) experiments inside an anechoic chamber.

(i) and (ii) were outdoor measurements at 11 GHz, whereas the indoor measurements (iii) were carried out at 20 GHz.

Chapter 7 shows the results of the various experiments in the experimental program. A validation of the experimental data is given.

Chapter 8 analyses the theoretical accuracy of the procedure and outlines the factors influencing the resolution and shows limitations of the procedure. The influence of noise in the measured data on the accuracy of the procedure is discussed.

Chapter 9 presents the conclusion and outlines further studies.

CHAPTER 2 BACKGROUND STUDIES

2.1 Multipath propagation

Multipath propagation is a common occurrence in radio-wave propagation and well documented in literature. Early publications in HF and microwave propagation like Bullington (1947) already realized that with shorter wavelength multipath propagation becomes more apparent. Multipath propagation means that signals travel from the source towards the receiver via different propagation paths. The receiver receives not only the direct line of sight (LOS) signal but also contributions reflected and scattered from or diffracted around structures on or in the vicinity of the direct path. At higher frequencies more structures likely to be large compared to the wavelength and hence act as sources for reflections.

The signal at the receiver is the resultant of the phasor addition of the individual signal component waves arriving via the various propagation paths. The individual signal contributions arrive at the receiver location with different phases depending on the individual path length. The received signal level can vary considerably over small distances of only a few wavelength (Jakes, 1974). Displacing the receiving antenna in a multipath situation over short distances will result in large variations in signal strength. The varying signal strength with distance shows pronounced amplitude minima and maxima (Hall and Barclay, 1989). The signal strength minima are experienced as deep fades which can be 40 dB or more below the maximum received signal level (Duffy, 1988).

Allen (1984) and Duffy (1988) summarize the effects of multipath propagation on long radio links. On long links different propagation paths arise from ground reflections and reflections or refractions from atmospheric layers caused by changes in the refractive index of the atmosphere (figure 2.1). The refractive index changes with time through weather and seasonal influences. Multipath propagation on long links is not static but time variant (Duffy, 1988).

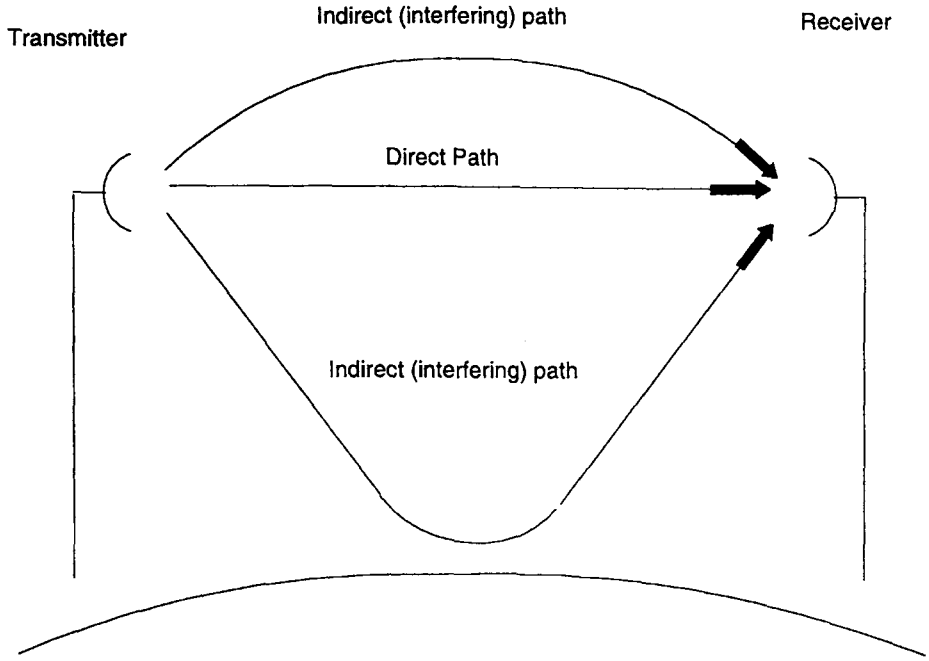

Figure 2.1 *Multipath propagation on long radio links (Duffy, 1988)*

On shorter radio links multipath propagation is mainly due to reflections, diffraction and scatter caused by obstacles such as buildings and other man-made and natural structures. This is particularly relevant in urban areas, see figure 2.1.

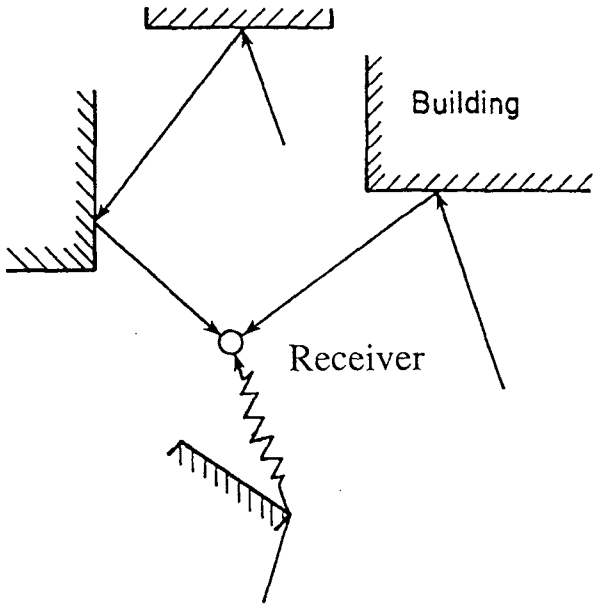

Figure 2.2 *Typical multipath situation in an urban environment (Hall and Barclay, 1989)*

Here the receiver might be at a low hight above ground, situated between buildings, often without a clear line of sight transmission from the signal source, Cichon et al, 1993. Multipath propagation in these situations is regarded as static, i.e. not time variant (Parsons and Gardiner, 1989). A static field of varying signal strength levels is the result of the interaction of the various signal components. Matthews and Mohebbi (1989) show a measurement signal levels in a multipath field. They created a three-dimensional display of the field by plotting the signal levels over the xy-plane of there measurement samples. The measurements were carried out at UHF frequencies.

Displacing the receiver over small distances through this field a spatial pattern of signal strength over distance can be recorded. This pattern is generally referred to as amplitude envelope (pattern), Jakes (1974) and Parsons (1992). Figure 2.3 shows such a pattern as given by Parsons and Gardiner (1989).

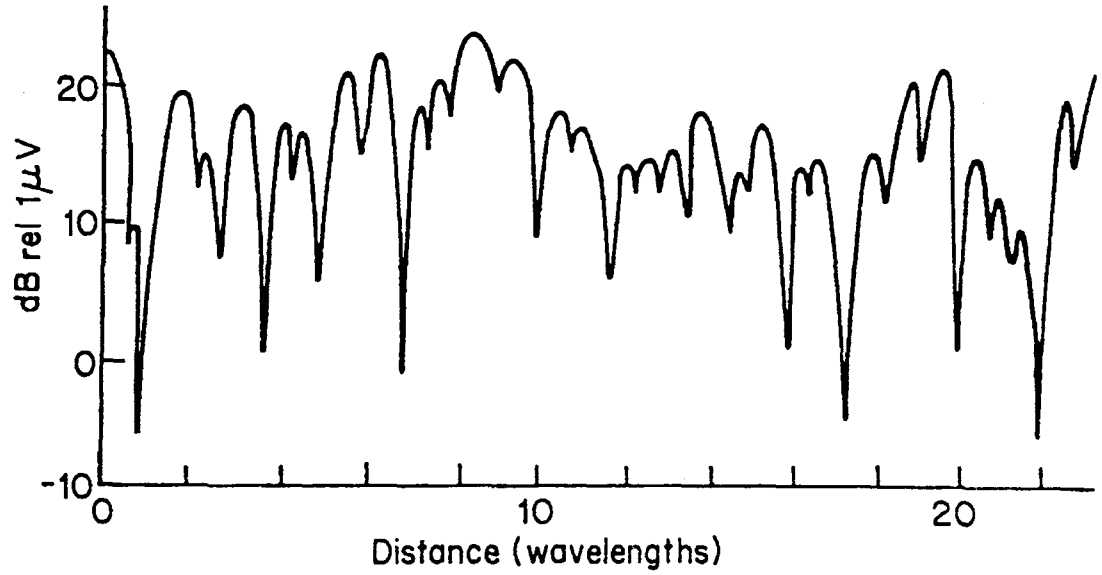

Figure 2.3 *Received amplitude envelope pattern with moving receiver under multipath conditions (Parsons and Gardiner, 1989)*

2.1.1. Effect of multipath propagation on radio links

Radio link systems are adversely affected by multipath propagation for three main reasons:

- Rapid changes of received signal strength with small displacements of receiving antenna, including deep fades in the signal level.
- Relative delayed arrival of signal components at the receiver caused by signal components travelling over different propagation paths.
- Both the above mentioned effects are strongly frequency dependent which has implications on wide-band systems.

Deep fades in the signal strength at locations where strong signal components combine in antiphase leads to insufficient signal strength levels and system outages. At locations of sufficient received signal levels the transmitted message will be affected by delayed signal components arriving later via longer propagation paths. The delays lead to distortions in analogue systems and cause errors in digital systems (Brown, Galzier, 1964). Interference from delayed signals limits transmission rates on digital links (Parsons and Gardiner 1989).

Phase differences caused by path length differences are dependent on the wavelength of the transmitted signal and hence the frequency. Locations of troughs and peaks in the spatial field of received signal levels differ for each frequency.

Figure 2.4 shows how a multipath notch, a signal fade at a certain frequency at a certain location can affect a digital radio system carrying several transmission channels causing adjacent channel interference.

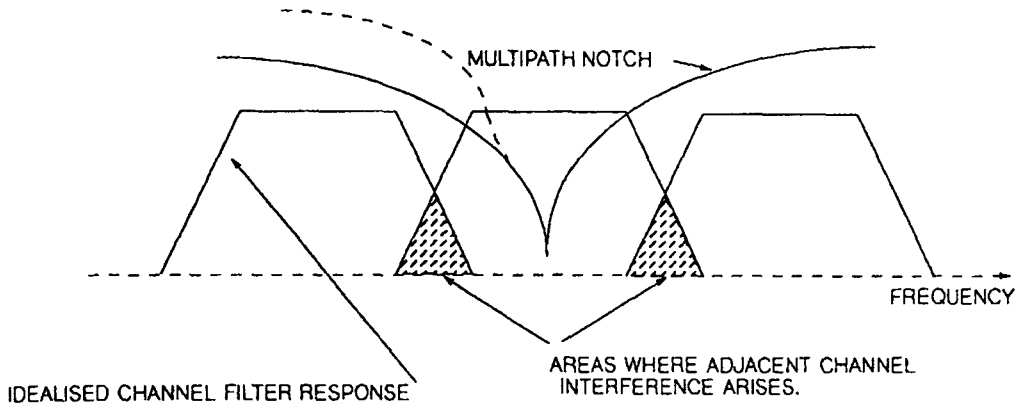

Figure 2.4 *Source of adjacent channel interference*

When transmitting a signal occupying a finite bandwidth the different propagation path lengths within the multipath medium have approximately the same electrical length for any closely spaced frequency components, their amplitudes and phase variations will be very similar. As the frequency separation increases the behaviour of the signals of different frequencies becomes increasingly uncorrelated, because the differential phase shifts along the various paths are quite different for each frequency. To asses the expected performance of radio links statistical parameters are used.

The signal delays are plotted as delay spreads of signal level over time delay. A coherence bandwidth is introduced (Jakes, 1974). The coherence bandwidth is a measure for the bandwidth over which spectral components are affected in a similar way by multipath propagation. Co (1972), and Matthews et al (1985) and Molkdar and Matthews (1988), give examples of such investigations in the UHF mobile communications band. Allen (1984) and Duffy (1988) show how these parameters influence the bit error rate (BER) for different modulation techniques on long radio paths. Langewellpott (1982) and Kürner and Wiesbeck (1994) investigate shorter urban links.

A great number of different methods and techniques to minimise multipath effects on radio channels are documented. Space and frequency diversity techniques utilise the fact that fades in the received signal are very localized and frequency dependent. Using several different locations or frequencies for the same information will minimise the multipath effects on the signal (Parsons and Gardiner, 1989), Beach and Swales (1989). Other papers concentrate on optimising different modulation and transmission techniques for multipath situations, for example Bernyukov (1988), Loulay and Holtzman (1984), Nossek (1989), Schultz and Höfgen (1984).

All the references listed in this section demonstrate that multipath propagation is generally undesirable and great effort is spent to minimise the problems associated with it. The geometry leading to the compound spatial field of signal levels in multipath situations is often not obvious when the receiving antenna is affected by a compound field of multipath signal components. Identification of constituent signal components and the quantification of their amplitudes and angles of arrival at the receiver would lead to an understanding of the signal sources giving rise to such a geometry. These factors can be taken into account at the system planning stage. Difficulties could be avoided employing techniques such as the use of higher directivity antennas, relocation of receiving terminals and or shielding them against interference.

2.1.2 Site-shielding

The technique of shielding radio terminals against unwanted interference utilizing terrain features, man-made obstacles or purpose built shields is know as site shielding. Early publications show examples of satellite earth stations being protected from interference from nearby terrestrial radio links. Bratnick (1973), Lucia (1970, 1972) and Gould and Schmitt (1977) show examples how earth stations can be protected by situating them in oval pit with extra protection by barrier walls or microwave fences. These measures require a considerable amount of construction work around the antenna. Lucia states a depth of 38.5 ft for the pit with respect to the highest point of the surrounding earth wall. Bratnick's paper shows a 16

ft hight concrete wall on a 10 ft high embankment surrounding a 15 ft deep pit. These dimensions illustrate the amount of construction work necessary to protect the earth station antennas. More recent site-shielding investigations try to utilize existing features for the protection of terminals (Sheeren 1984). Here especially in urban areas it is intended to place terminals in the shadow of existing buildings to achieve protection (van Dooren, Haslett, Levy, 1993, van Dooren, 1993, van Dooren and Govaerts, 1993). In an urban situation it is very unlikely to find an isolated building standing on its own as protection. A receiver placed in the shadow of an urban build will therefore always be subjected to a variety of signals reflected and scattered from adjacent buildings. Any solutions to the site-shielding problem in built up areas therefore require an in depth knowledge of the various signal components arriving by different propagation modes at the receiver (COST 235, 1996).

2.2 Resolution of multipath field components

As mentioned above it is possible to record an amplitude envelope pattern in a multipath situation when displacing the receiver through this field. This recorded pattern can be utilized to identify and quantify constituent multipath components. The interference of plane waves at microwave frequencies is very similar to the interference of monochromatic coherent light used to create holographic images.

2.2.1 Principle of holography in optics

Holographic images are created by the interference of a reference light beam with the light reflected from or shining through the object. The image (hologram) will be the result of this interference on the image plane, which can be light sensitive photographic film (or a plate) to have an image that can be repeated and copied (figure 2.5). If the hologram is created using a monochromatic laser, the principles involved (geometrical optics) are very similar to a multipath consisting of two components (Hecht and Zajac, 1974).

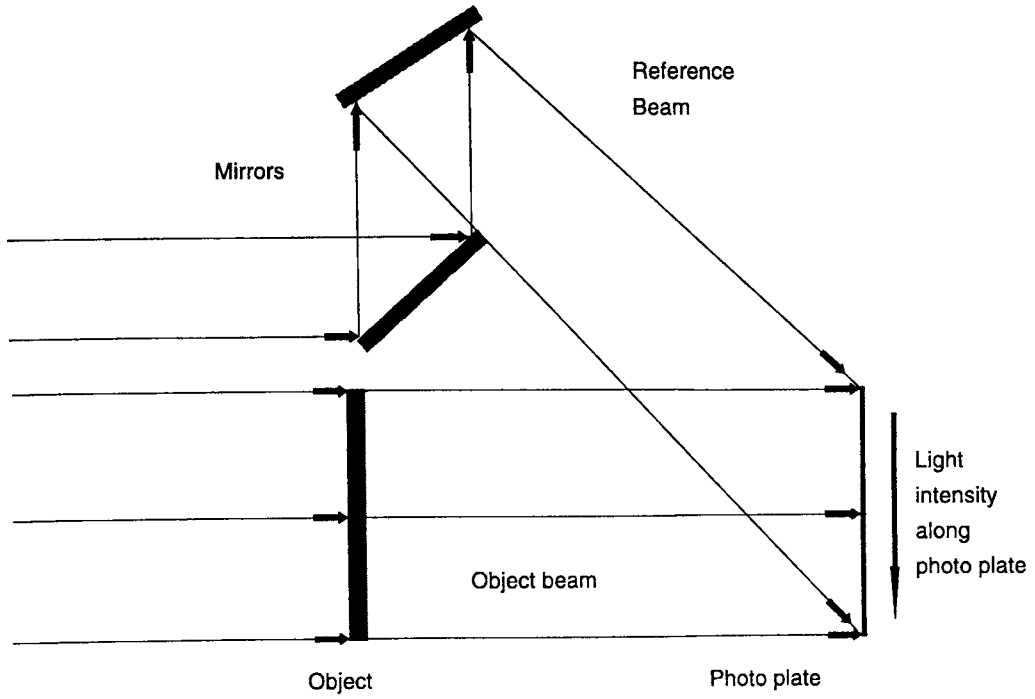

Figure 2.5 *Principle of holography with transparent object (Hecht and Zajac, 1974)*

2.2.2 Power density of a holographic image

The time averaged Poynting vector of an electromagnetic wave symbolized by <S> is defined as:

$$\langle S \rangle = \frac{c^2 \varepsilon_0}{2} |\vec{E_0} \times \vec{B_0}| \qquad (2.1)$$

where: c = speed of propagation of the EM wave

ε_0 = permittivity of vacuum

E_0 = electric field vector of a linearly polarized EM wave

B_0 = magnetic field vector of a linearly polarized EM wave

In optics the power density or Poynting vector is also defined as light irradiance often also still called light intensity I (Hecht and Zajac, 1974):

$$I = \langle S \rangle = \frac{c\varepsilon_0}{2} E_0^2 \tag{2.2}$$

According to Hecht and Zajac the resulting light irradiance along the photo plate of a hologram (like the one shown in figure 2.1.1, a case of 2 interfering light beams) using polarized monochromatic laser light is:

$$I = \frac{E_{0B}^2}{2} + \frac{E_{0O}^2}{2} + E_{0B}E_{0O}\cos(\Phi - \Phi_O) \tag{2.3}$$

Where E_{0B} and E_{0O} are the interfering components of the electric field, E_{0B} represents the electric field of the reference beam and E_{0O} that of the object beam (figure 2.1.1). Φ and Φ_O are:

$$\Phi = \frac{2\pi}{\lambda} x \sin\theta \quad \text{and} \quad \Phi_O = \frac{2\pi}{\lambda} x \sin\theta_O \quad \text{respectively.} \tag{2.4}$$

2.2.3 Adaptation of holographic principles for multipath resolution

A number of authors have addressed the use of holographic reconstruction methods using height gain functions on microwave links. Height gain functions are interference patterns in the vertical plane arising from the interference of ground reflection and reflected path in the atmosphere. Moving the receiver in a vertical line will reveal a similar interference pattern to the one observed in the horizontal plane in urban multipath situation, Ja (1975, 1976). See figure 2.6.

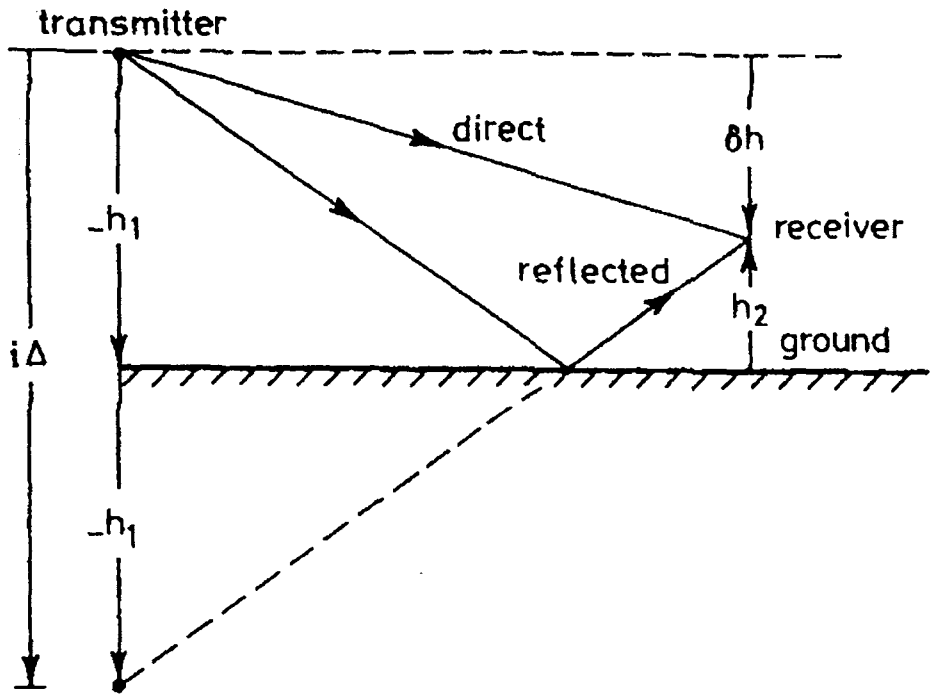

Figure 2.6 *Geometry resulting in height gain functions (Sayidmarie and Abbosh, 1993)*

Ja, Sayidmarie and Khildir (1989, 1991), Sayidmarie 1993) show the use of the height gain function to estimate angles of arrivals of a reflected component. The basic interference model for height gain functions is a two ray model. Ja (1975, 1976) shows a method using the sampled hight gain functions to reconstruct the location of signal sources. Ja applies the DFT to the square of the sampled height gain function to resolve angles of arrival and calculate the locations from these. He does not resolve any amplitudes, the frequency range used in investigation is 2 to 4 GHz.

Sayidmarie and Khildir (1989, 1991) use Ja's technique to calculate ground reflection coefficients as well as source locations at a frequency of 1.09 GHz. In the later paper Sayidmarie and Abbosh (1993) use a horizontal displacement of the receiving antenna to receive an amplitude envelope; the frequency used was 167.5 MHz. As before, Sayidmarie and Abbosh use this technique to calculate the reflection coefficient for signal reflected by the ground and the source height.

Narayanan et al (1996) adapt the methods used in the papers by Ja (1975, 1976) and Sayidmarie (1989, 1991) for the measurement of reflection coefficients of different ground surfaces at the millimetre-wave frequency of 95 Ghz. They use the same two component model as in the previous documents and gain additional information by applying a filtering process in the spatial frequency domain the separate what they call specular and diffuse components. They compare the different resulting diffuse components for measurements of different surfaces to determine a specular and a diffuse reflection coefficient for each surface depending on the grazing angle in each experiment.

All the papers mentioned above investigate methods to locate signal sources in a vertical plane, with the exception of Sayidmarie and Abbosh (1993) the receiving antenna is also displaced in a vertical direction. Common to all the above investigations is the use of a two ray model. The extension to more than 2 specular signal components is not been covered.

To adapt the holographic method to the resolution of multipath components in a horizontal field of n contributions these methods need to be developed further, which is the aim of this research programme.

The papers document the feasibility of using Fourier transform techniques on patterns of real data without additional phase information. Generally many documented signal processing techniques are applied to sets of complex input data samples containing information of amplitudes and phases, see section 2.3.

2.3 Choice of signal processing technique

Figure 2.2 depicting the received amplitude envelope when displacing the receiver through a multipath field shows a periodic or at least quasi periodic nature. The Fourier transform lends itself for spectral analysis of periodic signals (Beaucham and Yen, 1979). Webster and Scott (1987) use Fourier transform techniques to determine angles of arrival in tropospheric multipath propagation. They use an array of 12 antenna elements with a equal spacing of 51 wavelengths between elements and record both amplitude and phase of the signals arising at the elements. They determine angles of arrivals of signal components at different times of the day applying Fourier transform techniques to this complex data, the frequency used here was 16.65 GHz.

A wide range of different signal processing methods is documented in literature using a similar principle. All of these are based on complex input data received by an array of several antenna elements usually equidistantly spaced in a straight line. The exception is Moody (1980) who uses a circular array of antennas.

Examples for the processing of complex data obtained using a linear array of antennas are:

Bucker (1977) compares FFT and Prony algorithms on narrow-band signals in an ocean environment. He explains that Prony's method uses a series of exponential functions to represent a given function as opposed to the series of geometric functions used in the Fourier transform.

Gabriel (1980) describes a number superresolution techniques using array antennas to provide the input data for his algorithms.

Hug (1982), Kumaresan and Tuffs (1983), Johnson (1992), Mewes (1995), Sletten et al (1996) and Quiquis and Boulinguez (1997) give further examples of different signal processing techniques utilizing complex data received by array antennas.

Kay and Marple, (1981) list a comprehensive list of a number of different signal processing techniques, and compare the performances of those.

Extensive literature is available on the different resolution techniques, the ones listed here a re examples of the use of such techniques for similar resolution problems as the component multipath resolution problem subject of this research project. Many authors have developed methods with far better performance than the Fourier transform for specific applications. However many of these algorithm require substantial computational effort and more importantly only work on input data containing both amplitude and phase information of the received signal.

The aim of the research programme presented here is to develop a resolution procedure that can be implemented with inexpensive sufficiently simple hardware using only one receiving antenna recording amplitude information only. It was therefore concluded that the use of the Fourier transform as suggested in the literature on holography in section 2.2.3 was the best possible approach.

2.4 Summary and interim conclusion

Multipath propagation is widely observed on radio paths especially at microwave and millimetre-wave frequencies. The increased use of these frequency bands in urban areas and the need for efficient frequency planning means that multipath propagation needs to be addressed in these situations.

Radio links are adversely affected by multipath propagation due to unpredictable deep fades in the received signal strength at particular locations and delays caused to the signals components travelling on paths of different lengths. Both effects vary depending on the multipath geometry, which may not always be well defined.

The understanding of propagation mechanisms involved in generating a multipath field in the vicinity of buildings is also needed for the estimation of site-shielding properties of buildings and other structures.

A method to resolve the various constituent multipath field components would be extremely useful in these situations. The aim was to develop such a method with relatively simple engineering and measurement requirements.

Literature published on locating signal sources from height gain functions using Fourier transform techniques indicates that a received amplitude envelope can be utilized for the purpose of multipath resolution. However using holographic principles the relatively simple case of two interfering components considered in most of this literature will have to be expanded to n components.

The Fourier transform technique applied to the spatial amplitude envelope patterns containing amplitude information only proves to be a very effective tool in implementing a multipath resolution procedure.

CHAPTER 3 THEORY OF COMPONENT RESOLUTION

In principle two different kinds of signals leading to a multipath can be distinguished, depending on whether they originate mainly from specular reflection or from scatter (Narayanan et all, 1996). Surfaces whose roughness is small compared to the wavelength will cause specular reflection, whereas vegetation will scatter the signal into a random distribution of incoherent signals. For this reason this chapter consists of two parts: Part 3.1 describes theoretically the multipath field generated by discrete signals, like reflections from walls and other surfaces. This leads to the interference of coherent signal components with well defined phase angles. The second part (3.2) deals with scattered signals, with random phases generally and because of their large number may be considered as originating from a continuously distributed source.

3.1 Discrete Sources

The resolution of multipath fields produced by discrete sources deals with the resolution of the components of the interference pattern generated by discrete rays of signals. These can originate from specular reflections from surfaces, diffracted signals around the edges of buildings or other structures, and signals penetrating through structures. These signals recombine to form the multipath field. They originate from the same transmitter and hence are of the same frequency and can be considered coherent, so that fixed phase interrelationships can be assumed. Assuming discrete rays of signals means that the principles of geometrical optics apply (Born, Wolf, 1993). An application of the interference of two coherent signals may be found in the area of holography, where in two ray models especially many considerations are similar (Hecht, Zajac, 1974). This is briefly presented in chapter 2.2.1 on holography.

3.1.1 Theoretical description of the multipath field

The described procedure for the resolution of constituent components of a multipath field is based on the idea of recording the resultant interference pattern of the various components. The receiving antenna is placed at the location of interest (i.e. proposed receiver location) in the multipath field and then displaced linearly in small increments fraction of a wavelength long over a total distance of several wavelengths. While displacing the antenna the resultant signal strength is recorded at each point. The displacement is one increment at a time and the acquisition of each record is done while the receiving antenna is motionless. So there is no need to consider any Doppler shift of the received signal unlike in many mobile communication models, where the speed of the receiving mobile is significant (Jakes, 1974; Parsons 1992).

The signal strength is the resultant of the phasor addition of the individual contributions to the multipath field. The phase difference between the individual components varies differently for each component depending on its respective angle of arrival at the receiver relative to the direction of the displacement. So while moving the antenna the magnitude of the resultant field varies as a function of displacement. The recording of the absolute value, which represents the magnitude of the phasor addition, results in an interference pattern of magnitude versus distance, commonly known as the received amplitude envelope over distance (Jakes, 1974; Parsons, 1992). This pattern can be analyzed in the way described below yielding information about the magnitudes and angles of arrival of the individual contributions.

A typical multipath situation is shown in figure 3.1, where reflections from 2 buildings in the vicinity of the receiving antenna interfere with the original unobstructed signal arriving directly from the transmitter. The respective displacement of the receiving antenna for the purpose of recording the interference pattern is also shown. In this figure it should be noted that for the purpose of clarity the extent of the displacement is exaggerated in comparison with the dimensions of the buildings and their separation from the receiver.

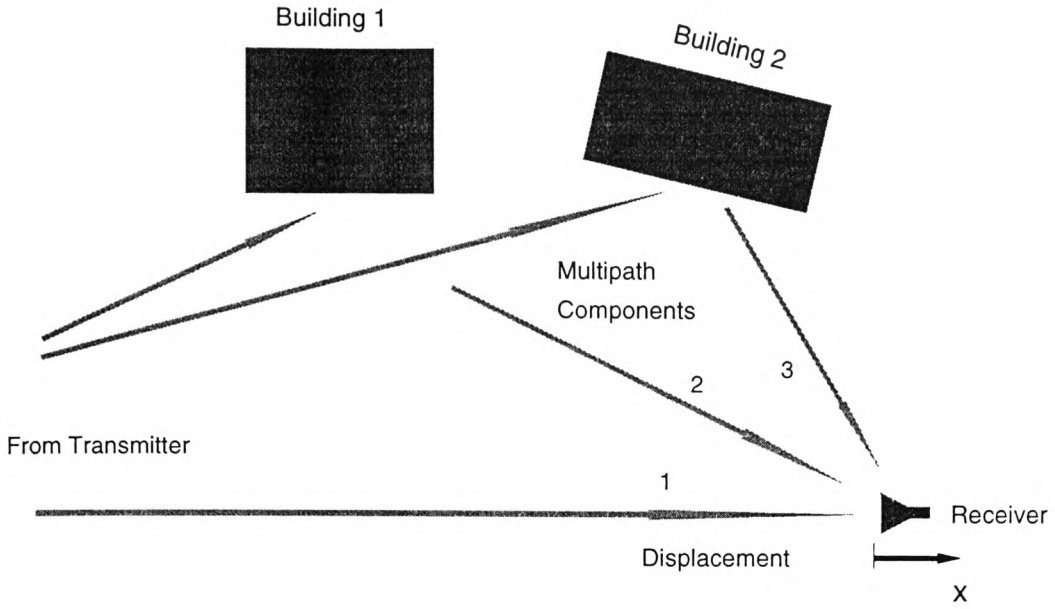

Figure 3.1 *Example of a multipath field, with constituent components indicated*

3.1.1.1 Two-component multipath field

The simplest case of a multipath situation is one consisting of two signal components, e.g. a direct component propagating from the transmitter to the receiver and a second component being reflected from a nearby building. This is shown in figure 3.2.

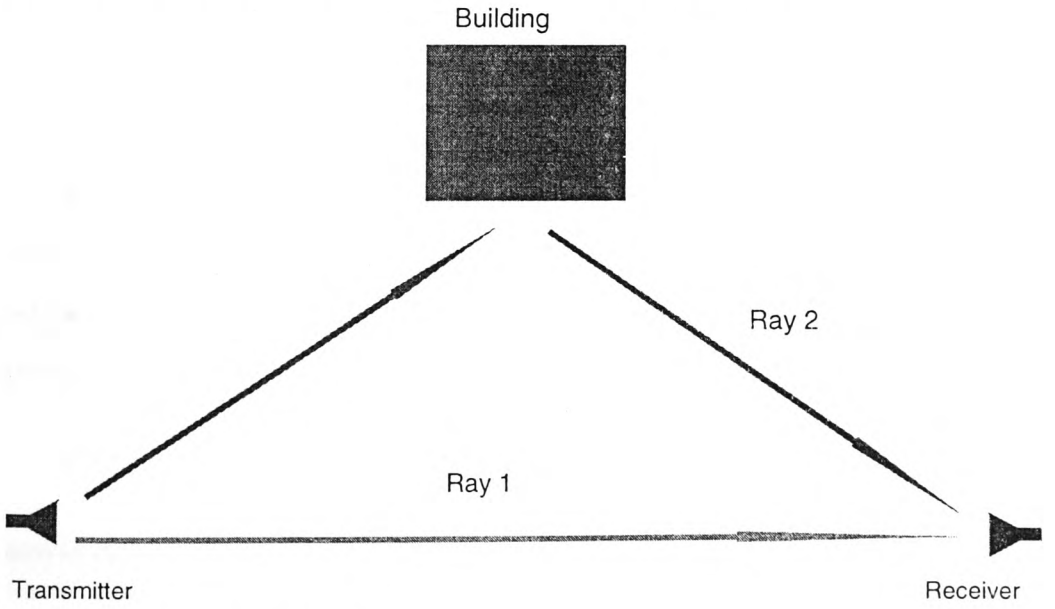

Figure 3.2 *A two component multipath*

At microwave frequencies (e.g. frequencies used in this investigation are 11.2 and 20 GHz with wavelengths of 2.7 and 1.5 cm respectively) involving typical multipath propagation path geometries it is justifiable that far field characteristics of the receiving antenna are assumed. The criterion widely used to determine the far field may be expressed as follows (Kraus, 1950):

$$D = \frac{2d^2}{\lambda} \tag{3.1}$$

where: D = the far field distance of the antenna

d = the largest dimension of the antenna

λ = the wavelength

In a typical urban environment the distance to the transmitter will be large in comparison to the far field distance D of the antennas involved. The receiving antenna will also in most cases be sufficiently far enough away from the reflecting or diffracting structures.

This means that plane wave propagation can be assumed. The voltage V induced in an antenna caused by an electric field E can be described considering the antenna angular gain pattern as a function of angle θ. If the directive gain of the receiving antenna is $G(\theta)$ in the direction of the arriving wave, the induced voltage follows as (Kraus, 1989):

$$\vec{V} = k\, G(\theta)\, \vec{E} \tag{3.2}$$

Where θ is the angle between the direction of propagation of the wave and the principal axis of the antenna. k is a system constant. If two or more plane waves arrive at the receiving antenna the voltage induced in the antenna is given by the phasor sum of the voltages induced individually by the constituent wave components. So in the case of two plane waves E_1 and E_2 arriving at the antenna (see figure 3.3) the received signal strength may be expressed as:

$$\vec{V} = \vec{V_1} + \vec{V_2} \tag{3.3}$$

The arrows denote voltage phasors V_1 and V_2, given by:

$$\vec{V_1} = k\, G(\theta_1)\, E_1 \tag{3.4}$$

$$\vec{V_2} = k\, G(\theta_2)\, E_2 e^{j\alpha} \tag{3.5}$$

where α is the phase difference between the two constituent fields E_1 and E_2 arising at the location of the receiving antenna.

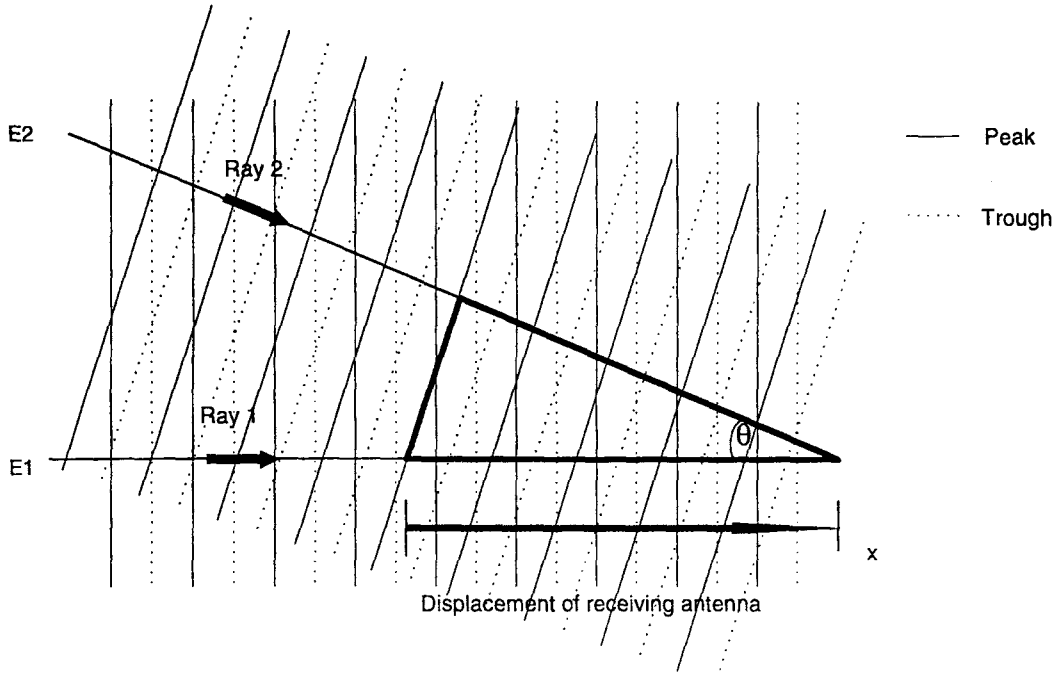

Figure 3.3 *Wave propagation in a two component multipath field*

Apart from the interaction of two plane waves Figure 3.3 also shows the displacement of the receiving antenna. In this case the antenna is displaced along the direction of propagation of one of the multipath field components. Theoretically the antenna can be displaced in any direction, over distances of a few wavelengths λ, but it is convenient to have the direction of displacement coinciding with one of the arriving components.

The signal received in such a case as a result of the above mentioned phasor sum is expected to vary between maximum and minimum values given respectively by:

$$V_{R_{max}} = k\,|\,G(\theta_1)E_1 + G(\theta_2)E_2\,| \tag{3.6}$$

$$V_{R_{min}} = k\,|\,G(\theta_1)E_1 - G(\theta_2)E_2\,| \tag{3.7}$$

A typical pattern that was observed in a two component multipath with a 60 cm parabolic reflector antenna as receiver at 11.2 GHz is shown in figure 3.4.

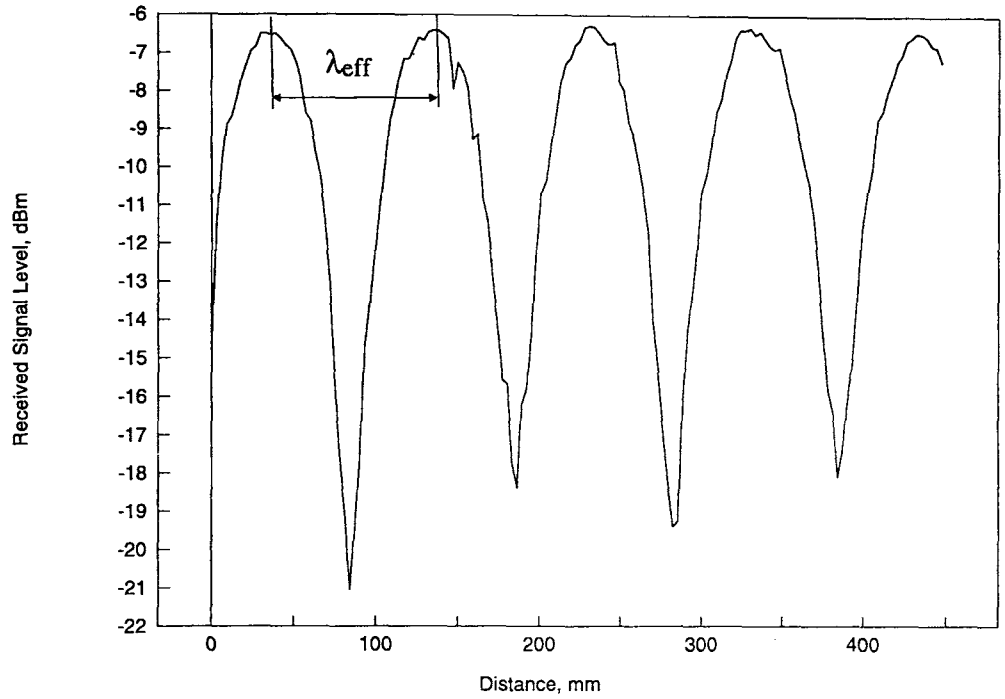

Figure 3.4 *Measured interference pattern in a two component multipath field, using a 60 cm parabolic reflector antenna*

The component resolution task consists of determining the two components V_1 and V_2 from a pattern like the one in figure 3.4 and for this relatively simple case the solution is straightforward. The maximum amplitude of the pattern in figure 3.4 is given when both components are in phase, so their amplitudes add up, whereas the minimum amplitude results from the component phasors being in antiphase, leading to a difference between the individual levels, i.e.:

$$| V_{R_{max}} | = V_1 + V_2 \tag{3.8}$$

$$| V_{R_{min}} | = V_1 - V_2 \tag{3.9}$$

From knowledge of the minimum and maximum values of the received interference pattern V_R it is easy to determine the amplitudes V_1 and V_2.

To resolve the spatial angles of arrival of the components (θ_1 and θ_2) relative to a reference direction the distance between successive maxima of the received signal V_R can be utilized. It is the distance between two points where the two contributions are in phase, and shall be defined as λ_{eff}, which is indicated in figure 3.4. Generalizing the situation in figure 3.3 to cases where the displacement direction of the receiving antenna does not coincide with the propagation direction of any of the signal component the relative phase angle α between the two phasors V_1 and V_2 can be expressed as:

$$\alpha = x\,(\cos\theta_2 - \cos\theta_1)\,\beta \tag{3.10}$$

Where: β is the phase constant $2\pi/\lambda$ and

x is the displacement of the antenna relative to the zero position

By definition, when $x = \lambda_{eff}$, the two phasors are in phase i.e. $\alpha = 2\pi$, so that equation 3.10 becomes:

$$2\pi = \lambda_{eff}\,(\cos\theta_2 - \cos\theta_1)\,2\pi/\lambda$$

or
$$\lambda_{eff} = \frac{\lambda}{|\cos\theta_2 - \cos\theta_1|} \tag{3.11}$$

If all the distances are normalized with respect to the wavelength of the radiation and the direction of displacement of the antenna is made to coincide with the direction of propagation of one of the field components, e.g. $\theta_1 = 0$ (for instance as indicated in fig 3.3) this leads to λ_{eff} becoming:

$$\lambda_{eff} = \frac{1}{|\cos\theta_2 - 1|} \tag{3.12}$$

Where λ_{eff} is given in normalised units of the wavelength λ.

So the angle of arrival θ_2, with respect to the direction of displacement in the case of a multipath field consisting of two components can be determined simply by noting the distance (λ_{eff}) between consecutive maxima of the recorded interference pattern V_R.

3.1.1.2 Multipath field consisting of more than two components

When the multipath consists of more than two components the situation becomes more complex. In most cases it will not be possible to solve analytically for the component amplitudes and their angles of arrival from the spatial plot of the interference pattern. The different component phasors will still acquire phase values such that at some points their phases are almost aligned or misaligned. This leads to the interference pattern thus exhibiting maximum and minimum values, some of which are absolute and others localised, where only some of the phasors happen to be in phase or in antiphase. The patterns formed this way show some periodicity or quasi-periodicity (see section 3.1.1.3), but their shape depends greatly on the path geometry involved, which will cause the individual components to arrive at certain angles with certain amplitudes. In general it has proved difficult to resolve patterns formed by three or more components analytically using the spatial domain functions unlike the situation in the two component case. However the theory derived for the two component case will be generalized to fields consisting of n components in the next section, where a method of resolution will be given.

The theory can be generalized for greater numbers of field components by assuming a receiving antenna responding to a compound multipath field produced by the interaction of several plane waves E_1, E_2 ... E_n having directions of propagation θ_1, θ_2 ... θ_n with respect to a reference direction taken conveniently as the principal axis of the antenna. The waves are assumed to be co-planar (2 D-model) which in practical cases can be justified, considering a distant transmitter and the reflecting and diffracting objects in the vicinity of the receiver mostly lying in the azimuth plane.

Figure 3.5 gives the top view, looking down on the receiving antenna in a typical multipath situation with several components, propagating horizontally with low elevation angles.

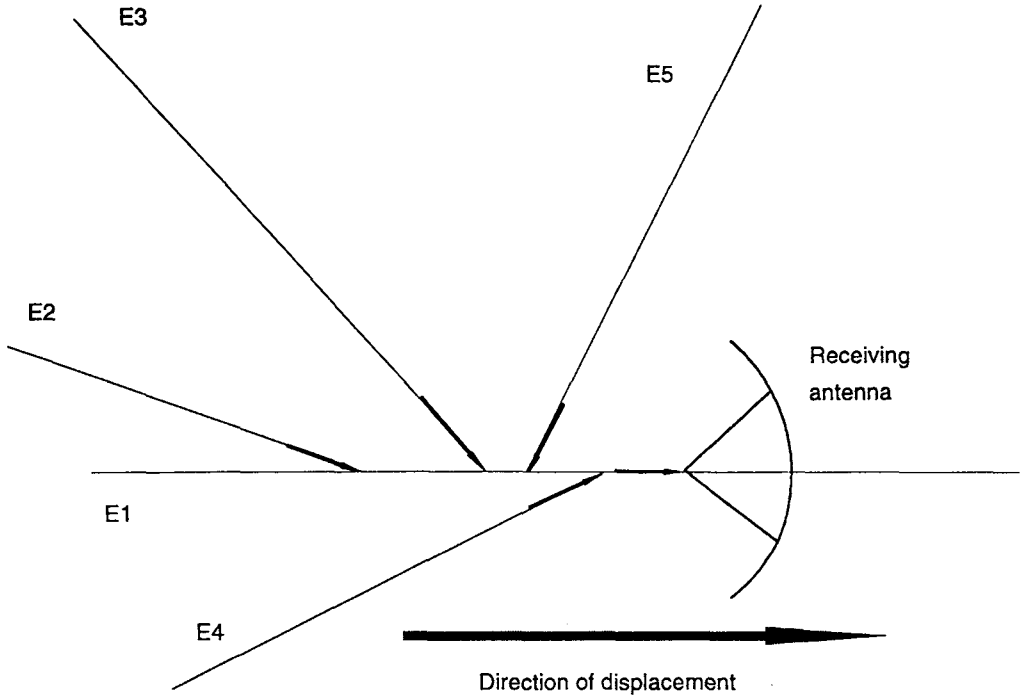

Figure 3.5 *Receiving antenna responding to several sources in a multipath field (top view)*

As in the two component case, to resolve the multipath field into its constituent components, the receiving antenna is displaced linearly along its principal axis over a distance of a few wavelengths λ in small discrete increments, a fraction of λ long. In displacing the antenna over a distance x, where x is very small relative to the distance between the receiving antenna and the sources giving rise to the multipath field the resultant signal received will display an interference pattern caused by the superposition of these components.

The received voltage at a given point is given by the phasor summation of the individual voltage contributions, i.e.:

$$\vec{V_R} = \sum_{r=1}^{n} A_r e^{j\alpha_r} \tag{3.13}$$

Where A_r and α_r represent the amplitude and relative phase of the received voltage caused by the contribution from the rth source.

A displacement x causes the individual angles α_r to change by the amount:

$$d\alpha_r = \beta x \cos\theta_r = \frac{2\pi}{\lambda} x \cos\theta_r \tag{3.14}$$

Where λ is the wavelength and β is the phase constant $2\pi/\lambda$.

Compared to the distance between transmitter and receiver as well as to those between reflecting and diffracting structures and the receiver, the displacement x is very small, so that the amplitudes A_r stay virtually constant, over the range of its variability. Hence the magnitude of a resultant voltage at an observation point can be expressed as:

$$V_{R_x} = \left| \sum_{r=1}^{n} A_r e^{j\alpha_r + \frac{2\pi}{\lambda} x \cos\theta_r} \right| \tag{3.15}$$

It is theoretically possible to choose an origin O at a point where all phasors are in phase (i.e. $\alpha_r = 0$, for all r). In this case V_R will be at an absolute maximum, given by:

$$\vec{V}_{R_O} = \sum_{r=1}^{n} A_r \tag{3.16}$$

Which leads to the simpler equation for V_{R_x} relative to origin O :

$$V_{R_x} = \left| \sum_{r=1}^{n} A_r e^{j\frac{2\pi}{\lambda} x \cos\theta_r} \right| \tag{3.17}$$

As mentioned in the previous paragraph, the simplest possible multipath case would be that resulting from two components, i.e. the direct path and one reflection. Solving equation 3.17 for n = 2 leads to:

$$V_{R_x} = \left| A_1 e^{j\frac{2\pi}{\lambda} x \cos\theta_1} + A_2 e^{j\frac{2\pi}{\lambda} x \cos\theta_2} \right| \tag{3.18}$$

For simplicity the exponent of the exponential function will be called $j\varphi_r$, so that:

$$V_{R_x} = \left| A_1 e^{j\varphi_1} + A_2 e^{j\varphi_2} \right| \tag{3.19}$$

Solving for the absolute value (magnitude) leads to:

$$V_{R_x} = \sqrt{A_1^2 + A_2^2 + 2A_1A_2\cos(\varphi_1 - \varphi_2)} \tag{3.20}$$

with: $\varphi_r = \frac{2\pi}{\lambda} x \cos\theta_r$ (3.21)

Equation 3.17 can be expanded for any number of components larger than n = 2.

For n = 3 using equation 3.21 it will be:

$$V_{R_x} = | A_1 e^{j\varphi_1} + A_2 e^{j\varphi_2} + A_3 e^{j\varphi_3} | \quad (3.22)$$

which leads to:

$$V_{R_x} = \sqrt{A_1^2 + A_2^2 + A_3^2 + 2A_1A_2\cos(\varphi_1 - \varphi_2) + 2A_1A_3\cos(\varphi_1 - \varphi_3) + 2A_2A_3\cos(\varphi_2 - \varphi_3)} \quad (3.23)$$

In the same manner as a component phasor has been added to eqn. 3.19 to result in eqn 3.22 this can be expanded to n components. As can be seen form the solutions of these vector additions, eqns. 3.20 and 3.23, adding a further multipath field component adds an additional squared amplitude A_n to the sum of the squares of amplitude values, it furthermore adds a cosine expression onto the sum of cosine expressions, and also a difference term with all the cosine terms present. As a general rule for the number of cosine terms (N_{kcos}) in the expression for V_{R_x} depending on the number of components i can be given by:

$$N_{kcos} = \sum_{i=1}^{n} i - 1,$$

Where N_{kcos} is the number of cosine terms in an equation with i signal components, and a maximum of n signal components. In practical cases the number of components is unlikely to exceed 4 significant signal components, although the expressions derived in this chapter can be expanded to infinitely more than 4. These expression for V_{R_x} describe the received amplitude envelope in a multipath field when displacing the receiver linearly. To resolve the constituent components a method is needed to find solutions for the amplitudes $A_1, A_2,...,A_n$ and the angles of arrival $\theta_1, \theta_2,...,\theta_r$. The phase terms $\varphi_1, \varphi_2,...,\varphi_n$ express the angles of arrival through equation 3.21.

The resolution of the amplitude envelope can be achieved using Fourier transform techniques as described in chapter 4, with chapter 5 describing the development of a working resolution procedure. Here it is considered useful to present two typical examples of received signal envelopes, which are discussed to get an insight into the resolution problem and its subsequent analysis.

The graphs shown in section 3.1.2.1 were created using a computer simulation of a path geometry, simulating the resultant amplitude envelope received in a multipath field. This is explained in the following section.

3.1.2 Computer simulation of the multipath field

A computer simulation was developed to investigate the behaviour of the envelope received in different multipath situations. These could be conveniently modelled, yielding results which were found very useful in developing and optimising the component resolution procedure. This simulation will be used here to give two typical examples of multipath signals. In chapter 4 a number of simulated examples are presented for which solutions are given in chapter 5.

To be independent of the signal frequency the calculations were scaled and normalized to units of wavelength λ. The displacement x is expressed in units of the wavelength λ. Let i be the number of points over the whole distance of displacement and N the number of points per wavelength. The ratio i/N determines the number of wavelengths over which the simulation is carried out. The displacement x can hence be written as:

$$x = \frac{i}{N}\lambda \tag{3.24}$$

So V_{Rx} from equation 3.24 can be expressed as:

$$V_{R_x} = \left| \sum_{r=1}^{n} A_r e^{j\frac{2\pi}{N} i \cos\theta_r} \right| \tag{3.25}$$

The result of this simulation is an amplitude envelope representing the interference pattern

received in a multipath field with moving receiver in volts over displacement scaled in wavelength λ. The following two examples have been generated using this simulation and serve the purpose of showing the expected nature of multipath interference patterns.

3.1.2.1 Two examples of simulated signal envelopes

Two examples of simulated interference patterns are presented here. The first one (figure 3.6), is typical for a received signal envelope in a multipath caused by the interference of two signal components. The second one (figure 3.7) is an example of an envelope expected in a multipath caused by three signal components. The amplitudes and angles of arrival of the constituent components of these multipath examples are listed in the subcaptions of figs. 3.6 and 3.7.

Two component multipath:

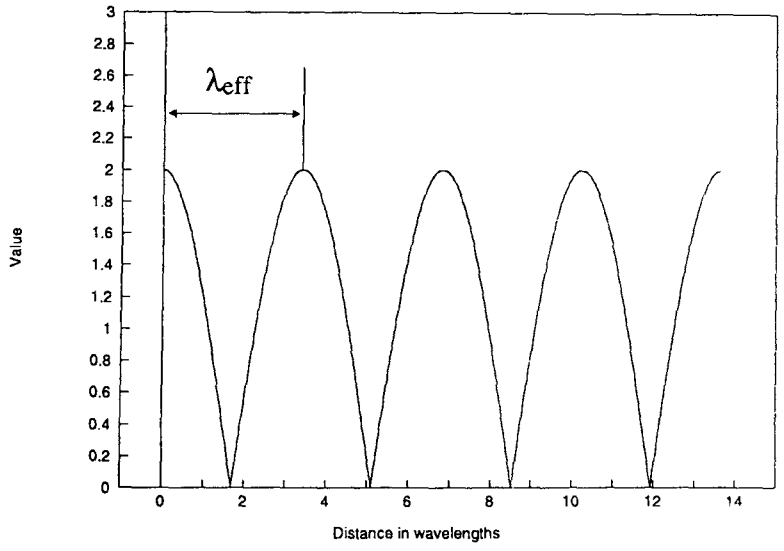

Figure 3.6 *Simulated interference pattern in a 2 component multipath*

Amplitudes: $A_1 = 1.0,\ A_2 = 1.0$

Angles: $\theta_1 = 0°,\ \theta_2 = 45°$

Three component multipath

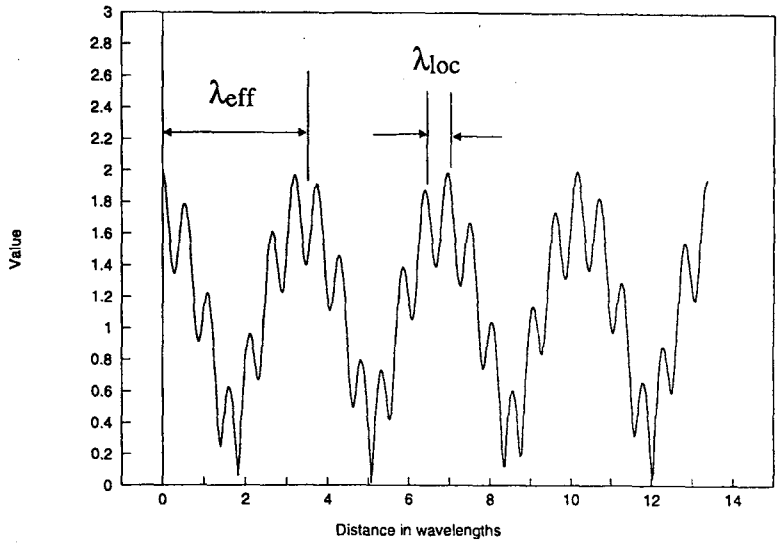

Figure 3.7 *Simulated interference pattern in a 3 component multipath*

Amplitudes: $A_1 = 1.0$, $A_2 = 0.7$, $A_3 = 0.3$

Angles: $\theta_1 = 0°$, $\theta_2 = 45°$, $\theta_3 = 150°$

Analysing the shapes of the amplitude envelope received in a multipath field, in every case this appears to exhibit a periodic or quasi-periodic behaviour. In the simple case of two components the signal is clearly periodic, whereas in cases of three or more components the signal shows quasi-periodicity. At an early stage in the investigations this quasi-periodicity observed in measured patterns led to the consideration of Fourier transform analysis techniques for the purpose of resolving the unknown amplitudes A_r and angles of arrival θ_r. The next section outlines the behaviour of the expected interference patterns in a multipath field (like the two examples shown above), which were generated by computer simulation.

3.1.3 Quasi-periodicity of the interference pattern

The solution of the multipath problem may be obtained, it was determined, by applying Fourier transform techniques to the recorded interference pattern. Fourier transform techniques give best results on periodic signals (Brigham, 1988), therefore it will be useful to analyze the possible periodic nature of the interference pattern.

In the case of the multipath being caused by two components the shape of the received amplitude envelope is periodic. As the receiver is being displaced the resulting relative phase angle (α) between the two component phasors varies in fractions of 2π, depending on the ratio x/λ. The displacement x is linear, so α changes linearly in fractions of 2π. If the displacement is performed over distances greater than one wavelength α will also reach multiples of 2π. The amplitude pattern varies with $\cos\alpha$, and because of the periodic behaviour of the cosine function for angles above 2π the result is a periodic pattern. This can be observed in figure 3.6.

In any cases where the number of constituent multipath components exceeds 2 however the situation becomes more complex. The resultant envelope is the result of the interaction of various phasors.

With displacement x the phases of these individual phasors will change by differing amounts over certain lengths of displacement, depending on their angles of arrival. The resulting spatial cycles for each phasor are independent of each other, so that localised minima and maxima in the recorded amplitude pattern are reached at certain displacement distances, governed by the resulting phasor sum at each point. The resulting shape of the interference pattern exhibits quasi-periodicity, rather than perfect periodicity as in the two component case. Also unlike in the case of two constituent multipath components, in cases with $n > 2$ depending on the geometry leading to the multipath field (angles of arrivals of components), it can be difficult to relate the observed periodicities to the individual components directly from the spatial pattern. In some cases a situation is encountered like the one demonstrated in figure 3.7 where two periodicities with distance can be identified. This may be referred to

as λ_{eff} and λ_{loc}. Again this is the case when one of the components is chosen to be in line with the direction of displacement of the receiving antenna.

The derivation for the periodicities λ_{eff} and λ_{loc} is similar to the one given for λ_{eff} for the two component case in section 3.1.1.1. Again considering the general case (different from figure 3.3) the displacement of the antenna x not being parallel to the field component E_1 but at an arbitrary angle. The resulting phase angle caused by the interaction of all components can be seen as the superposition of the differences of two components at the time, so that for these individual points where the two phasors are in phase we may calculate:

$$\alpha = \frac{2\pi}{\lambda} x \,(\cos\theta_2 - \cos\theta_1) \tag{3.26}$$

As before it applies that a maximum will be reached at $\alpha = 2\pi$, this was defined as the distance λ_{eff}, so the result is equation 3.11 again:

$$2\pi = \lambda_{eff}\,(\cos\theta_2 - \cos\theta_1)\; 2\pi/\lambda$$

Normalizing the displacement in units of λ, λ_{eff} results as:

$$\lambda_{eff} = \frac{1}{|\,(\cos\theta_2 - \cos\theta_1)\,|} \tag{3.27}$$

The remaining components will be superimposed, so that the derivation is similar, i.e. in the case of three components there will be a local maximum whenever α_2 and α_3 are in phase, substituting the indices in equation 3.27 leads to:

$$\lambda_{loc} = \frac{1}{|\,(\cos\theta_3 - \cos\theta_1)\,|} \tag{3.28}$$

The three component case is shown in figure 3.5, where λ_{eff} and λ_{loc} are marked for angles of arrival of components A_2 and A_3 of 45° and 150°, component A_1 was arriving at 0°, which means it was in line with the displacement of the antenna.

3.1.3.1 Auto-correlation of the interference pattern

To investigate whether a given signal is periodic or not the auto-correlation function (Beauchamp and Yuen) is used. This information is obtained by making measurements of the amplitude of the signal at two times, separated by a delay τ, finding their product, and averaging over the time of the record. The product is the auto-correlation, and the resulting curve is the auto-correlation function:

$$R_x(\tau) = \lim_{T \to \infty} \frac{1}{T} \int_0^T x(t)\, x(t+\tau)\, d\tau \tag{3.29}$$

For a completely random signal even a slight variation in delay will result in a reduction of the product, $x(t)x(t+\tau)$ to a very small value, so that a large value will only be obtained at or close to $\tau = 0$. Whereas for the case of periodic components a large shift in τ equal to half a period will be required before any substantial change in $R(\tau)$ will be apparent.

Figure 3.8 shows the auto-correlation of a random signal in comparison to the auto-correlation of the interference pattern signal in a multipath in figure 3.9. The signal for which the auto-correlation has been obtained is the one shown before in figure 3.7.

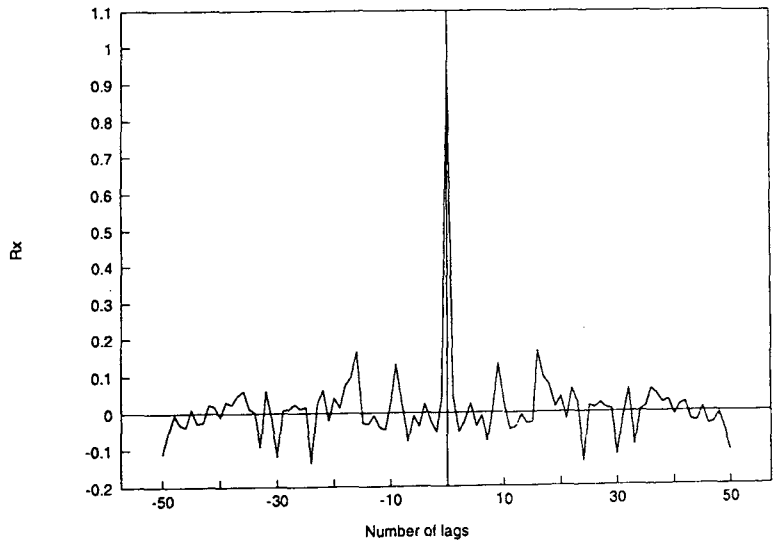

Figure 3.8 *Auto-correlation $R_x(\tau)$ of a random signal*

The two component interference pattern is clearly a periodic signal. It consists of the addition of a constant and one cosine term. The square rooting process does not effect its periodicity, since only amplitudes ≥ 0 are present (absolute value of received voltage V_{R_x}.

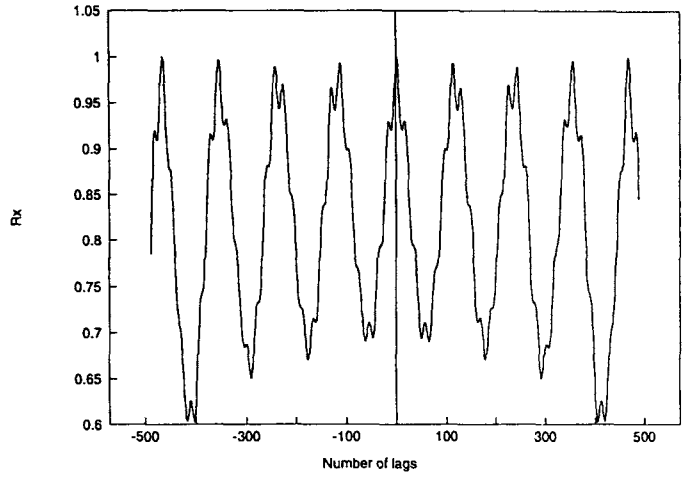

Figure 3.9 *Auto-correlation $R_x(\tau)$ of an interference pattern in a multipath field*

The auto-correlation function of a typical three component interference pattern (figure 3.7) as shown in figure 3.9 clearly indicates its quasi-periodic nature. Shifts of τ reveal large amplitude changes which show a repetitive pattern, but those repetitions, although very similar are not exact images of the previous one. However this quasi-periodic nature was found to be a strong justification for the application of Fourier transform techniques to the received amplitude envelope.

3.1.4 Summary and interim conclusion of chapter 3.1

In a multipath field that has been caused by the interaction of an original signal with reflected and diffracted rays of this signal, information about this multipath field can be gained from the spatial pattern obtained by displacing a receiving antenna over a small distance inside this field. When displacing the antenna in small increments, a fraction of a wavelengths at time, over a few wavelengths, the resulting amplitude envelope can be recorded. This interference pattern is the result of the addition of the electric field phasors causing induced voltages in the antenna. The magnitude of this amplitude envelope as a function of distance is generally described by a non-linear equation. This pattern exhibits either a perfectly periodic behaviour if the field consist of only two signal components or is quasi-periodic when there are three or more constituent signal components. The interference pattern in cases of two components is relatively simple to analyze and has been utilized in other areas , such as holography. Fields with larger number of constituent components are more complex situations. And here constituent signal components cannot be determined straightforwardly as in the two component case.

Chapter 4 describes how the multipath resolution can be achieved using Fourier transform techniques.

3.2 Continuous Sources

To resolve signal components in cases where the constituent components can also result from continuous sources like vegetation scatter a different technique is necessary. The difference with scatter signals is that these cannot be considered coherent anymore as in the above case For these cases a different technique is required. This is referred to as deconvolution and is discussed in section 3.2.1. Schulz and Höfgen (1984), Jensen and Pandelis (1983), Stefanos and Christos (1985) utilized similar techniques.

3.2.1 Deconvolution Techniques

This technique will be based on rotating the receiving antenna in a multipath situation rather than displacing it linearly. In this description it could be assumed that a receiving antenna of gain G(θ) is placed in a combined field arising from the interaction of a continuous distribution of transmitting sources. The antenna could be pointed such that its principal axis makes an angle θ with respect to a reference direction.

If V_i represents the voltage received by the antenna due to the source i alone causing a wave propagating at angle α_i as shown, then Vi may be written as:

$$\vec{V_i} = A_i\, G\,(\theta - \alpha_i)\, e^{j\gamma_i} \tag{3.30}$$

where

A_i is the voltage which would be received by an antenna of gain 1 placed in the location of the actual antenna due to source i alone

γ_i phase angle of V_i measured with respect to some arbitrary reference

$G(\theta - \alpha_i)$ is the gain of the receiving antenna in direction of source i.

For n sources the voltage received is the phasor sum of V_i:

$$\vec{V_R}\,(\theta) = \sum_{i=1}^{n} A_i\, G\,(\theta - \alpha_i)\, e^{j\gamma_i} \tag{3.31}$$

Equation (3.31) implies that the sources are co-planar and contained within the plane of rotation of the receiving antenna. As the antenna is rotated the amplitudes A_i remain unchanged as θ is varied since by definition A_i is the voltage received by an antenna of gain 1. However γ varies due to path length changes as well as phase changes associated with side lobes. In other words γ_i is a function of θ:

Hence $$\vec{V_R}\,(\theta) = \sum_{i=1}^{n} A_i\, G\,(\theta - \alpha_i)\, e^{j\gamma_i(\theta)} \tag{3.32}$$

Equation (3.32) applies to a discrete distribution of sources and represents an alternative form of equation (3.5). In equation (3.5) the gain is absorbed in the voltage amplitude A_r received by the actual antenna whereas in (3.32) the gain is explicitly stated. This equation can be generalised for the case where the antenna is placed in a continuous distribution of sources. $A(\alpha)d\alpha$ is the voltage received due to sources contained in a small angle $d\alpha$ by a reference antenna gain of 1. Under these conditions equation (3.32) becomes:

$$\vec{V_R}(\theta) = \int_0^{2\pi} A(\alpha)\, G(\theta - \alpha)\, e^{j\gamma(\theta,\alpha)}\, d\alpha \tag{3.33}$$

Signal separation in this case consists of the determination of the function $A(\alpha)$ from the knowledge of the received voltage V_R as a function of the antenna rotation θ. Solution considerations of equation (3.33) are discussed below.

3.2.1.1 Ignoring the Phase Term

If the phase term in equation (3.33) can be ignored, an assumption which may be justified when the antenna is receiving a randomly scattered signal from buildings or obstacles surrounding the antenna (3.33) can be reduced to:

$$\vec{V_R}(\theta) = \int_0^{2\pi} A(\alpha)\, G(\theta - \alpha)\, d\alpha \tag{3.34}$$

This represents a convolution process which may be solved using Fourier transform methods. Ft{ } denotes Fourier transform inside the curly brackets so that:

$$\mathrm{Ft}\{V_R(\theta)\} = F_1(u) \tag{3.35}$$

$$\mathrm{Ft}\{A(\alpha)\} = F_2(u) \tag{3.36}$$

$$\mathrm{Ft}\{G(\theta)\} = F_3(u) \tag{3.37}$$

and

$$F_1(u) = F_2(u) \times F_3(u) \quad (\times \text{ denotes multiplication}) \tag{3.38}$$

The solution of (3.34) thus involves the following procedure.

(i) Measure the received voltage $V_R(\theta)$ as a function of the rotation angle θ.

(ii) Measure the gain function $G(\theta)$ of the antenna.

(iii) Determine the Fourier transforms of $V_R(\theta)$ and $G(\theta)$ numerically if necessary.

(iv) Determine $F_2(u)$ using equation (3.38).

(v) Carry out the inverse Fourier transform of $F_2(u)$ numerically if necessary. This yields the function $A(\alpha)$ which is the required solution.

3.2.1.2 Including the Phase Term

The phase term in equation (3.33) makes the solution of the equation more complex. The form of the function $\gamma(\theta,\alpha)$ is crucial to the solution of the equation.

It is reasonable to assume that

$$\gamma(\theta,\alpha) = \gamma(\theta - \alpha) \tag{3.39}$$

This results in equation (3.35) becoming

$$\vec{V}(\theta) = \int_0^{2\pi} A(\alpha)\, G(\theta - \alpha)\, e^{j\gamma(\theta-\alpha)} d\alpha \tag{3.40}$$

$$\vec{V}(\theta) = A(\theta) * G(\theta)\, e^{j\gamma(\theta)} \tag{3.41}$$

Where * denotes convolution.

Equation (3.41) may be solved using Fourier transform techniques as explained above. However it is now necessary to measure or determine not only the magnitude of the gain function $G(\theta)$ but also its phase $\gamma(\theta)$ as functions of the rotation angle θ.

Equation (3.40) shows that signal processing techniques such as convolution and transform methods can be used to advantage in signal separation studies. Further investigation of these methods could yield very useful results in modelling and characterisation of buildings and obstacles in site shielding and propagation work.

3.2.2 Experimental requirements

This method will require as mentioned earlier the knowledge of the radiation pattern of the receiving antenna not only in amplitude but also in phase.

One possible way of acquiring the phase information needed could be to compare the received signal to that of a fixed reference antenna and noting the difference in phase between the two (Matthews and Mohebbi, 1989). Also the antenna angular pattern of the receiving antenna has to be determined with respect to amplitude and phase, rather than just the usual amplitude radiation pattern. After this preparatory stage the measurements can be carried out by rotating the receiving antenna in a field of various different contributions, and comparing its phase with that of the reference antenna.

CHAPTER 4 RESOLUTION OF MULTIPATH INTERFERENCE PATTERN WITH FOURIER TRANSFORM TECHNIQUES

The previous chapter described the interference pattern received by an antenna when displaced linearly in a multipath field. The quasi-periodic nature of the received pattern suggests that its spatial frequency spectrum may be utilized to obtain information about the angles of arrival of the constituent multipath components and their relative amplitude. Preliminary results obtained from the application of DFT analysis to the received pattern showed that such information can be obtained in a few simulated cases. These are given in 4.1.1.

The following describes how the information about the amplitudes and angles of arrival of the constituent multipath components can be retrieved from the spectrum of the recorded amplitude envelope. This envelope represents a spatial pattern rather than a time signal since the variations in amplitude envelope occur due to the receiver displacement instead of time. The Fourier analysis will yield a spectrum of spatial frequencies, scaled in (distance) $^{-1}$. This terminology was previously used in mobile communications, Jakes 1974).

In the first section of this chapter a few simulated examples of amplitude envelopes and their DFTs are presented to indicate the dependence of the generated spectrum on the relevant multipath parameters, i.e. amplitudes and angles of arrival of the constituent multipath components. In order to determine these parameters from any recorded interference pattern mathematical linkage between the amplitude envelope in the spatial domain and its spectrum in the spatial frequency domain has to be made.

Two methods of establishing this linkage will be given here. The first method one uses the recorded magnitude envelope directly by applying a DFT to it. The resulting DFT shows a number of spatial frequency components many of which are spurious and undesirable for the purpose of component resolution. Moreover this method necessitates a complex substitution using binomial series expansions to explain the results in the spatial frequency domain so that the desired information on the constituent multipath components can be derived from it.

To overcome the difficulties encountered with the first method a second approach has been developed using the square of the amplitude envelope to which we apply the Fourier transform. This leads to far less frequency components in the spatial frequency domain. Here the information about the multipath components can be extracted from the resulting spatial frequency domain using relatively simple relationships. This has led to this method being chosen as the preferable solution.

4.1 Interpretation of the spatial frequency domain

The interference pattern recorded when displacing the receiving antenna along a straight line in a multipath field was obtained as a set data of amplitude samples over the distance observed. As mentioned above this will be referred to as spatial domain. The application of the Fourier transform to this pattern gives rise to the spatial frequency domain. The values of spectral lines in this spatial frequency domain and the frequencies at which they arise will be investigated for useful information on the parameters to be determined.

In section 3.1.3 the terms λ_{eff} and λ_{loc} for the periodicities that arise in the interference pattern of a multipath field composed of 3 components were introduced. The defining equations of chapter 3 for λ_{eff} and λ_{loc} can be used to link the spectral lines in the spatial frequency domain to the angles of arrival of the components relative to a reference direction.

$$\lambda_{eff} = \frac{1}{|\cos\theta_2 - \cos\theta_1|} = \frac{1}{f_{sp12}} \tag{3.27}$$

$$\lambda_{loc} = \frac{1}{|\cos\theta_3 - \cos\theta_1|} = \frac{1}{f_{sp13}} \tag{3.28}$$

These equations simplify if the receiving antenna is moved along the propagation direction of one of the components. For example displacing the antenna in the direction of the propagation of the first component the angle of arrival θ_1 will be 0. The arising spatial frequencies can be directly linked to λ_{eff} and λ_{loc} by:

$$f_{sp12} = | \cos\theta_2 - 1 | = \frac{1}{\lambda_{eff}} \tag{4.1}$$

$$f_{sp13} = | \cos\theta_3 - 1 | = \frac{1}{\lambda_{loc}} \tag{4.2}$$

For $\theta_1 = 0$ the angles of arrival (θ_2, θ_3) can be calculated from the spatial frequencies (f_{sp12}, f_{sp13}) as follows:

$$\theta_2 = arcos\,(1 - f_{sp12}), \qquad \theta_3 = arcos\,(1 - f_{sp13}) \tag{4.3}$$

In general, a multipath field resulting from the interaction of n components equating $\theta_1 = 0$ results in the angles of arrival θ_2, θ_3, ... ,θ_n becoming:

$$\theta_j = arcos\,(1 - f_{sp1j}) \qquad \text{with} \quad j = 2, 3, \ldots, n \tag{4.4}$$

where θ_j expresses the angle of arrival of the jth component with respect to the direction along which the antenna is moved.

4.1.1 Simulated examples

A computer simulation is described in section 3.1.2, which simulates the recorded amplitude envelope expected for given multipath geometries. Using this simulation four examples of different multipath geometries are shown to demonstrate that the DFT of these envelopes varies according to the chosen geometry. Figure 4.1 shows the simulated amplitude envelope for a multipath resulting from two components (a) and its DFT (b). Figures 4.2 (a) to 4.4 (a) show simulations of amplitude envelopes of three different multipath geometries resulting from the interaction of three components and their DFTs are given in figures 4.2(b) to 4.4 (b) respectively.

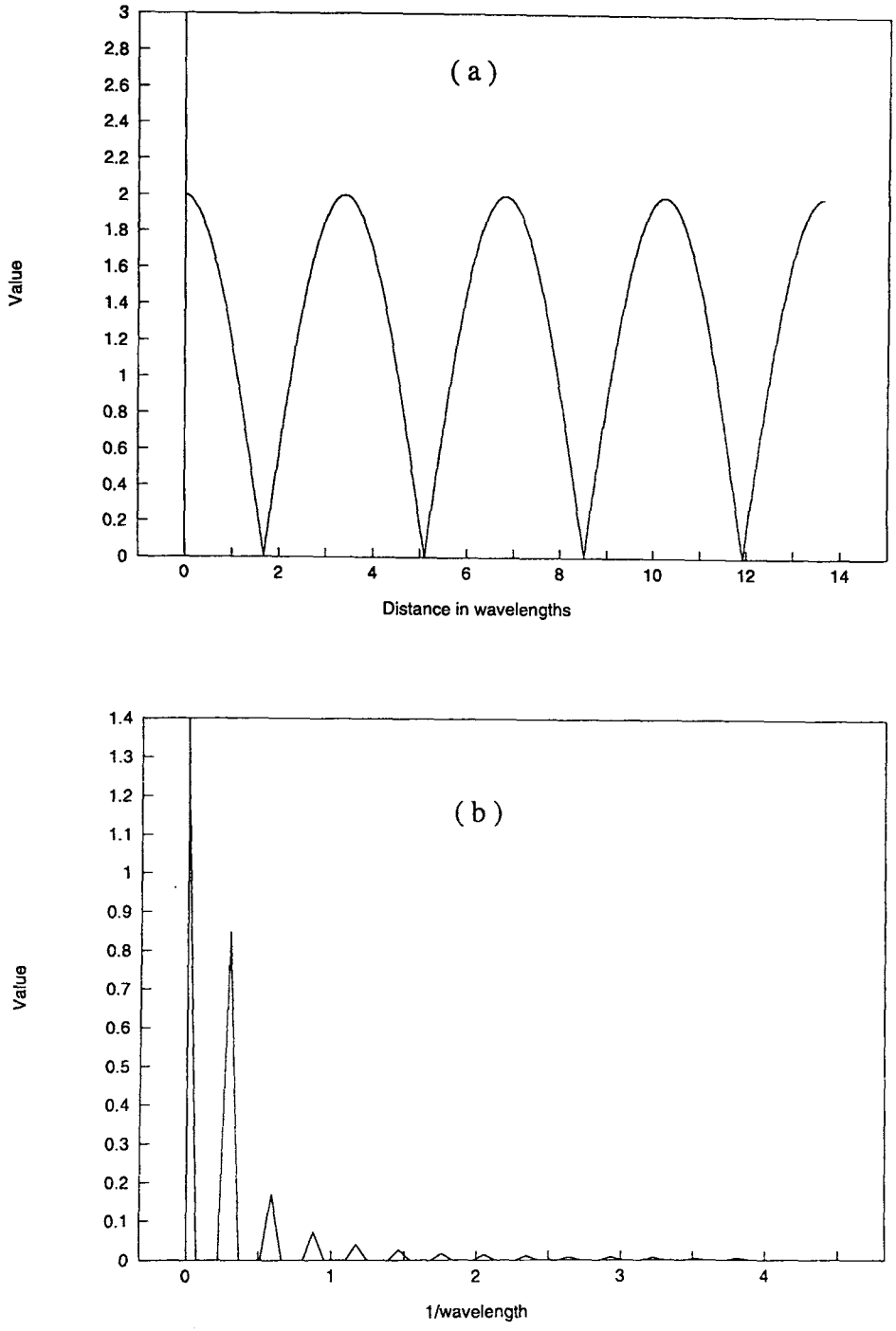

Figure 4.1 *Simulated amplitude envelope (a) and its DFT (b) for a multipath of 2 components:* $A_1 = 1.0, A_2 = 1.0;$ $\theta_1 = 0°, \theta_2 = 45°$

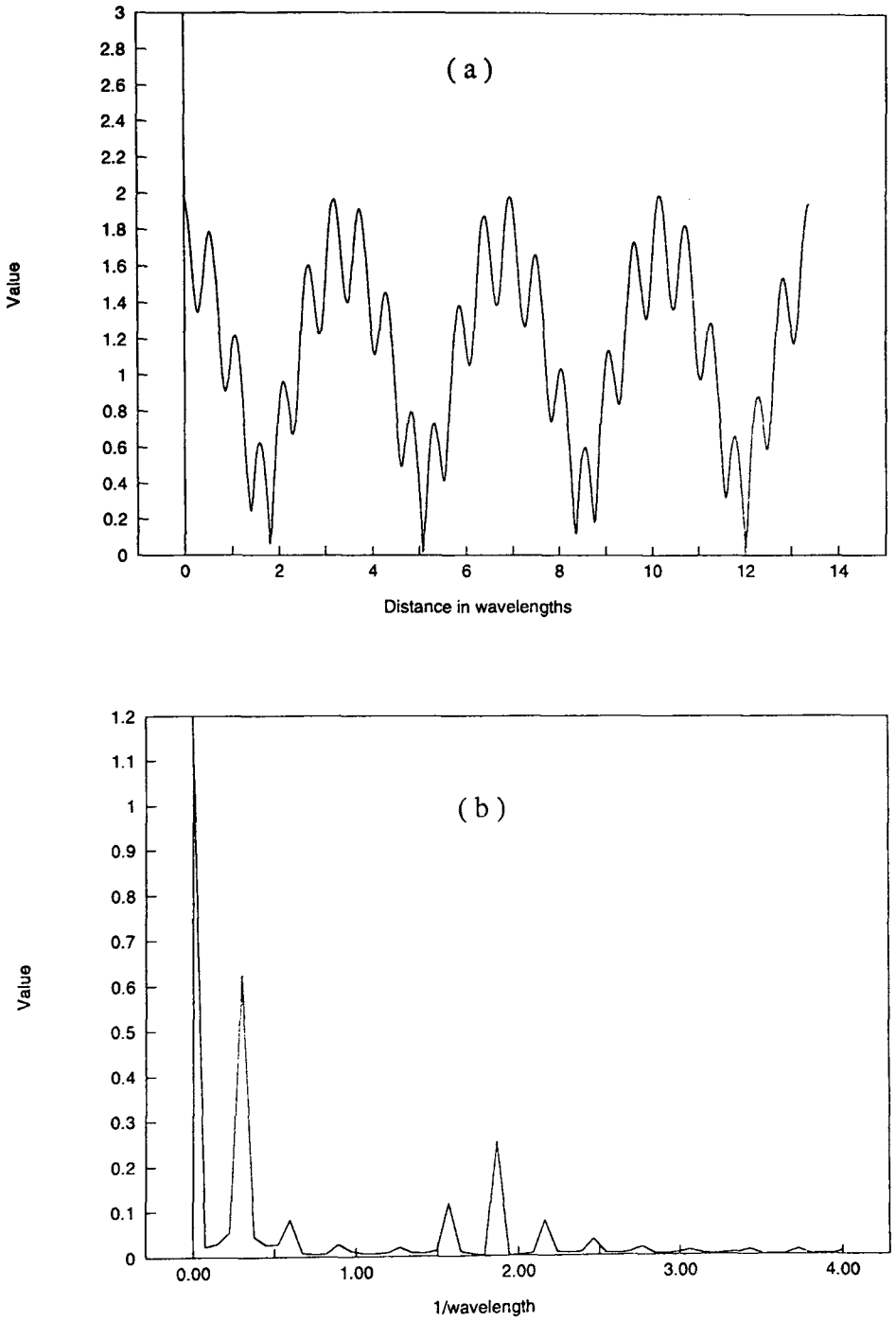

Figure 4.2 *Simulated amplitude envelope (a) and its DFT (b) for a multipath of 3 components:* $A_1 = 1.0, A_2 = 0.7, A_3 = 0.3;$ $\theta_1 = 0°, \theta_2 = 45°, \theta_3 = 150°$

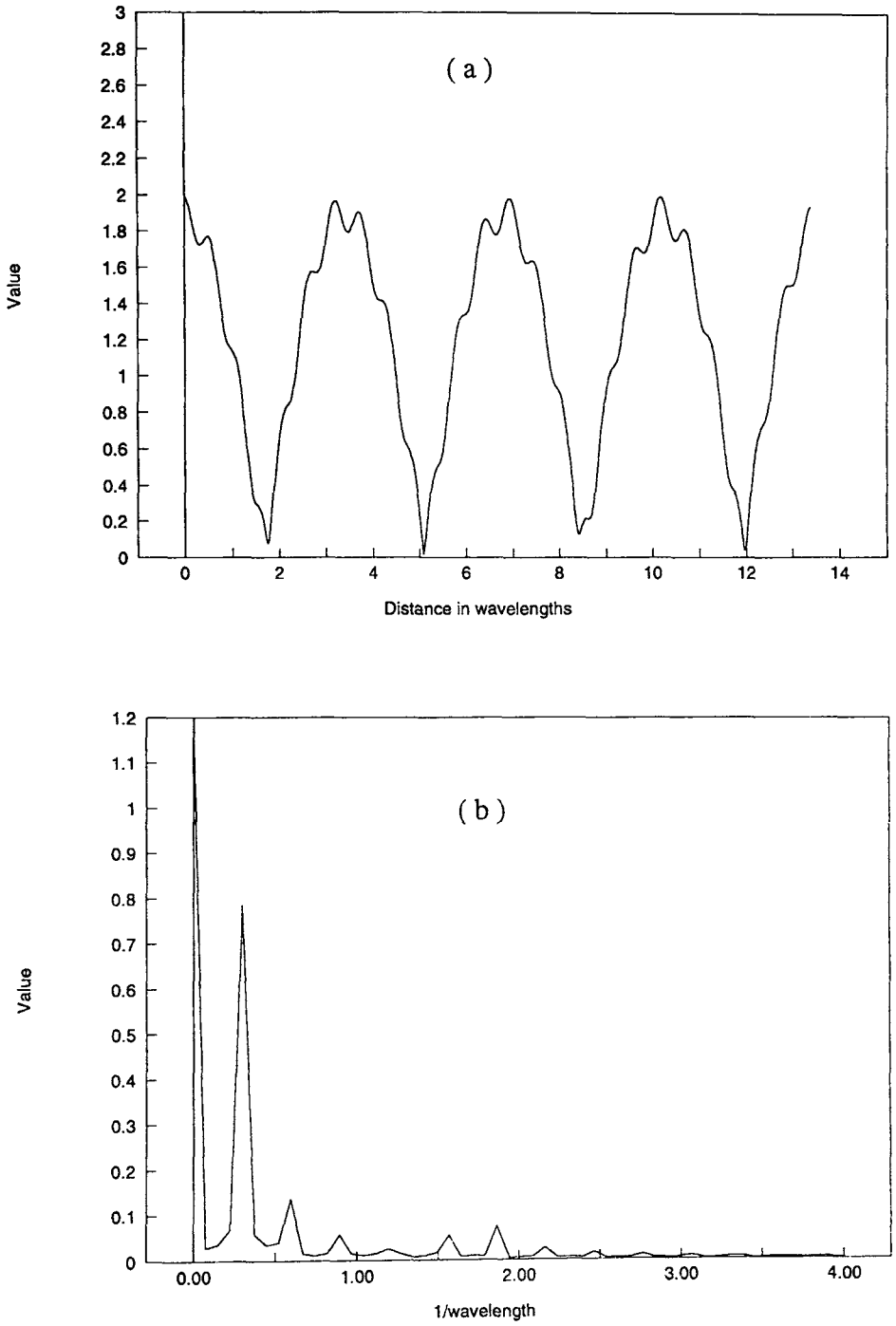

Figure 4.3 *Simulated amplitude envelope (a) and its DFT (b) for a multipath of 3 components:* $A_1 = 1.0, A_2 = 0.9, A_3 = 0.1;$ $\theta_1 = 0^\circ, \theta_2 = 45^\circ, \theta_3 = 150^\circ$

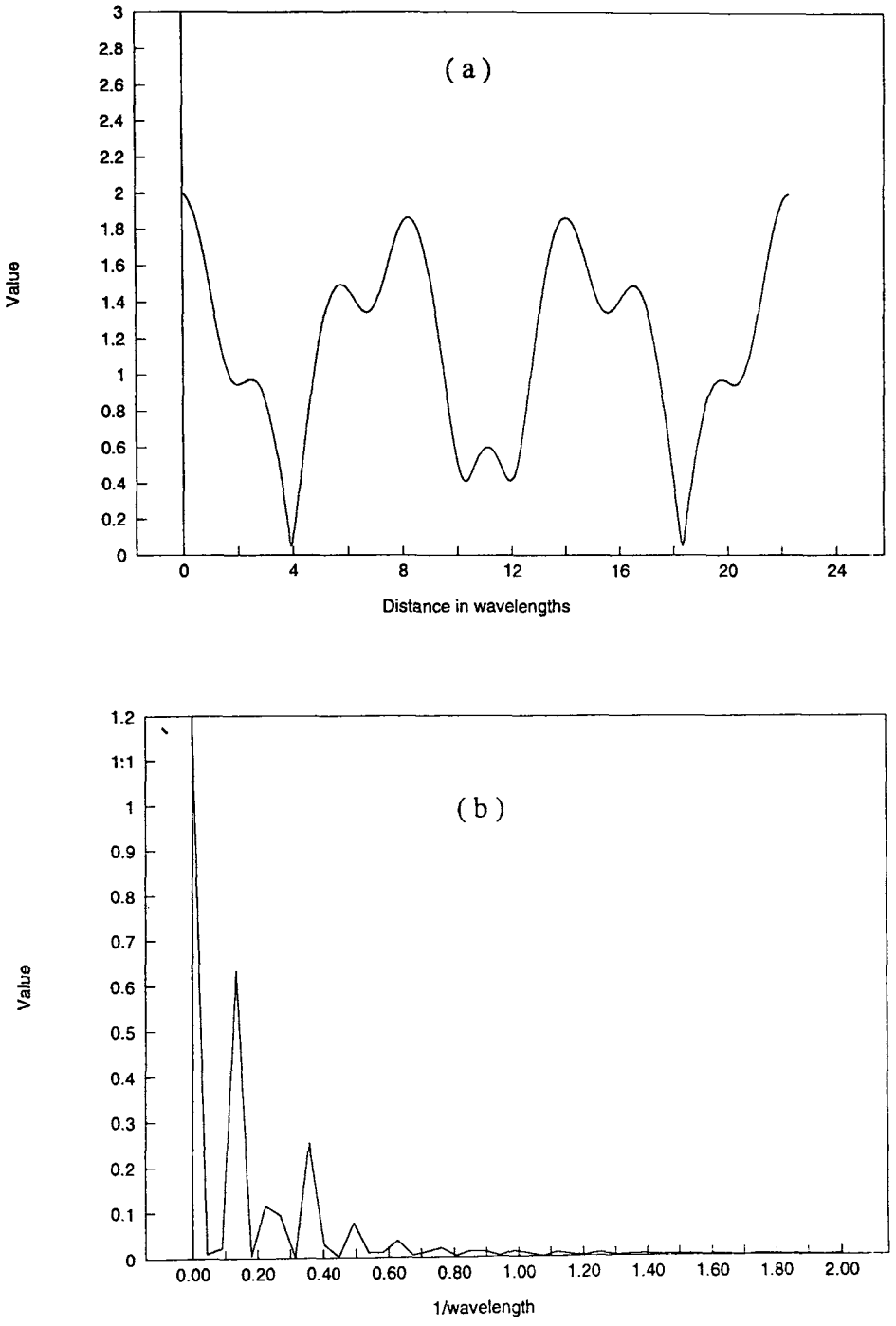

Figure 4.4 *Simulated amplitude envelope (a) and its DFT (b) for a multipath of 3 components:* $A_1 = 1.0, A_2 = 0.7, A_3 = 0.3;$ $\theta_1 = 0°, \theta_2 = 30°, \theta_3 = 50°$

For each of the simulated examples above spatial frequencies corresponding to the chosen angles of arrival of the components can be calculated using equations 4.1 and 4.2. These values are listed in table 4.1 for comparison with the spatial frequencies of the lines in figures 4.1 to 4.5. The angle of arrival of component 1 was chosen as 0°, leads to no spatial frequency related to this component.

	Component 2		Component 3	
	Angle of arrival	Spatial frequency	Angle of arrival	Spatial frequency
Figure 4.1	45°	0.29 1/λ	---	---
Figure 4.2 & 4.3	45°	0.29 1/λ	150°	1.87 1/λ
Figure 4.4	30°	0.13 1/λ	50°	0.6 1/λ

Table 4.1 *Relation of angles of arrival and spatial frequencies in simulated examples*

So far the following conclusions can be drawn from these simulations:

(i) A spectral line exists in each DFT at the spatial frequency corresponding to an angle of arrival not equal to 0 in each example.

(ii) The amplitude of the spectral line is dependent on the amplitude of the signal component arriving with the corresponding angle of arrival. This is especially evident from comparing figures 4.2 and 4.3).

(iii) There are other spatial frequencies are also apparent in the spatial spectra yielded in the different examples.

4.1.1.1 The spurious spatial frequencies

It was found that additional frequency components at frequencies other than f_{sp} in the two component case are harmonics of the first line at f_{sp}. This can easily be seen in figure 4.2 (b) by the spacing of each line, which is f_{sp}. In the other examples spatial frequency lines were found at multiples of the f_{sp1j}. Additionally there were lines found at sum and difference frequencies of both the original f_{sp}s and their harmonics in various possible combinations. Many of these sum and difference terms will be relatively small in amplitude as the amplitudes of higher order harmonics become smaller but nevertheless as figures 4.2 to 4.4 (b) show their are many spectral lines present in each DFT. The large number of spectral lines will make it difficult to derive the multipath parameters i.e. component amplitude and angles of arrival, from the amplitude envelope of an unknown multipath geometry. A method to avoid the occurrence of these spurious frequency components is discussed in section 4.3.

In order to relate the DFT result to the recorded amplitude envelope and with that to the multipath geometry, it is useful to review briefly the Fourier transform in the form of the Fourier integral for the spatial amplitude envelope. If h(x) represents the function of amplitude values depending on antenna displacement x the Fourier integral follows as:

$$H(f) = \int_{-\infty}^{\infty} h(x)\, e^{-j2\pi fx} dx \tag{4.5}$$

where: x is the displacement of the receiving antenna

f is the spatial frequency

H(f) is the resulting spectrum in the spatial frequency domain

h(x) is the amplitude envelope in the spatial domain

For the two component case the spatial domain function (amplitude envelope) h(x) is (eqn. 3.20):

$$h(x) = \sqrt{A_1^2 + A_2^2 + 2A_1A_2\cos(\varphi_1 - \varphi_2)} \tag{4.6}$$

with: $\varphi_r = \frac{2\pi}{\lambda} x \cos\theta_r$ (3.21)

The Fourier integral to solve would hence be:

$$H(f) = \int_{-\infty}^{\infty} \sqrt{A_1^2 + A_2^2 + 2A_1A_2\cos(\varphi_1 - \varphi_2)} \; e^{-j2\pi fx}\, dx \tag{4.7}$$

This integral is intractable due to the complexity of the integrand. For more than two components more terms are added to the integrand and its complexity is increased further.

The general Fourier integral describing the Fourier transform of a recorded amplitude in a multipath field with n components can be written as:

$$H(f) = \int_{-\infty}^{\infty} \left| \sum_{r=1}^{n} A_r e^{j\frac{2\pi}{\lambda} x \cos\theta_r} \right| \; e^{-j2\pi fx}\, dx \tag{4.8}$$

An alternative method of solving the Fourier integral arising in this application had to be considered, which used an approximation of the square root expression by binomial series. This is presented in section 4.2.

4.2 Binomial series approximation

A possible solution of the Fourier integral (eqn. 4.7) could be found by approximating the square root expression of h(x) by a binomial series.

The general binomial series is:

$$(a \pm x)^m = a^m \left[1 \pm \frac{x}{a}\right]^m = \sum \binom{n}{m} x^m a^{n-m} \tag{4.9}$$

for a = 1 this simplifies to:

$$(1 \pm x)^m = 1 \pm \binom{m}{1} x + \binom{m}{2} x^2 \pm \binom{m}{3} x^3 \pm \ldots + (\pm 1)^n \frac{m(m-1)\,(m-2)\ldots(m-(n+1))}{n\,!} x^n + \ldots \tag{4.10}$$

The series converges for $x \leq 1$

4.2.1 Two components

First a solution for the two component case will be given. For that eqn. 3.20 will be normalized by making the strongest component say A_1 equal to 1 so that $A_2 = k$ and $k < 1$. This means that amplitude levels are normalized to the value of the strongest component. This leads to the following expression for equation 3.20:

$$V_{R_x} = [1 + k^2 + 2k\cos\varphi]^{1/2} \tag{4.11}$$

Which can also be written as:

$$V_{R_x} = (1 + k^2)^{1/2}\,(1 + \frac{2k\cos\varphi}{1 + k^2})^{1/2} \quad \text{since} \quad 1 - 2k + k^2 \geq 0\,, \quad 2k \leq 1 + k^2 \tag{4.12}$$

The RHS of eqn. 4.12 consists of two parts, whereby the left-hand part $(1 + k^2)^{1/2}$ can be expressed as a binomial series, whereas in the other part a substitution needs to be made:

$$M = \frac{2k\cos\varphi}{1 + k^2} \qquad \text{for} \qquad M \leq 1 \tag{4.13}$$

So the expression in eqn. 4.12 is turned into a product of two terms:

$$V_{R_x} = (1 + k^2)^{1/2}\,(1 + M)^{1/2} \tag{4.14}$$

The left-hand $(1 + k^2)^{1/2}$ term does not present much difficulty to be expanded as binomial series, whereas the right-hand one includes a cosine function. Subsequent calculations showed that it was a relatively slowly converging function. This meant that the series had to be expanded up generally up to the 9th term, producing cosine terms of ninth order.
Additional theorems for the cosine function up to the 9th order are as follows:

$$\cos^2\alpha = \frac{1}{2}(1+\cos 2\alpha)$$

$$\cos^3\alpha = \frac{1}{4}(2\cos\alpha + \cos 3\alpha)$$

$$\cos^4\alpha = \frac{1}{8}(4\cos 2\alpha + \cos 4\alpha + 3)$$

$$\cos^5\alpha = \frac{1}{16}(5\cos 3\alpha + \cos 5\alpha + 10\cos\alpha)$$

$$\cos^6\alpha = \frac{1}{32}(6\cos 4\alpha + \cos 6\alpha + 15\cos 2\alpha + 10)$$

$$\cos^7\alpha = \frac{1}{64}(35\cos 2\alpha + 21\cos 3\alpha + 7\cos 5\alpha + \cos 7\alpha)$$

$$\cos^8\alpha = \frac{1}{128}(56\cos 2\alpha + 28\cos 4\alpha + 8\cos 6\alpha + \cos 8\alpha + 35)$$

$$\cos^9\alpha = \frac{1}{256}(126\cos\alpha + 84\cos 3\alpha + 36\cos 5\alpha + 9\cos 7\alpha + \cos 9\alpha) \qquad (4.15)$$

The approximation of eqn. 4.14 using two different binomial series for the two factors can be written as:

$$V_{R_x} = \left(1 + \frac{1}{2}k^2 - \frac{1}{8}k^4 + \frac{1}{16}k^6 \pm \ldots\right)\left(1 + \frac{1}{2}\frac{2k\cos\varphi}{1+k^2} - \frac{1}{8}\frac{(2k\cos\varphi)^2}{(1+k^2)^2} \pm \ldots\right) \qquad (4.16)$$

In the second binomial series representing the second factor in this expression any $\cos\varphi$ term will indicate a spectral line in the spatial frequency domain. This series in the right-hand half of eqn 4.16 has to be expanded to higher order terms in order to make it converge. For cosine terms of an order equal to or higher than 2 equations 4.15 indicate the presence of multiples of the angle in the arguments of the cosine function. These multiples of the angle φ will be found in the binomial series terms of order 2 or higher. This explains the occurrence of other frequency lines in the spatial frequency domain other than those directly related to the angles of arrival of multipath components. This presents an additional problem of accurately identifying those spectral lines to be useful in the determination of the angles of arrival.

In order to find expressions for the individual spectral lines of interest the resulting binomial series has to be searched so that the terms relating to each line can be collected which results in the following equations:

$$D.C.\ term = (1 + \frac{k^2}{2} - \frac{k^4}{8} + \frac{k^6}{16} \pm ...)\,(1 - \frac{\frac{1}{8}(2k\cos\varphi)^2}{(1+k^2)^2} \pm ...) \tag{4.17}$$

The amplitude envelope of a two component multipath is a periodic signal, where the periodicity observed is λ_{eff}. This corresponds with the fundamental spatial frequency at $1/\lambda_{eff}$ its amplitude is given by:

$$amplid._{1/\lambda_{eff}} = (1 + \frac{k^2}{2} - \frac{k^4}{8} + \frac{k^6}{16} \pm ...)\,(\frac{k}{1+k^2} \pm ...) \tag{4.18}$$

The first harmonic of this line at double the spatial frequency ($2/\lambda_{eff}$) can be derived as:

$$amplid._{2/\lambda_{eff}} = (1 + \frac{1}{2}k^2 - \frac{1}{8}k^4 + \frac{1}{16}k^6 \pm ...)\,(\frac{\frac{1}{4}k^2}{(1+k^2)^{2)}} + ...) \tag{4.19}$$

The speed of the convergence of the series depends on the relative amplitude A_1/A_2. If A_2 is relatively small compared to A_1 the series will converge more quickly. Depending on the speed of convergence a sufficient number of terms for each series would have to be considered and the resulting system of equations would have to be solved for A_1/A_2. However a two component multipath can be resolved much more easily without frequency analysis from the spatial domain pattern as shown in section 3.1.1.1. Whereas it is not possible to resolve any multipath geometry resulting from more than two components in the same manner applicable to a 2 component multipath. This means a solution for these cases, $n > 2$, is required. We start by examining the derivation for a three component case which follows.

4.2.2 Three components

In the three component case equation (3.23), (see section 3.1.1.2), can be expressed by a binomial series:

$$V_{R_x} = \sqrt{A_1^2+A_2^2+A_3^3 + 2A_1A_2\cos(\varphi_1 - \varphi_2) + 2A_1A_3\cos(\varphi_1 - \varphi_3) + A_2A_3\cos(\varphi_2 - \varphi_3)} \quad (3.23)$$

The following simplifications were introduced:

$$\varphi_{12} = \varphi_2 - \varphi_1 \quad (4.20)$$

$$\varphi_{13} = \varphi_3 - \varphi_1 \quad (4.21)$$

$$\varphi_{23} = \varphi_3 - \varphi_2 \quad (4.22)$$

$$k_1 = \frac{A_2}{A_1} \quad (4.23)$$

$$k_2 = \frac{A_3}{A_1} \quad (4.24)$$

so that:

$$V_{R_x} = (1 + k_1 + k_2)[1 - \frac{4(k_1 \sin^2(\frac{\varphi_{12}}{2}) + k_2 \sin^2(\frac{\varphi_{13}}{2}) + k_1k_2 \sin^2(\frac{\varphi_{23}}{2})}{(1 + k_1 + k_2)^2}]^{1/2} \quad (4.25)$$

or: $V_{R_x} = (1 + k_1 + k_2)\,[1 - x]^{1/2}$ where:

$$x = [1 - \frac{4(k_1 \sin^2(\frac{\varphi_{12}}{2}) + k_2 \sin^2(\frac{\varphi_{13}}{2}) + k_1k_2 \sin^2(\frac{\varphi_{23}}{2})}{(1 + k_1 + k_2)^2}]^{1/2} \quad (4.26)$$

Again it can be shown, that $x \leq 1$. As such the term $(1 - x)^{1/2}$ can be expanded as a binomial series enabling terms to be collected and assigned to the various spatial frequency components, their harmonics and intermodulation products. The series expansion will in general be tedious revealing relationships between the relative amplitudes of the spatial frequency spectra and their frequencies, which cannot be simply presented. The degree of convergence of the series is a function of the value x. Where this value is less than 0.5 indicating a predominant component relative to the other two, the series converges rather quickly, rendering it sufficient to consider only the first two or three terms. With x increasing towards 1, which corresponds with the three components being comparable in amplitude to

each other, the convergence is slow and many more terms are needed. As an example the DC-term will be obtained from the series of equation 4.25. An expression for this is given in the section below.

$$V_{R_x} = (1 + k_1 + k_2)\,(1 - x)^{1/2}$$

$$= (1 + k_1 + k_2)\,(1 - \frac{1}{2}x + \frac{1}{8}x^2 \pm \ldots)$$

$$= (1 + k_1 + k_2)\,(1 - \frac{1}{2}\,\frac{4(k_1 \sin^2\frac{\varphi_{12}}{2} + k_2 \sin^2\frac{\varphi_{13}}{2} + k_1k_2 \sin^2\frac{\varphi_{23}}{2})}{(1 + k_1 + k_2)^2}$$

$$+\frac{1}{8}\,\frac{16\,(k_1 \sin^2\frac{\varphi_{12}}{2} + k_2 \sin^2\frac{\varphi_{13}}{2} + k_1k_2 \sin^2\frac{\varphi_{23}}{2})^2}{(1 + k_1 + k_2)^4} \pm \ldots) \qquad (4.27)$$

It can be shown that even when the expansion contains only 3 terms, the identification and collection of terms becomes rather complicated.

$$D.C.\ term = (1 + k_1 + k_2)\,(1 - \frac{(k_1 + k_2 + k_1k_2)}{(1 + k_1 + k_2)^2} + \frac{2\,(\frac{3}{8}(k_1^2 + k_2^2 + k_1^2k_2^2)}{(1 + k_1 + k_2)^4} \pm \ldots)$$

$$= (1 + k_1 + k_2)\,(1 - \frac{k_1 + k_2 + k_1k_2}{(1 + k_1 + k_2)^2} + \frac{3\,(k_1^2 + k_2^2 + k_1^2k_2^2)}{4\,(1 + k_1 + k_2)^4} \pm \ldots) \qquad (4.28)$$

The above shows the difficulties in trying to analytically determine the relative amplitudes of various signal components from a knowledge of the envelope of the signal received under multipath conditions. Deriving equations for the other spatial frequency lines in the spectrum will result in equations of even greater complexity. When the amplitudes of all, or some of the, multipath components become comparable, convergence of the series slows down, and

more terms in the series have to be considered, further increasing the complexity of the equations. As in the two component case this system of equations would have to be solved in order to determine the relative amplitudes of the components in the multipath field. Moreover even after obtaining these results the problem of identifying the correct spatial frequency lines for the unknown angles of arrival remains and needs to be resolved.

For multipath geometries arising from two interfering components the spatial frequency lines will be the fundamental, corresponding with the angle of arrival, and a set of harmonics. Here an identification of the relevant lines is feasible. In cases of three and more components however cross terms arise from sum and difference terms of the fundamental component and the various harmonics of each component. Correct identification in an unknown multipath geometry can to be very difficult with this large number of spectral lines. In addition when using the DFT this produces a sampled spatial frequency domain. It will be possible for spatial frequency lines to merge when two (or more) lines fall into one sampling interval and further complicate the correct identification of relevant spatial frequency lines. A solution has to be found that reduces the number of spatial frequency lines not directly related to the angles of arrival of multipath components.

This solution is described in section 4.3.

4.3 Solution by squaring the interference pattern

Section 4.2 indicates the problems faced when trying to solve the result of a Fourier transform of the recorded amplitude envelope in a multipath field for the multipath parameters. The difficulties described are the result of the square root in equations 3.20 and 3.23. The square root is a non-linear process resulting in extra frequency components being introduced in the spatial spectrum. To reverse this non-linearity the square of the envelope will be used in the following for the Fourier transform. It will be shown that this results in a system of relatively simple equations which can be solved for the amplitudes of constituent multipath components. It is also possible to identify spatial frequencies corresponding to the angles of arrival of these components.

Squaring the received amplitude envelope in a two component multipath field results in:

$$V_{R_x}^2 = A_1^2 + A_2^2 + 2A_1A_2\cos(\varphi_1 - \varphi_2) \tag{4.29}$$

with: $$\varphi_r = \frac{2\pi}{\lambda} x \cos\theta_r \tag{3.21}$$

This resulting equation is very similar to the equation describing the light irradiance (intensity) of a holographic image along the photographic plane (Hecht and Zajac, 1974). This is discussed in chapter 2. The light irradiance represents a power density (Poynting vector) of the light, similarly the resulting equation for $V_{R_x}^2$ can be interpreted as Poynting vector at location x of the resulting multipath field.

This function consists of a constant term $(A_1^2 + A_2^2)$ and the cosine term $(2A_1A_2\cos(\varphi_1 - \varphi_2))$. With the substitution:

$$c = \frac{1}{\lambda_{eff}} = \frac{1}{\lambda}(\cos\theta_1 - \cos\theta_2) \tag{4.30}$$

it can be written as:

$$V_{R_x}^2 = A_1^2 + A_2^2 + 2A_1A_2\cos(2\pi xc) \tag{4.31}$$

This resembles a finite Fourier series with a DC-coefficient and a cosine function (one spectral line). Solving the Fourier integral of this function should result in a DC-component and one spectral line:

With the Dirac-pulse:

$$\delta(f) = \int_{-\infty}^{\infty} e^{-j2\pi fx} dx \tag{4.32}$$

the resulting spatial frequency domain function H(f) is:

$$H(f) = (A_1^2 + A_2^2)\,\delta(f) + A_1A_2\,\delta(f - c) + A_1A_2\,\delta(f + c) \tag{4.33}$$

This equation is the representation of three Dirac pulses at DC and frequencies + and - c, which represents the Fourier transform of a sinusoid plus DC - value (Brigham, 1988).
It can be expanded to three and more components, the calculation of the Fourier integral will be carried out for the three component case here as an example.

For $n = 3$ (three components) the square of the amplitude envelope is described by:

$$V_{R_x}^2 = A_1^2 + A_2^2 + A_3^2 + 2A_1A_2\cos(\varphi_1 - \varphi_2) + 2A_1A_3\cos(\varphi_1 - \varphi_3) + 2A_2A_3\cos(\varphi_2 - \varphi_3) \quad (4.34)$$

with: $$\varphi_r = \frac{2\pi}{\lambda} x \cos\theta_r \quad (3.21)$$

This expression contains a constant term $A_1^2 + A_2^2 + A_{3_2}$ and three cosine functions. A similar substitution to the one in the two component case can be made, i.e.:

$$c_{ij} = \frac{1}{\lambda}(\cos\theta_i - \cos\theta_j) \quad (4.35)$$

The Fourier transform of eqn 4.34 is calculated by the Fourier integral where the function in the spatial domain (h(x)) can be written as:

$$h(x) = A_1^2 + A_2^2 + A_3^2 + 2A_1A_2\cos(2\pi x c_{12}) + 2A_1A_3\cos(2\pi x c_{13}) + 2A_2A_3\cos(2\pi x c_{23}) \quad (4.36)$$

The Fourier integral is equation 4.5 with h(x) being equation 4.36.
Substituting :

$$\cos(2\pi x c_{ij}) = \frac{e^{j2\pi x c_{ij}} + e^{-j2\pi x c_{ij}}}{2} \quad (4.37)$$

Leads to:

$$H(f) = \int_{-\infty}^{\infty} (A_1^2 + A_2^2 + A_3^2 + 2A_1A_2\left(\frac{e^{j2\pi x c_{12}} + e^{-j2\pi x c_{12}}}{2}\right) + 2A_1A_3\left(\frac{e^{j2\pi x c_{13}} + e^{-j2\pi x c_{13}}}{2}\right)$$

$$+ 2A_2A_3\left(\frac{e^{j2\pi x c_{23}} + e^{-j2\pi x c_{23}}}{2}\right)) e^{-j2\pi f x}\, dx \quad (4.38)$$

$$= (A_1^2 + A_2^2 + A_3^3) \int_{-\infty}^{\infty} e^{-j2\pi fx}\, dx + A_1A_2 \int_{-\infty}^{\infty} (e^{-j2\pi x(f-c_{12})} + e^{-j2\pi x(f+c_{12})})\, dx$$

$$+ A_1A_3 \int_{-\infty}^{\infty} (e^{-j2\pi x(f-c_{13})} + e^{-j2\pi x(f+c_{13})})\, dx$$

$$+ A_2A_3 \int_{-\infty}^{\infty} (e^{-j2\pi x(f-c_{23})} + e^{-j2\pi x(f+c_{23})})\, dx \qquad (4.39)$$

Using the Dirac-pulse 4.32 the result in the spatial frequency domain is:

$$H(f) = (A_1^2 + A_2^2 + A_3^2)\, \delta(f) + A_1A_2\, (\delta(f-c_{12}) + \delta(f+c_{12}))$$
$$+ A_1A_3\, (\delta(f-c_{13}) + \delta(f+c_{13})) + A_2A_3\, (\delta(f-c_{23}) + \delta(f+c_{23})) \qquad (4.40)$$

Equation 4.40 represents the spectrum of the square of the recorded amplitude envelope in a multipath field where the receiving antenna is displaced along the direction of propagation of component 1.

The spectrum consists of both positive and negative frequencies, as generally found with the Fourier transform (Brigham,1988). The resulting spectrum shows a DC-component and three spectral lines in each of the positive and negative frequency ranges. Since the spectrum is even function the true value of the spectral line amplitudes is double the magnitude read in either the positive or negative frequencies. The DC is only represented once, which means its amplitude does not need to be multiplied.

Since the receiving antenna is moved along the direction of propagation of one of the multipath components two of the three non DC lines relate to the angles of arrival by equation 4.4. The third is a difference term resulting from $\cos(\varphi_2 - \varphi_3)$ in equation 4.34. The amplitude values of the spectral lines result in a system of equations which can be used to determine the unknown amplitudes of the signal components composing the multipath:

D.C. term value : $Val_{DC} = A_1^2 + A_2^2 + A_3^2$ (4.37)

value of spec. line at f_{sp12} : $Val_{12} = 2A_1A_2$ (4.38)

value of spec. line at f_{sp23} : $Val_{23} = 2A_2A_3$ (4.39)

value of spec. line at f_{sp13} : $Val_{13} = 2A_1A_3$ (4.40)

This gives four equations which may be used to calculate the three wanted values A_1, A_2 and A_3. One of the former equations is not independent.

The calculation of the constituent components' magnitudes in the three component case now involves much simpler equations than having to solve infinitely long binomial series expressions encountered in the case of the unsquared time domain signal:

$$A_1 = [\frac{Val_{DC}}{2} + \frac{\sqrt{Val_{DC}^2 - Val_{12}^2 - Val_{13}^2}}{2}]^{1/2} \quad (4.41)$$

$$A_2 = \frac{Val_{12}}{2A_1} \quad (4.42)$$

$$A_3 = \frac{Val_{13}}{2A_1} \quad (4.43)$$

For a two component case these equations are even simpler, according to eqn. 4.30, there are only two lines in the spatial frequency domain, a DC-level and a line at one frequency. Hence:

$$Val_{DC} = A_1^2 + A_2^2 \quad (4.44)$$

$$val_{12} = 2A_1A_2 \quad (4.45)$$

Which leads to:

$$A_1 = [\frac{Val_{DC}}{2} + \frac{\sqrt{Val_{DC}^2 - Val_{12}^2}}{2}]^{1/2} \quad (4.46)$$

$$A_2 = \frac{Val_{12}}{2A_1} \tag{4.47}$$

These results are illustrated in the graphs of simulated squared amplitude envelopes and their DFTs in the following section.

4.3.1 Simulated examples using the squared interference pattern

The same examples of amplitude envelopes in multipath geometries, that were shown in section 4.1 will be presented again here for reasons of comparison. In this section part (a) of figures 4.5 to 4.8 shows a simulation of the square of the amplitude envelope for the multipath geometries described by their characteristics given in the figure subtitles. Part (b) of each figure shows the corresponding DFT of the squared amplitude envelope.

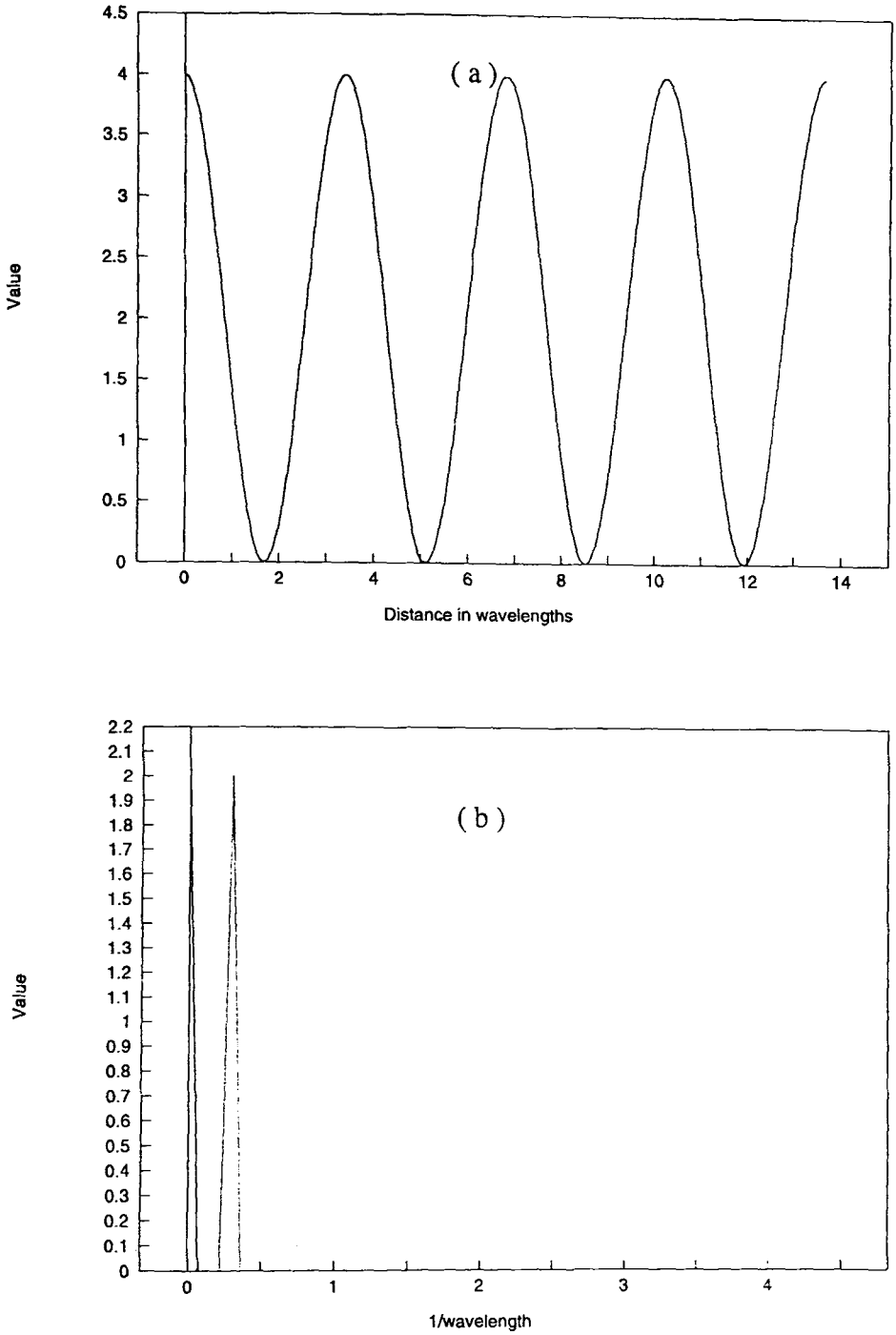

Figure 4.5 *Simulated square of amplitude envelope (a) and its DFT (b) for a multipath of 2 components:* $A_1 = 1.0, A_2 = 1.0;$ $\theta_1 = 0^\circ, \theta_2 = 45^\circ$

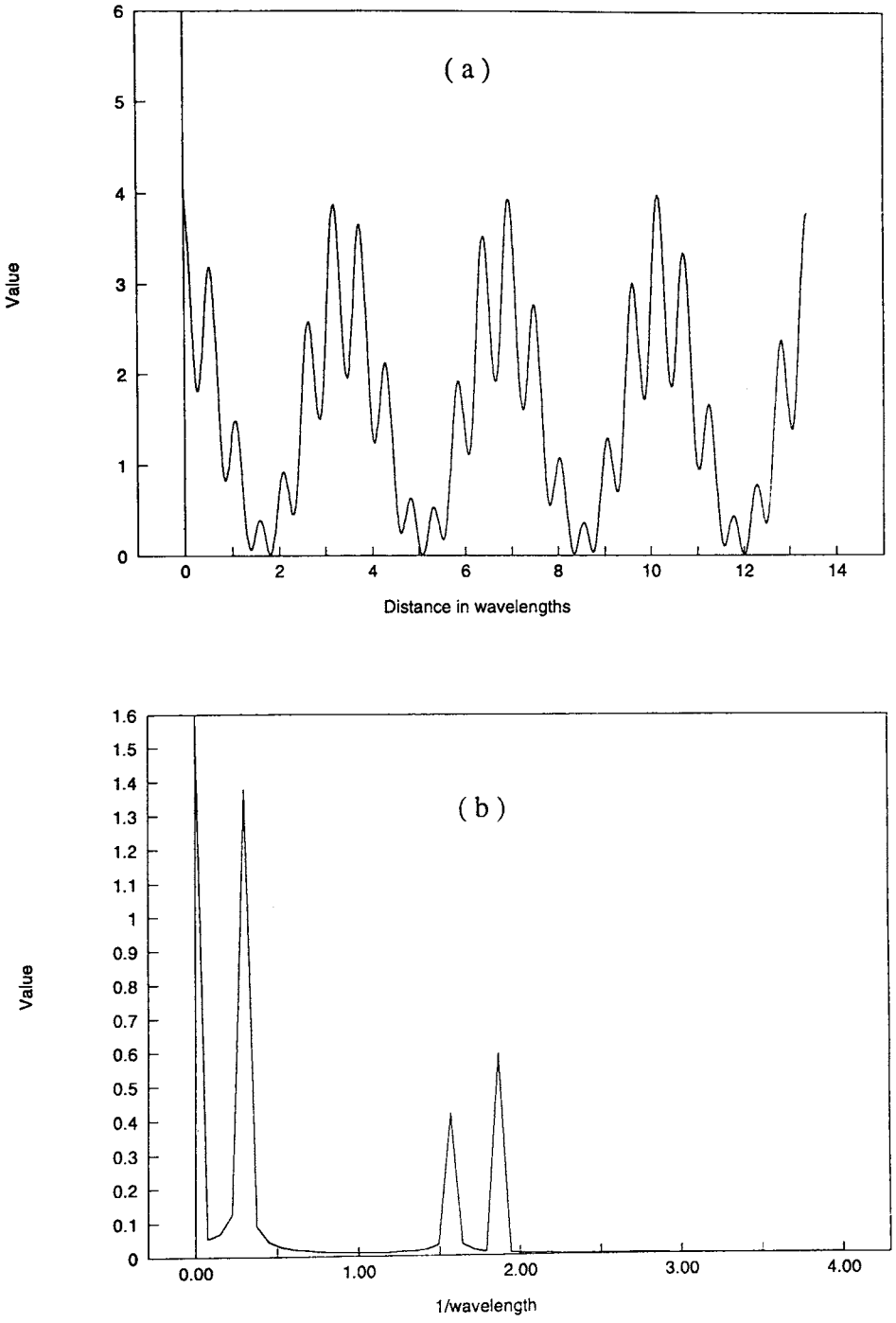

Figure 4.6 *Simulated square of amplitude envelope (a) and its DFT (b) for a multipath of 3 components:* $A_1 = 1.0, A_2 = 0.7, A_3 = 0.3;$ $\theta_1 = 0°, \theta_2 = 45°, \theta_3 = 150°$

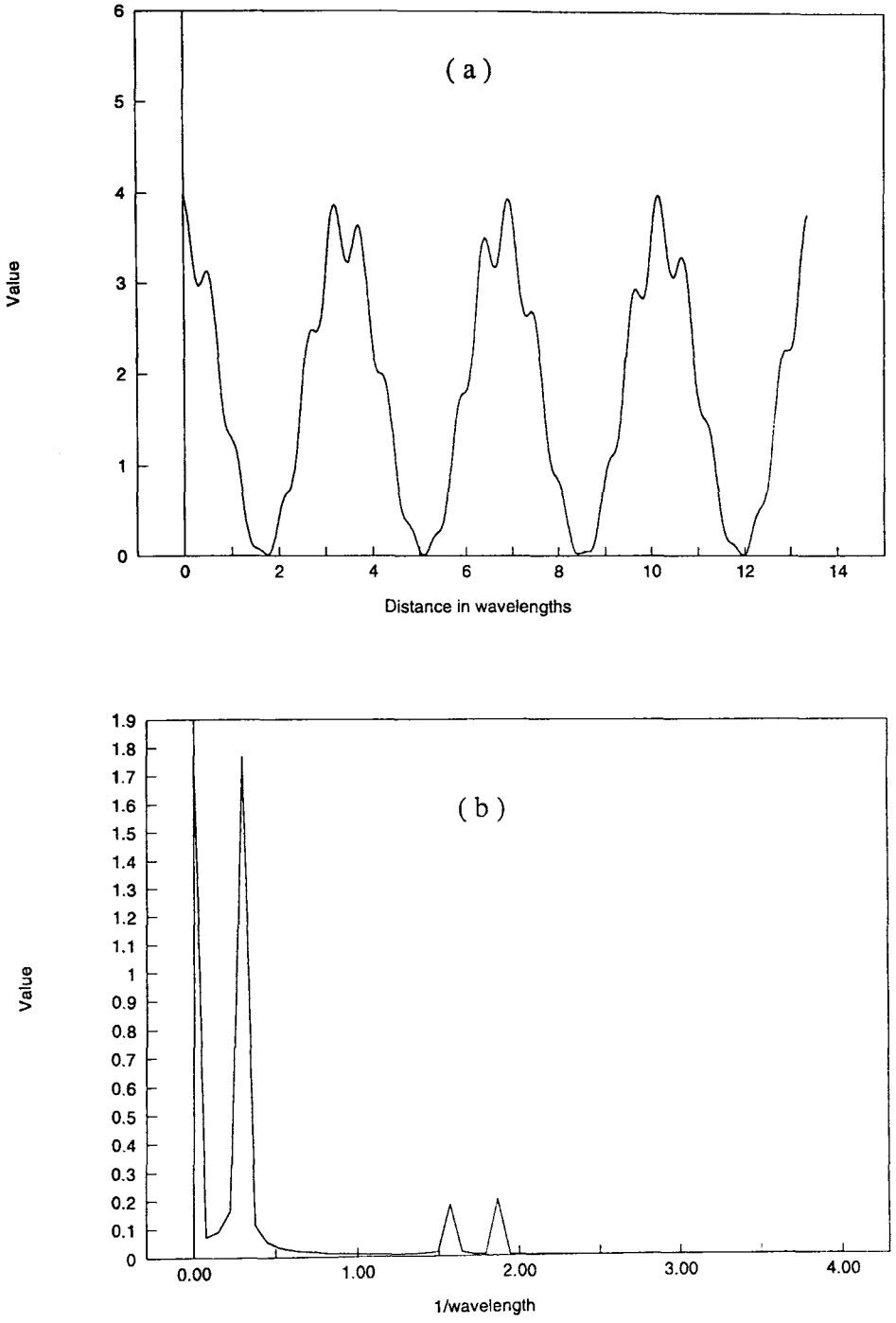

Figure 4.7 *Simulated square of amplitude envelope (a) and its DFT (b) for a multipath of 3 components:* $A_1 = 1.0, A_2 = 0.9, A_3 = 0.1;$ $\theta_1 = 0^\circ, \theta_2 = 45^\circ, \theta_3 = 150^\circ$

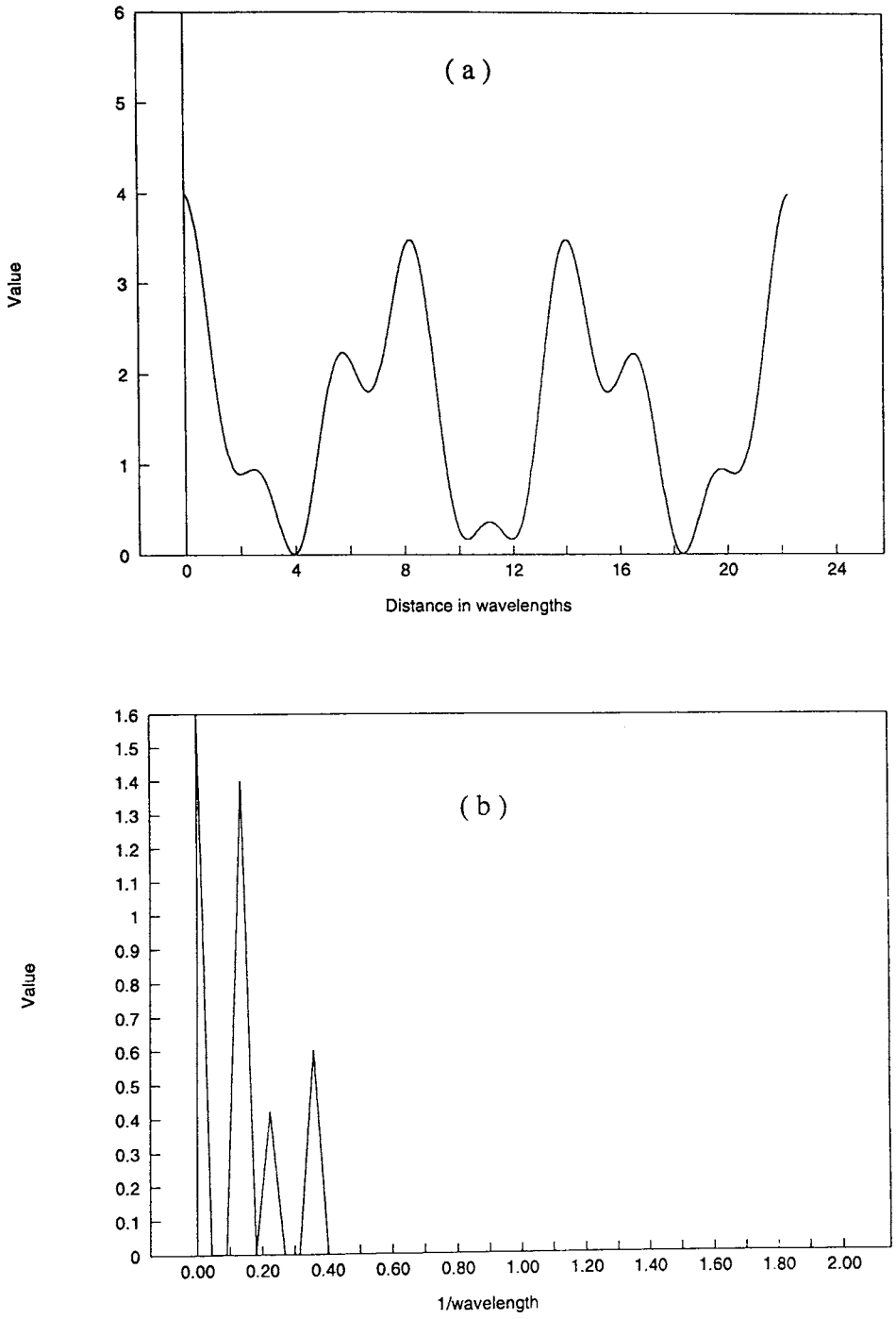

Figure 4.8 *Simulated square of amplitude envelope (a) and its DFT (b) for a multipath of 3 components:* $A_1 = 1.0, A_2 = 0.7, A_3 = 0.3;$ $\theta_1 = 0°, \theta_2 = 30°, \theta_3 = 50°$

The DFTs in the above examples can be used to derive the describing multipath parameters for unknown multipath geometries, i.e. component amplitudes and angles of arrival. The chosen component amplitude values in the above simulation can be used to calculate the expected spectral line amplitudes using eqns 4.37 to 4.40. These amplitudes are summarized in table 6.2. Comparing these spectral line calculated amplitudes with the graphs of the DFTs in figures 4.5 to 4.8 (b) shows that the DFT results in spectral lines of the expected magnitude and equations 4.41 to 4.43 can be used to determine the amplitudes of the multipath components.

	Amplitudes of the spectral lines at spatial frequencies:			
	DC	f_{sp12}	f_{sp23}	f_{sp13}
	Val_{DC}	Val_{12}	Val_{23}	Val_{13}
Figure 4.6	2.0	2.0	---	---
Figure 4.7 & 4.9	1.58	1.4	0.42	0.6
Figure 4.8	1.82	1.8	0.18	0.2

Table 6.2 *Amplitudes of spatial frequency lines in spatial spectra of squared simulated amplitude envelope*

These examples also show that the spatial frequencies at which the lines are found in the spatial frequency domain can be used to determine the angles of arrival.

4.3.2 Identification of the spectral line(s) corresponding with difference term

In the three component cases (fig. 4.6 to 4.8) a fourth line is evident in the spectrum. This line is due to the difference term $\cos\varphi_2 - \cos\varphi_3$ in the equation for the square of the amplitude envelope (4.34). The equation to relate this spectral line f_{sp23} to the angles of arrival is:

$$f_{sp23} = |\cos\theta_3 - \cos\theta_2| \tag{4.48}$$

Using equations 4.1 and 4.2 shows that f_{sp23} is the result of $f_{sp13} - f_{sp12}$, which is also evident in figures 4.6 to 4.8. The spectral line resulting from the difference term of the cosine of the two angles of arrival can be distinguished from the lines directly related to the angles of arrival by calculating the difference in frequency between the other two lines. If a line exists at a spatial frequency that is the result of the difference between two other spatial frequencies, then this line can be identified as the difference term, not directly related to the angles of arrival.

For any multipath geometry consisting of more than three components expanding equation 4.34 will lead to an additional cosine term directly related to any addition angle of arrival of the geometry. Additional difference terms will also be found. The number of cosine terms k_{cos} depending on the number of multipath components n can be calculated as (see section 3.1.1.2):

$$k_{cos} = \sum_{i=1}^{n} i - 1 \tag{4.49}$$

The criterion to distinguish the difference terms from terms directly related to angles of arrival is the same as in the three component case, any spatial frequency that is the result of the difference of any two others indicates a difference term.

4.4 Summary and interim conclusion of chapter 4

It can be shown that the quasi-periodicity of a recorded amplitude envelope in a multipath situation leads to a spatial spectrum, which contains useful information about the multipath components. With the amplitude envelope being recorded over distance by displacing the receiver antenna, the transform of this spatial interference pattern leads to a spectrum of spatial frequencies. The Fourier transform of the envelope function yields a spectrum which contains a large number of spatial frequency components. There are spatial frequency lines in the spectrum related to the angles of arrival of the multipath components. But the large number of spurious components will make correct identification of theses lines very difficult for unknown multipath geometries arising in practice.

The large number of spurious spatial frequency components is caused by the non-linear characterisation of the square root function arising in the equation for the amplitude envelope. Squaring the recorded envelope recorded in a multipath field removes this non-linearity and yields data whose DFT results in a spectrum with only a small number of spectral lines. The magnitude of these lines and the spatial frequencies at which they arise can be used to establish the amplitude and angles of arrival of the signal components giving rise to the multipath field. Although in situations where the multipath field results from the interaction of more than two signal components a small number of difference terms are found in the spectrum, these can be identified. The experimental programme, detailed in chapters 6 with results in chapter 7, showed that multipath geometries in the outdoor environment will rarely arise from more than of 4 significant components. In the case of a four component multipath the spectrum of the square of the amplitude envelope will show 7 spatial frequency lines, three of which are difference terms. These can easily be distinguished from spatial frequencies lines relating to angles of arrival since their spatial frequencies result from the frequency differences related to the four components.

Chapter 5 describes a procedure developed that resolves multipath components in amplitude and angle of arrival from recorded amplitude envelopes using the discrete Fourier transform (DFT).

CHAPTER 5 DEVELOPMENT OF RESOLUTION PROCEDURE USING DFT

This chapter describes the development of the computer procedure to resolve constituent multipath component from a recorded amplitude envelope. The general principle of utilizing the Fourier transform for the purpose of component resolution is described in chapter 4. This section concentrates on the Discrete Fourier transform (DFT) and its properties as well as shortcomings. The developed procedure applies the DFT to the recorded interference pattern in a multipath situation. The interference pattern or amplitude envelope is obtained by displacing the receiver antenna in small increments over a distance of a few wavelengths. This results in a record represented as a set of amplitude samples spaced regularly by appropriately small distance displacements. The DFT can in many cases give different results to those obtained by applying the Fourier transform using the Fourier integral, which Brigham (1988) calls the continuous Fourier transform. The differences on the one hand arise from the fact that the DFT is applied to sampled signals as input and also produces a spectrum consisting of sample values. Secondly in Fourier transform analysis the signal is generally assumed to be of infinite length, which is not the case for sampled data records. The most important problem in the context of component resolution was found to be related to the spectral leakage associated with the DFT. This is analyzed in the next section.

5.1 Spectral leakage using DFT

The DFT is applied to sampled signals of finite lengths with N being the number of samples of that record. The Fourier integral (eqn. 4.5) in the case of the DFT is represented by series of N terms. The sampled time domain function with sampling interval Δt is represented by a series of values $x(k\Delta t)$. The sampled frequency domain function is a series of values $C(n\Delta f)$ where Δf is the sampling interval in the frequency domain. The DFT is defined as (Jones and Watson, 1990):

$$C(n) = \sum_{k=0}^{N-1} x(k)\, e^{-j\frac{2\pi nk}{N}} \qquad with \quad n = 0, 1, 2, \ldots, N-1 \tag{5.1}$$

This indicates a time limited (truncated) signal in the time domain where the truncation interval or window is of the duration of the record length N.
Spectral leakage arises in the spectrum of the DFT when the cycle length of a signal is not equal to an integer fraction of the record length (Brigham, 1988; Harris, 1978).

Brigham explains spectral leakage by graphically developing the DFT. He compares two examples, in the first one the period of the signal coincides with the truncation interval in the time domain, prior to the DFT. In the second example signal period and truncation interval do not coincide. This development is shown in figures 5.1 to 5.4. Figure 5.1 shows the graphical development of the DFT of a cosine function with period T_0 coinciding with the truncation interval T_0. Figure 5.4 shows the same development for a cosine function of period T_1 which is different from the truncation interval T_0. The time domain is shown on the left hand side of figures 5.1 and 5.4 and the frequency domain in the right hand one. Brigham uses a double lined hexagon to indicate Fourier transform from functions on the left to those on the right. He also indicates convolution by the asterisk *.
In the two figures 5.1 and 5.4 the cosine function h(t) and its transform H(f) are shown in fig.(a). The sampling function $\Delta_0(t)$ and its transform follow in fig.(b). Multiplication of the two in the time domain leads to convolution of their transforms in the frequency domain fig.(c). The time domain window x(t) and its transform X(f) are shown in fig.(d). Applying the window leads to a truncated record of the sampled signal with N samples fig.(e) and the resulting frequency domain is the convolution of the transforms of all the multiplied functions. Multiplication in one domain is equivalent to convolution in the other. The same applies when the sampling function in the frequency domain is introduced fig.(f), a train of dirac pulses with spacing $1/T_0$. Since the Fourier transform transforms signals in the same way from one domain to the other this train of pulses has a representation in the time domain also shown in fig.(f). Multiplication of the sampling function with the signal so far fig.(e) in the frequency domain leads to the result of the DFT shown in fig.(g). The bidirectional nature of the Fourier transform between domains leads to the result in the time domain also shown in fig.(g). It is the result of the convolution of the truncated record in fig.(e) with the transform of the frequency domain sampling function fig.(f). This convolution leads to a repetition of

the truncated signal at $-T_0$ and T_0. Comparing figures 5.1 and 5.2 shows that when the truncation interval and the signal period do not coincide a discontinuity arises at the point of repetition in the time domain, which indicates the presence of additional frequencies in the spectrum.

Figures 5.2 and 5.3 show expanded views of the frequency domain in figures 5.1(e) and 5.4(e). They show the sinc function that results from the convolution of the transform, the sampled cosine function fig.(c) and transform of the rectangular truncation interval (d) in the frequency domain. The resulting sinc function is sampled with the frequency domain sampling function $\Delta_1(f)$ in both cases. In the case of the truncation interval and the signal period coinciding the sinc function is sampled once at its peak value. All other sampling points in the frequency domain fall into the zeros of the sinc function (figure 5.2). On the other hand as shown in figure 5.3, when the truncation interval is not equal to the signal period the sinc function in the frequency domain is sampled at different locations. It is not sampled at its peak any more and further spectral contributions are found at other frequencies. This leads to the familiar lowering of the amplitude of that spectral line and the widening near the frequency axis where leakage occurs.

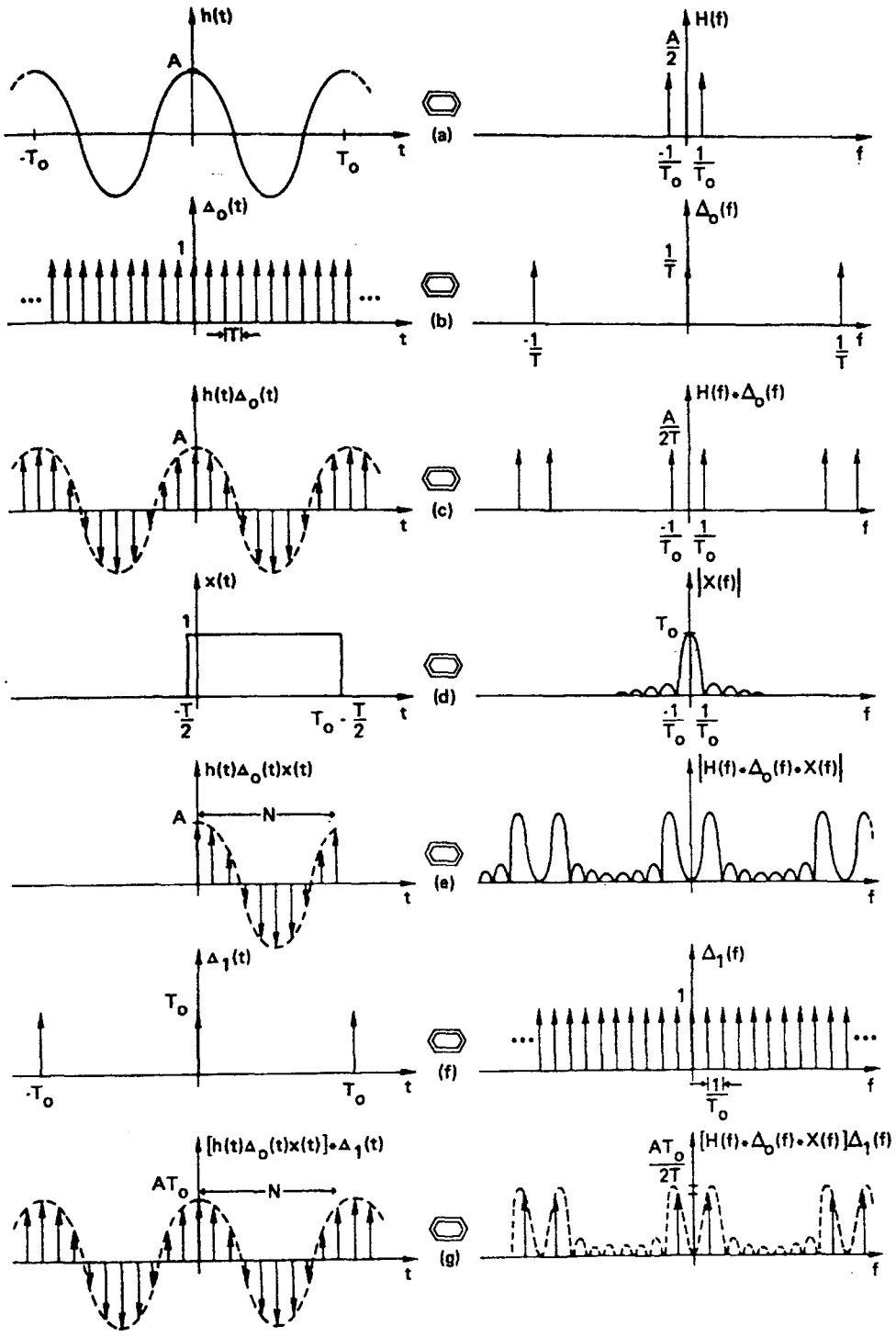

Figure 5.1 *Graphical development of DFT of a time limited sampled function, period equal to truncation interval (Brigham, 1988)*

Fourier transform is indicated by: ⟺

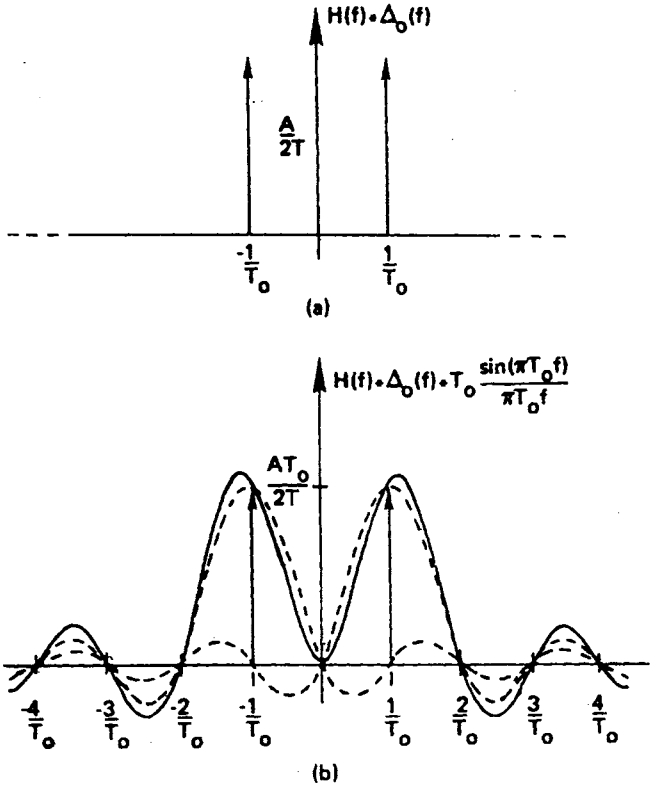

Figure 5.2 *Expanded view of figure 5.1(g) (Brigham 1988)*

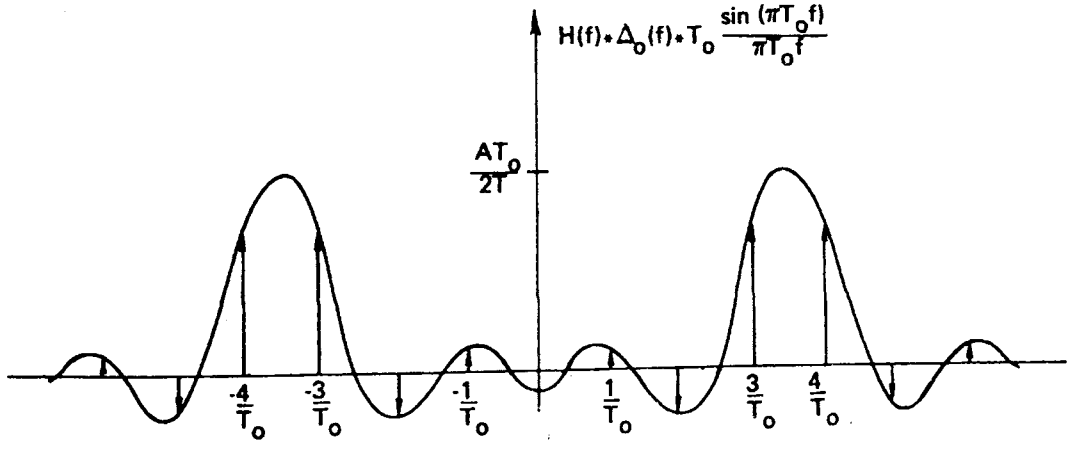

Figure 5.3 *Expanded view of figure 5.4(g) (Brigham, 1988)*

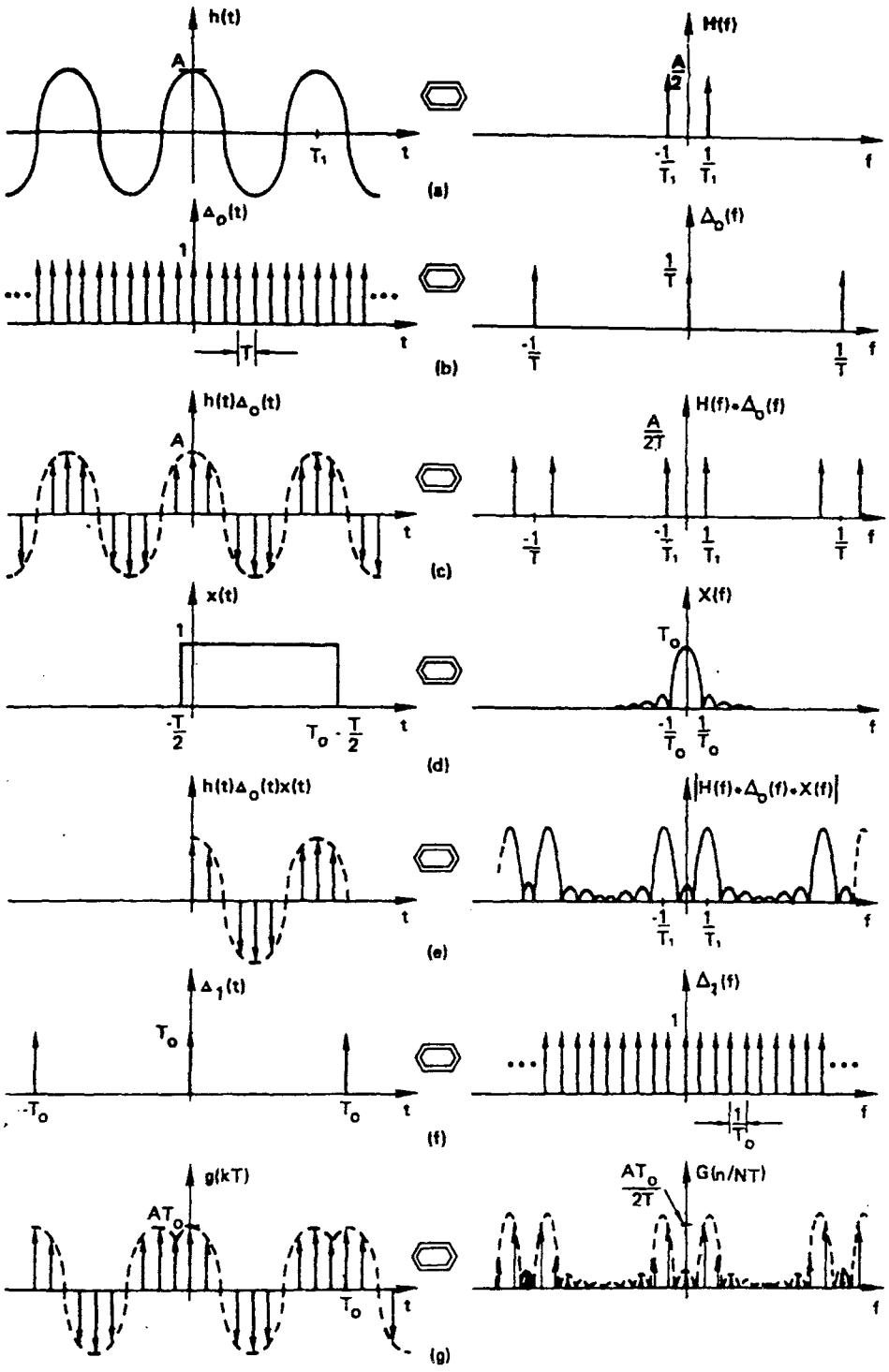

Figure 5.4 *Graphical development of DFT of a time limited sampled function, period not equal to truncation interval (Brigham, 1988)*

Fourier transform is indicated by: ⟺

5.1.1 Significance of leakage errors for component resolution procedure

Spectral leakage will arise using the DFT when the record length or truncation interval of the sampled signal is not equal to an integer multiple of its period (section 5.1). In an unknown multipath environment the signal components leading to the multipath field arrive at arbitrary and unknown angles of arrival at the receiving antenna. Furthermore it is unlikely that their is any relationship between the different angles of arrival. Therefore the spectrum of the recorded amplitude envelope must be considered to have spatial frequency values, depending on the angles of arrival, which are equally likely to arise at arbitrary spatial frequency values. This means harmonic relationships where spatial frequencies are integer multiples of each other cannot be assumed. Consequently it is not possible to choose a truncation interval in the spatial domain of a length that would be an integer multiple of all signal periods of signal components present in the interference pattern. Thus spectral leakage will arise in the spatial frequency domain thus distorting the resulting spectral lines.

An illustration of the leakage problem when applying the DFT to a multipath interference pattern is given in figures 5.5 and 5.6. These two figures show two spatial frequency domain plots for the same multipath geometry. The multipath is modelled as a three component case with the following parameters of its components: $A_1 = 1$; $\theta_1 = 0°$; $A_2 = 0.7$; $\theta_2 = 45°$; $A_3 = 0.3$; $\theta_3 = 150°$. The two figures 5.5 and 5.6 show the result of two DFTs applied to the square of the simulated amplitude envelope. The difference in generating the two graphs is the length of the truncation interval in the spatial domain. In the first case the truncation interval prior to the DFT is an integer multiple of λ_{eff} (figure 5.5), whereas in the second case the truncation interval was equal to an integer multiple of λ_{loc} (figure 5.6). λ_{eff} and λ_{loc} are explained in section 3.1.3. The relations between the spatial frequencies and the angles of arrival are given in section 4.3.

Comparing the two graphs the influence of the different truncation interval length is evident. Figure 5.5 shows a spreading out of the highest spatial frequency and reduced amplitude values, whereas the lower spatial frequency is represented correctly. The reverse is true in

figure 5.6. This shows that measures to minimize the errors caused by spectral leakage are necessary.

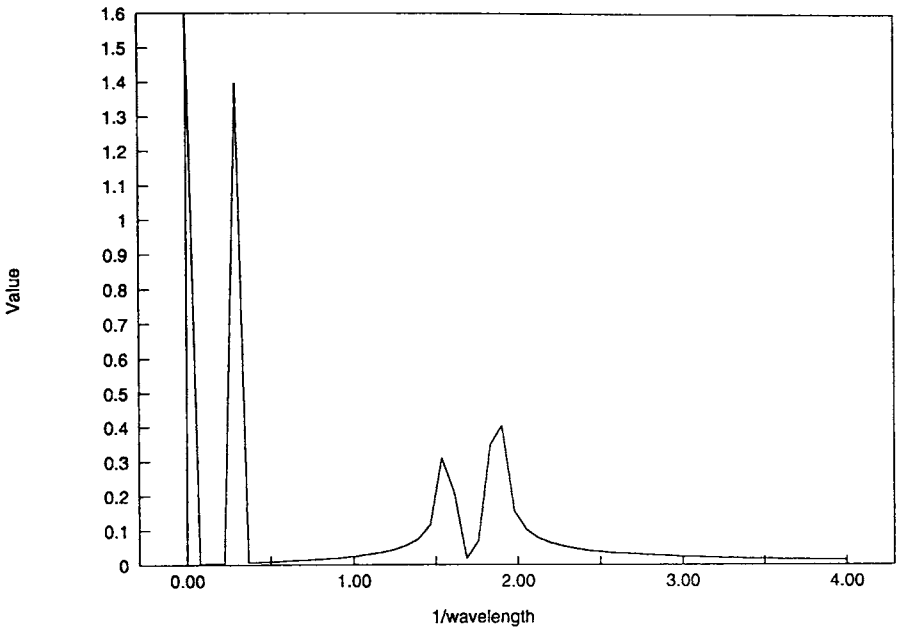

Figure 5.5 *Fourier transform of 3 component squared envelop, truncation interval equal to period of lower spatial frequency (f_{sp12})*

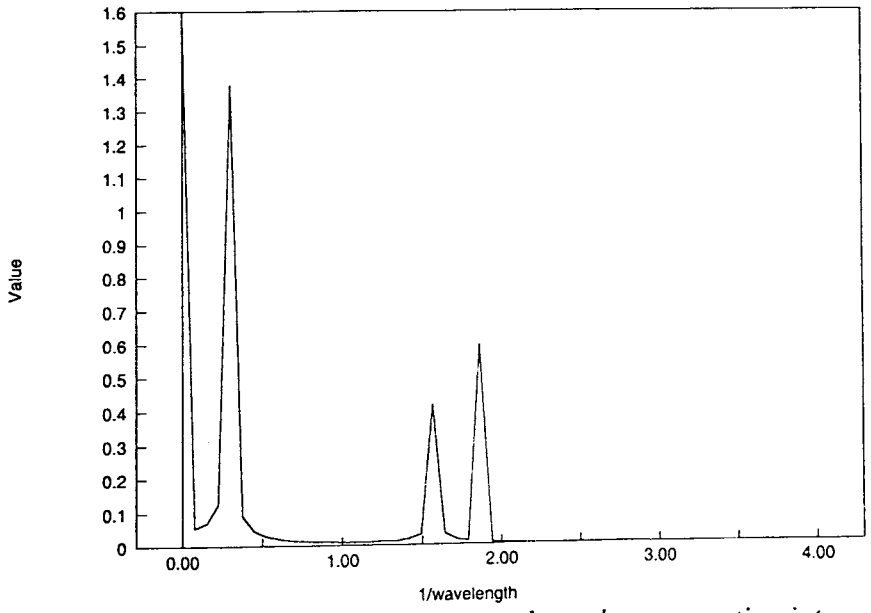

Figure 5.6 *Fourier transform of 3 component squared envelop, truncation interval equal to period of higher spatial frequency (f_{sp13})*

5.2 Minimisation of errors due to spectral leakage

5.2.1 Error minimisation using windowing functions prior to DFT

Commonly a reduction of errors due to possible spectral leakage is achieved by multiplying the signal with a window function. The window function adds weights to the set of sampled data points prior to the DFT (Bergland, 1969; Brigham 1988). Common to all the windowing functions used is that they weight sample points in the middle of a data set by 1, whereas amplitudes slope off towards the first and last samples in each record. Multiplying the data samples with such a function will reduce the observed discontinuities describe in section 5.1 by forcing the sample magnitudes at either end of the record to be of similar value. Therefore the occurrence of additional frequency components in the spectrum is reduced in cases where the signal period is not an integer multiple of the truncation interval of the record.

A rectangular window, a truncation of the record without adding weights, leads to a convolution of the spectrum with a sinc function. In section 5.1 it was shown that the errors due to leakage arise in the spectrum when the sample points in the spectrum fall into the side lobes and the lower parts of the main lobe of the sinc function (Figure 5.4). The windowing functions often resemble a bell shape (Brigham 1988; Harris, 1978). The are designed so that their transforms will have much lower side lobes than the sinc function and a wider main lobe. The aim is that for non integer multiples between truncation interval and signal period the side lobe contribution are suppressed, whereas it is desirable that the spectral sample point within the main lobe remains of the same level.

The method of using window functions has two drawbacks:

a) The resolution in the spectrum is reduced, since several spectral lines falling into the main lobe can not be distinguished and
b) The overall signal content is reduced by attenuating the amplitudes of number of data points in the original signal. This attenuation has to be compensated for in the spectrum to achieve correct amplitude values of the spectral lines.

Error reduction using data windowing is well documented in the literature (Markel, 1971; Eberhard, 1973; Babic and Temes, 1976; Harris, 1978). Many different windows exist for many different applications (Thomson, Robbins et al, 1976; Harris, 1978; Webster, 1980; Nuttal 1981; Kwong and Kim, 1995), see also appendix.

With the aid of the computer simulation described in section 3.1.2 different interference patterns for different multipath geometries were utilized. They provided input data to test how well given geometries could be resolved from the spectra resulting from the application of the DFT after different windows were utilized. One window producing the best results was found to be the Kaiser-Bessel window (see appendix) discussed by Harris (1978).

Typical results for the resolution of multipath components that can be achieved in this way are listed in tables 5.1 and 5.2. The left hand half of these tables lists the multipath parameters as component amplitudes (A_1, A_2, A_3) and their angles of arrival (θ_2, θ_3). θ_1 is chosen 0 in both cases. **Bold** figures represent the values assumed by the simulation whereas figures in normal print are values resolved from spectrum resulting from the DFT with prior application of the Kaiser-Bessel window. The right hand half of the tables list values in the spectrum itself. Using eqns. 4.1, 4.2, 4.37, 4.38, 4.40 spatial frequencies (f_{sp12} and f_{sp13}) and spectral line amplitudes (Val_{DC}, Val_{12}, Val_{13}) can be derived that represent the aforementioned multipath parameters in a spectrum not distorted by leakage. These figures are shown in **bold** to enable the assessment of the accuracy of spectral lines determined as a result of applying the DFT with Kaiser-Bessel window.

Simulated geometry	Resolved parameters	Error	Theoretical spectral values	Values result. from DFT.	Error
$A_1 = 1.0$	1.055	5.5 %	**$Val_{DC} = 1.58$**	1.576	-0.27 %
$A_2 = 0.7$	0.625	-11 %	**$Val_{12} = 1.4$**	1.320	-5.7 %
$A_3 = 0.3$	0.267	-11 %	**$Val_{13} = 0.6$**	0.563	-6.1 %
$\theta_2 = 45°$	43.4°	-3.6 %	**$f_{sp12} = 0.2929$**	0.273	-6.6 %
$\theta_3 = 150°$	147.8°	-1.5 %	**$f_{sp13} = 1.866$**	1.846	-1.1 %

Table 5.1 *Accuracy of component parameters resolved (DFT with Kaiser-Bessel window)*

Simulated geometry	Resolved parameters	Error	Theoretical spectral values	Values result. from DFT	Error
$A_1 = 1.0$	1.102	10 %	**$Val_{DC} = 1.82$**	1.815	-0.28 %
$A_2 = 0.9$	0.770	-14 %	**$Val_{12} = 1.8$**	1.697	-5.7 %
$A_3 = 0.1$	0.085	-15 %	**$Val_{13} = 0.2$**	0.187	-6.5 %
$\theta_2 = 45°$	43.4°	-3.6 %	**$f_{sp12} = 0.2929$**	0.273	-6.6 %
$\theta_3 = 150°$	147.8°	-1.5 %	**$f_{sp13} = 1.866$**	1.846	-1.1 %

Table 5.2 *As table 5.1 with different amplitude values*

Tables 5.1 and 5.2 compare the theoretical values for the amplitudes of the spatial frequency lines for the given multipath geometries with those found in the DFT spectra. It shows that using the Kaiser-Bessel window an accuracy in the order of ± 6 % can be achieved. This represents a great improvement over the use of a rectangular window, where as documented in literature (Brigham, 1988) and also illustrated in figure 5.7 spectral amplitudes can fall as low 60 % of the true value. However the multipath component amplitudes and angles of arrival have to be calculated from these values using the equations derived in sections 4.1 and 4.3:

$$\theta_1 = 0° \text{ (by choice)}, \quad \theta_2 = arcos\,(1 - f_{sp12}),\ \theta_3 = arcos\,(1 - f_{sp13}) \tag{4.3}$$

$$A_1 = [\frac{Val_{DC}}{2} + \frac{\sqrt{Val_{DC}^2 - Val_{12}^2 - Val_{13}^2}}{2}]^{1/2} \tag{4.41}$$

$$A_2 = \frac{Val_{12}}{2A_1} \tag{4.42}$$

$$A_3 = \frac{Val_{13}}{2A_1} \tag{4.43}$$

Tables 5.1 and 5.2 show that the multipath component amplitudes in these examples are resolved only with ± 15 % accuracy, due to error accumulation when using eqns. 4.41 to 4.43. This was found to be a typical error using the Kaiser-Bessel window other windows produced either similar or worse results. Were this method to be applied to measured interference pattern the measurement errors would add to these methodical ones and increase the inaccuracy even further. The accuracy that can be achieved in this was felt to be insufficient so that a different method was developed which is described in section 5.2.2.

5.2.2 Leakage error reduction using an adaptive window size

The leakage problem arises whenever the length of the truncation interval of the record for the DFT is not equal to an integer multiple of the period of the signal component in question (Brigham 1988). In the case of a multipath amplitude envelope the expected spatial frequencies will generally not be integer multiples of each other, so that it will be impossible to choose a truncation interval to suit all spatial frequencies. The classic approach of applying a window function prior to the DFT was found to be too inaccurate to achieve reliable results.

Digital computers are now able to perform a succession of DFTs in very short time. The approach chosen is therefore one whereby starting with the full set of the sampled data record its length is reduced by one point at the time and a DFT is applied every time. The resulting spectral lines are stored in a array of both spatial frequency and magnitude of each line after each DFT. As the record of the amplitude envelope gets gradually reduced in length for different spectral lines there will be record lengths matching an integer multiple of the corresponding signal period for this particular spatial frequency. The amplitude of this frequency is expected to reach a maximum in this case. The array of amplitude values obtained for each record length for each spectral line will have to searched for the maximum value. This would then represent the correct amplitude of this spectral line. The change of amplitude of the spectral lines with varying record length (or window size) is demonstrated in figure 5.7. It shows amplitude variation of the four resulting spectral lines in the spectrum of the square of the simulated amplitude envelope of a three component multipath. The simulated geometry is: $A_1 = 1.0$, $\theta_1 = 0°$, $A_2 = 0.7$, $\theta_2 = 45°$ and $A_3 = 0.3$, $\theta_3 = 150°$.

The spectrum resulting from the DFT of the square of an interference pattern shows the following four lines (see section 4.3): Val_{DC} at spatial frequency 0, Val_{12} at frequency f_{sp12}, Val_{13} at frequency f_{sp13}, and the difference term Val_{23} at frequency f_{sp23}. The graph shows the amplitudes of these lines changing with the length of the window. The full length of the simulated record was 512 sample points and was gradually reduced to 240 points plotted on the abscissa of figure 5.7. The variation of amplitude for each line is evident. There are only small amplitude variations in the DC component, because the overall nature of the

interference pattern is not changed when varying the record length. The amplitude of each spatial frequency line (Val_{12} to Val_{23}) varies significantly with the change of record length, with a considerable range between the minimum and the maximum values obtained. The range of variability is shown in figure 5.7.

As expected the lower spatial frequency component changes less frequently with the change of window length than the higher spatial frequencies as there are less cycles of the lower frequency present in the record. A small change in the value of the DC-level (Val_{DC}) can also be observed. Varying of the record length does influence the mean level and hence the DC-value of that record. The investigations showed that the DC-level was found to be of the correct value, calculated using eqn. 4.37, for the same record lengths as for the strongest spatial frequency line, here Val_{12}.

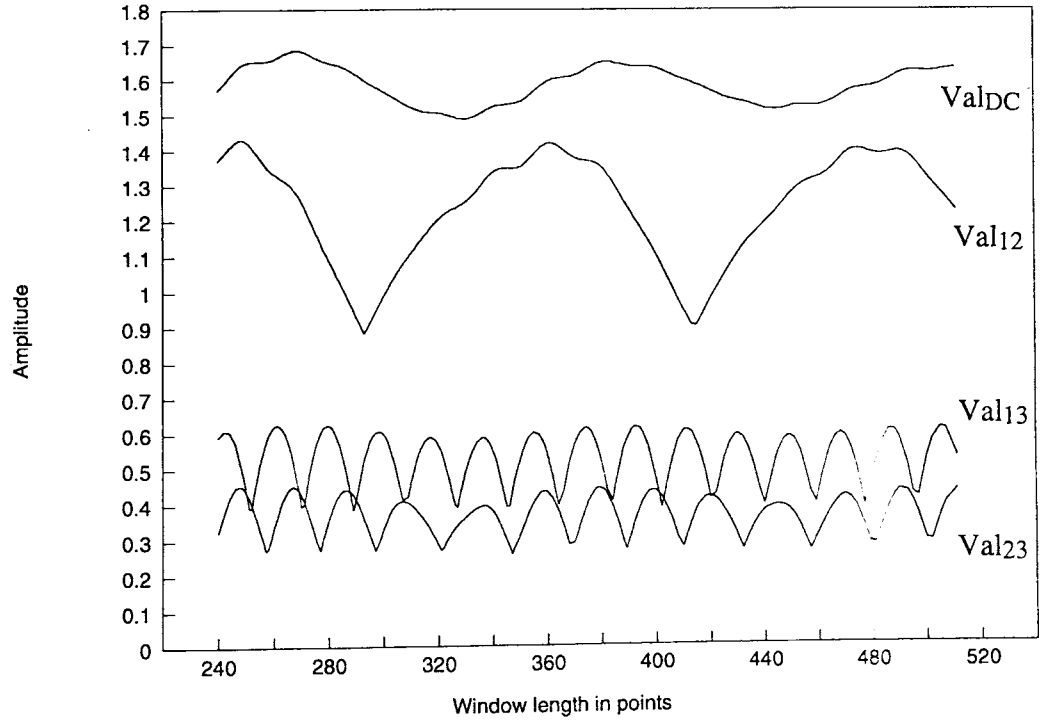

Figure 5.7 *Change of spectral line amplitude with changing record length*

5.2.2.1 Identification of correct truncation interval for each line

Figure 5.8 represents a 3D-graph of the array resulting from the spectra of successive DFTs. The spatial frequency axis has been scaled in multiples of 1/NT, which is the reciprocal of the record length of N sample points with duration T. The reduction of record length (i.e. window size) is indicated by -n (minus n), starting at 0 points being deducted from the original record, ending in this graph at 100 deducted from the original length.

From this array of values of the correct amplitude value for each spectral line at its correct spatial frequency has to be extracted. The identification of the correct spectral frequency value is explained in section 5.2.2.2, identification of the correct amplitude value in section 5.2.2.3.

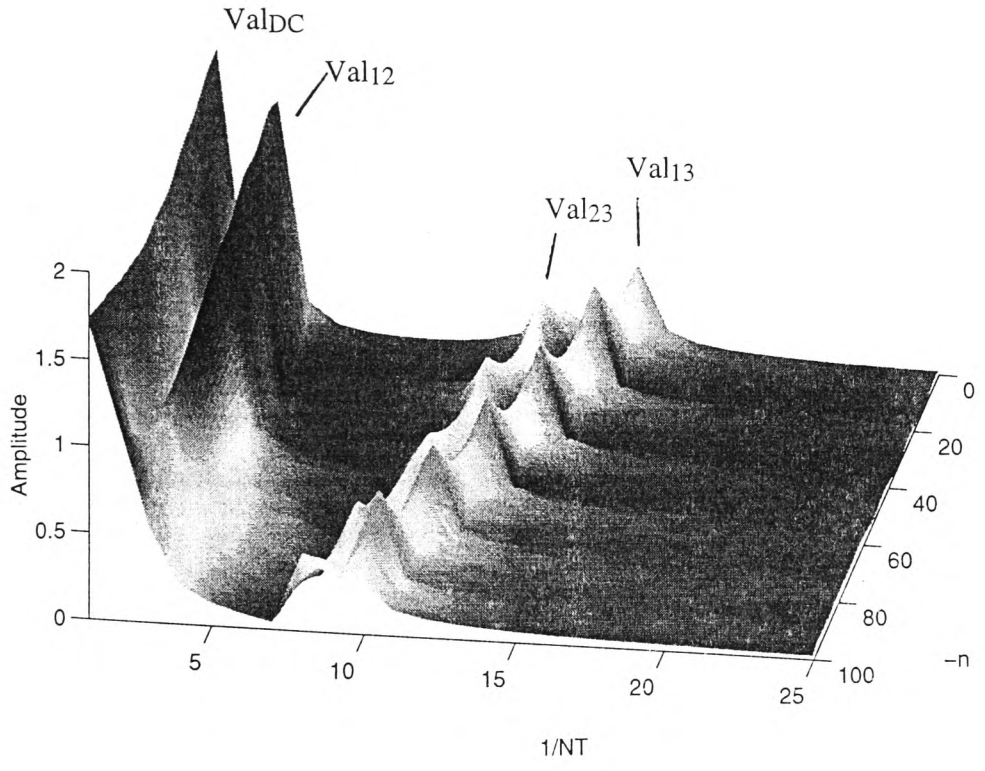

Figure 5.8 *3D-graph of resulting FTs with changing truncation interval in the spatial domain*

5.2.2.2 Identification of correct spatial frequency values

The sampling distance between successive sample points in the frequency domain equals the reciprocal of the record length (in distance) in the spatial domain. The variation of the record length in the spatial domain before each DFT is applied will result in a change in the length of the sampling interval in the spatial frequency domain. Care has to be exercised when assigning spatial frequency values to the number of sampling points where the spectral line arises. The procedure using the adaptive window size has to assign a spatial frequency to each line after each DFT using the reciprocal of the particular record length used in the spatial domain. The amplitude values can then be collected for each spatial frequency of every DFT and compared after the last DFT. Since the length of the sampling interval in the spatial frequency domain changes with each change of the record length there will be instances when a decision in the middle of two sampling intervals has to be made as to what frequency is represented by each point. This also has to be incorporated in the procedure.

5.2.2.3 Identification of correct amplitude values

Applying successive DFTs with changing record lengths, it was expected that the each spectral line would reach its maximum amplitude where the length of the truncation interval is equal to an integer multiple of the cycle length of this frequency component. Figure 5.7 suggests that this would be the case. However close examination showed that a slightly higher amplitude would be reached when the record length differed slightly from the integer multiple of the cycle length. Varying the record length on signals with known spectra, the amplitude value of a given spectral line will at a certain record length exceed the theoretical value. Changing the record length further this amplitude will reduce again. This was found to be a leakage related phenomenon of the DFT which meant that an additional criterion to the maximum amplitude of the spectral line with changing record length is required.

To demonstrate this behaviour a signal was generated consisting of the sum of a DC-level and a sine-wave, both of amplitude 1. For the window size that was an exact integer multiple

of the cycle length of this signal it was chosen to contain 4 cycles. Figure 5.9 shows the results of four different DFTs of this signal, where the record length has been altered slightly between each DFT. One DFT was carried at a window length that was exactly 4 cycles of this signal, marked as 'exact'. One DFT was applied to a record of this signal which was one sampling point shorter, marked as '-1pnt' in the legend. And two DFTs were applied to records longer than the original one, one longer by one point ('+1pnt') and one longer by two sampling points ('+2pnts').

The variations between the four graphs are small, but both the top and the bottom of the graph are of interest. Therefore figure 5.10 shows an expanded view of the top section of figure 5.9. And figure 5.11 shows an expanded view of figure 5.9 near the abscissa.

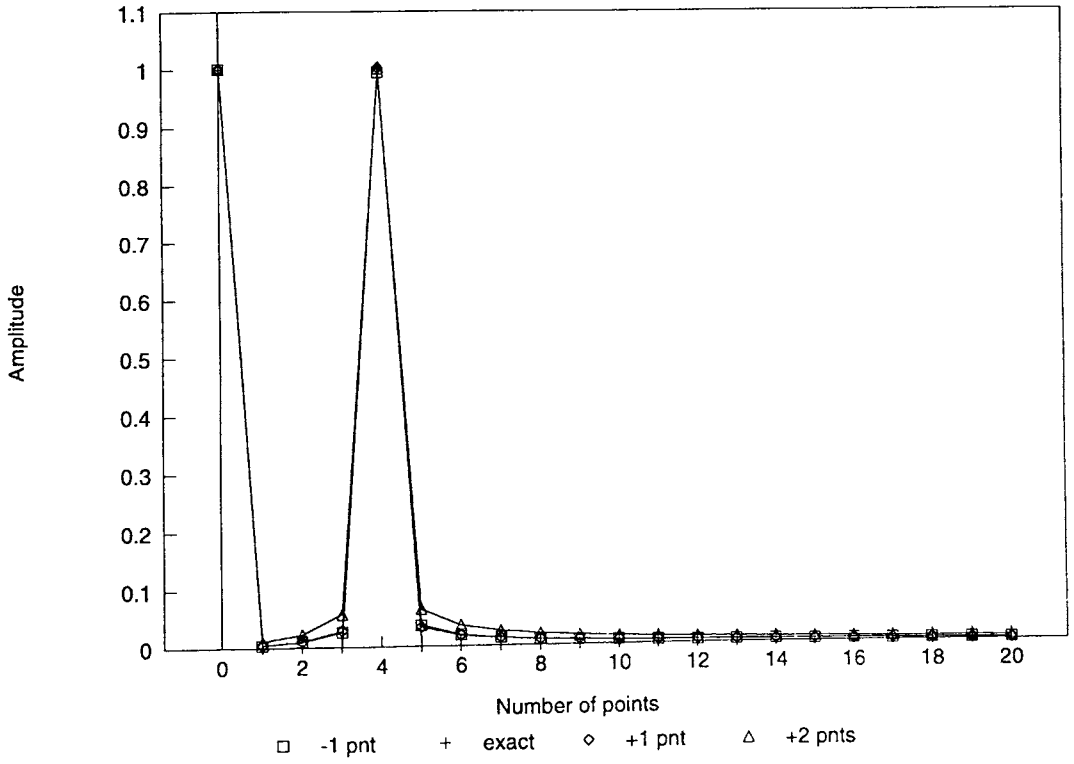

Figure 5.9 *DFTs of a DC + sine-wave signal with 4 different record lengths*

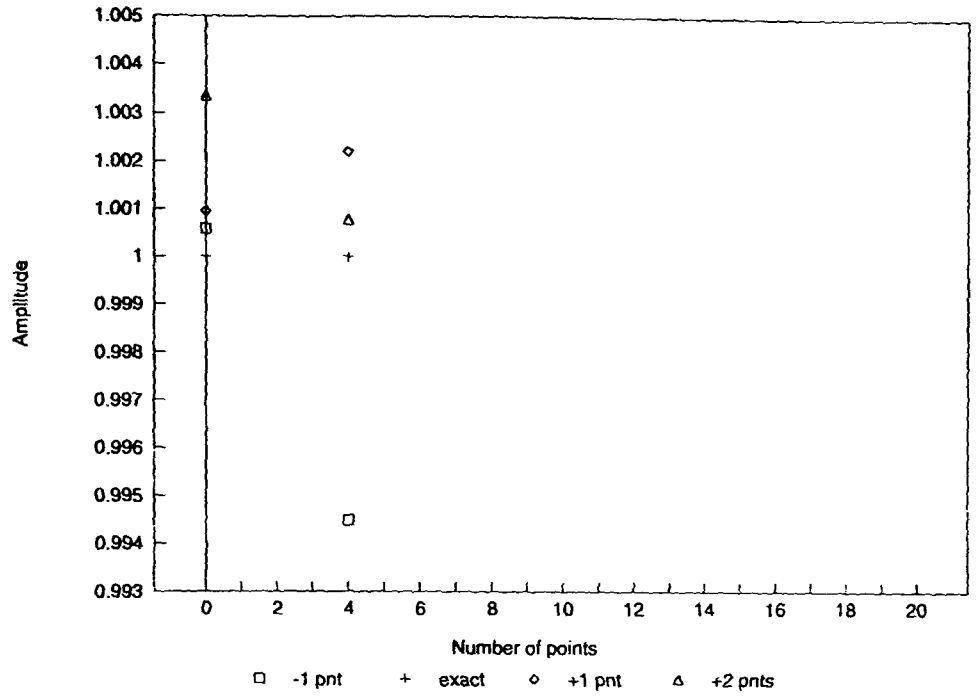

Figure 5.10 *Expanded view of top section of figure 5.9*

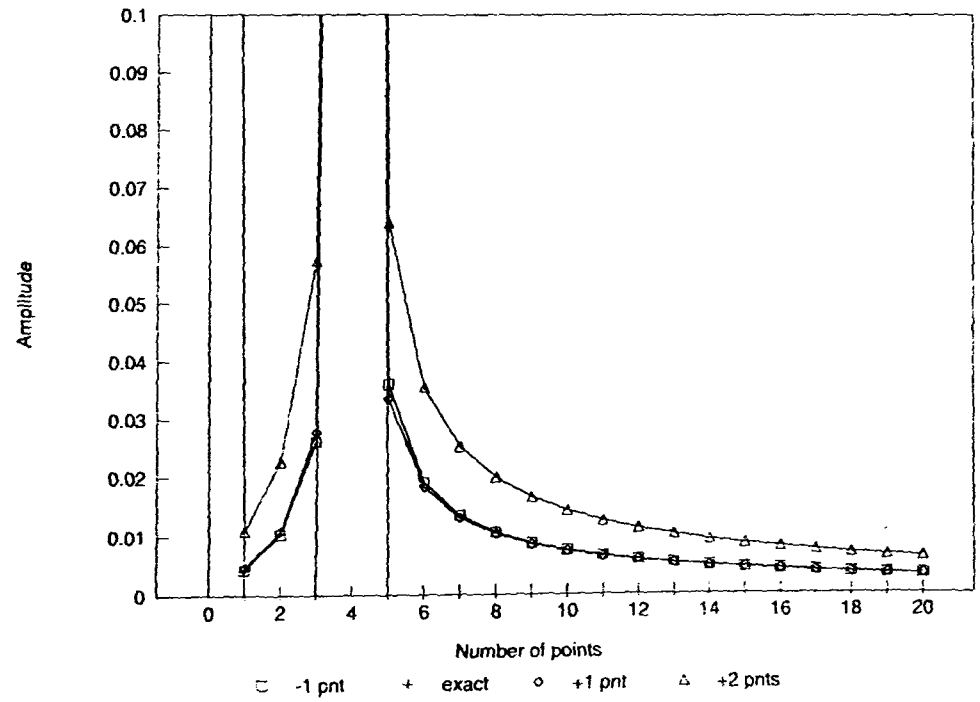

Figure 5.11 *Expanded view of bottom section of figure 5.9*

The figures show that both the spectral line for the DC level and for the sine-wave are exceeding the correct amplitude value slightly at certain window length, are of the true value at an exact integer multiple of the cycle time of the signal (best seen in figure 5.10). It can also be seen, that in the case of an excess amplitude value there is leakage present in the vicinity of the spectral line of the sine-wave. This can be observed best in figure 5.11.

In order to obtain correct spectral line amplitudes a criterion to test for minimum leakage as well as finding the maximum amplitude after each DFT was introduced into the resolution procedure.

Although the differences of the amplitude values in the last example are small, incorporating a minimum leakage criterion proved that a significant increase in the accuracy of the resolution of simulated multipath geometries can be obtained.

5.3 Results of improved procedure applied to simulated amplitude envelopes

Tables 5.3 to 5.10 show results of the developed resolution procedure for four different simulated (using the simulation described in section 3.1.2) multipath geometries. The most left hand column in the tables list the parameters (amplitudes and angles of arrival) for the simulated multipath geometries, representing the true values in **bold** figures. As in the examples before the angle of arrival of the first component (θ_1) was chosen to be 0°. The other columns list how these parameters were resolved by the developed procedure both with and without using the leakage test criterion. The error compared to the values for simulated geometries is also listed in each case. It can be seen that a significant improvement is achieved using the minimum leakage criterion. It can also be seen that using the adaptive window size yields much more accurate results than a single DFT after using a window-function. This can be seen comparing the results shown in tables 5.3 to 5.10 with the ones obtained using a single DFT shown in tables 5.1 and 5.2.

	Adaptive window size, **no** minimum leakage test		Adaptive window size, **plus** minimum leakage test	
Simul. geometry	Procedure result	Error	Procedure result	Error
$A_1 = 1.0$	0.9878	-1.2 %	0.9993	-0.07 %
$A_2 = 0.7$	0.7100	1.4 %	0.6991	-0.14 %
$A_3 = 0.3$	0.3095	3.5 %	0.3022	0.72 %
$\theta_2 = 45°$	45.149°	0.33 %	44.999°	-0.001 %
$\theta_3 = 150°$	150.180°	0.12 %	149.855°	-0.09 %

Table 5.3 *Improved resolution procedure results using adaptive window size*

	Adaptive window size, **no** minimum leakage test		Adaptive window size, **plus** minimum leakage test	
Simul. geometry	Procedure result	Error	Procedure result	Error
$A_1 = 1.0$	1.0194	1.9 %	1.013	1.3 %
$A_2 = 0.5$	0.4973	-0.54 %	0.4962	-0.77 %
$A_3 = 0.5$	0.4952	-0.94 %	0.4963	-0.74 %
$\theta_2 = 45°$	45.199°	0.44 %	44.099°	-0.22 %
$\theta_3 = 150°$	150.180°	0.12 %	149.855°	-0.09 %

Table 5.4 *Improved resolution procedure results using adaptive window size*

	Adaptive window size, **no** minimum leakage test		Adaptive window size, **plus** minimum leakage test	
Simul. geometry	Procedure result	Error	Procedure result	Error
$A_1 = 1.0$	1.0049	0.49 %	1.0007	0.07 %
$A_2 = 0.9$	0.8951	-0.54 %	0.8988	-0.13 %
$A_3 = 0.1$	0.1066	6.6 %	0.1009	0.89 %
$\theta_2 = 45°$	44.950°	-0.11 %	44.999°	-0.001 %
$\theta_3 = 150°$	151.744°	1.16 %	150.29°	0.20 %

Table 5.5 *Improved resolution procedure results using adaptive window size*

	Adaptive window size, **no** minimum leakage test		Adaptive window size, **plus** minimum leakage test	
Simul. geometry	Procedure result	Error	Procedure result	Error
$A_1 = 1.0$	1.0119	1.2 %	1.0081	0.82 %
$A_2 = 0.7$	0.7203	2.9 %	0.7180	2.6 %
$A_3 = 0.3$	0.3099	3.3 %	0.2975	-0.84 %
$\theta_2 = 30°$	29.559°	-1.5 %	29.724°	-0.92 %
$\theta_3 = 50°$	50.424°	0.85 %	49.995°	-0.01 %

Table 5.6 *Improved resolution procedure results using adaptive window size*

	Adaptive window size, **no** minimum leakage test		Adaptive window size, **plus** minimum leakage test	
Simul. geometry	Procedure result	Error	Procedure result	Error
$A_1 = 1.0$	1.0125	1.3 %	1.0023	0.23 %
$A_2 = 0.5$	0.5349	7.0 %	0.5284	5.7 %
$A_3 = 0.5$	0.5001	0.02 %	0.4889	-2.2 %
$\theta_2 = 30^\circ$	29.494°	-1.7 %	29.429°	-1.9 %
$\theta_3 = 50^\circ$	50.208°	0.42 %	49.995°	-0.01 %

Table 5.7 *Improved resolution procedure results using adaptive window size*

	Adaptive window size, **no** minimum leakage test		Adaptive window size, **plus** minimum leakage test	
Simul. geometry	Procedure result	Error	Procedure result	Error
$A_1 = 1.0$	1.0401	4.0 %	1.0004	0.04 %
$A_2 = 0.9$	0.8766	-2.6 %	0.8999	-0.01 %
$A_3 = 0.1$	0.1234	23 %	0.1006	0.62 %
$\theta_2 = 30^\circ$	29.658°	-1.1 %	29.995°	-0.02 %
$\theta_3 = 50^\circ$	50.588°	1.2 %	50.054°	0.11 %

Table 5.8 *Improved resolution procedure results using adaptive window size*

	Adaptive window size, **no** minimum leakage test		Adaptive window size, **plus** minimum leakage test	
Simul. geometry	Procedure result	Error	Procedure result	Error
$A_1 = 1.0$	0.9713	-2.9 %	0.9905	-0.95 %
$A_2 = 0.7$	0.7213	3.0 %	0.7065	0.93 %
$A_3 = 0.3$	0.3421	14.0 %	0.3184	6.1 %
$\theta_2 = 60^\circ$	60.075°	0.13 %	60.000°	0.0 %
$\theta_3 = 70^\circ$	70.337°	0.48 %	70.370°	0.53 %

Table 5.9 *Improved resolution procedure results using adaptive window size*

	Adaptive window size, **no** minimum leakage test		Adaptive window size, **plus** minimum leakage test	
Simul. geometry	Procedure result	Error	Procedure result	Error
$A_1 = 1.0$	0.9809	-1.91 %	1.0043	0.43 %
$A_2 = 0.5$	0.5140	2.8 %	0.4986	-0.28 %
$A_3 = 0.5$	0.5268	5.4 %	0.4842	-3.16 %
$\theta_2 = 60^\circ$	60.151°	0.25 %	60.000°	0.0 %
$\theta_3 = 70^\circ$	70.146°	0.21 %	70.028°	0.04 %

Table 5.10 *Improved resolution procedure results using adaptive window size*

5.4 Summary of the developed resolution procedure

The developed resolution procedure performs the following tasks:

- It calculates the square of a recorded amplitude envelope.
- It applies a DFT to squared envelope.
- Then it reduces the record length by 1 sample point and applies another DFT, this is repeated for a given number of times.
- After each DFT the amplitudes and spatial frequencies are stored in a array. The spatial frequencies are rescaled after each DFT using the changed record length.
- For the amplitude values of each spectral line a routine is applied. It uses a combined the search of the result array for the maximum amplitude value and for minimum leakage.
- The values found for the spatial frequencies and the spectral line amplitudes are used to determine the amplitudes and angles of arrival of the multipath components using equations 4.3, 4.41 to 4.43.

5.5 Interim conclusion of chapter 5

When using the DFT leakage errors have to be taken into account whenever the record length window of the signal to which the DFT is applied is not an integer multiple of its period. The spatial frequency components in the spectrum of the square of the received amplitude envelope in a multipath field cannot be considered to exhibit an integer relationship. Due to a lack of harmonic relationship, errors due to spectral leakage cannot be eliminated. To minimize these errors the sampled signal record is generally multiplied with a window function prior to applying the DFT. This well established method (Brigham, 1988) was implemented on spatial interference patterns (amplitude envelopes), but for component resolution purposes the results achieved were found to be unsatisfactory. To improve the accuracy of the resolved multipath components a techniques was developed that applies successive DFTs to the signal record while the record length is varied prior to each DFT

application. Within the sampling resolution in the spatial domain it is possible to find window sizes for each frequency that are integer multiples of their period in the spatial domain. Collecting the results from these DFTs and implementing a maximum amplitude and minimum leakage finding routine it is possible to retrieve the relevant multipath parameters with good accuracy. It was possible to develop a computer routine that incorporates this method and achieves resolution of angles of arrival and amplitudes of multipath components from a given interference pattern.

Chapters 6 and 7 describe the equipment experimental program and results obtained from it to verify the resolution procedure applied in the practical environment.

CHAPTER 6 EXPERIMENTAL VERIFICATION

6.1 Introduction

The component resolution procedure described in section 5 was developed using amplitude envelopes created with the simulation described in section 3.1.2. The procedure was optimized using this simulation. This improved the accuracy with which simulated multipath geometries could be resolved. However the developed procedure is intended to be applied to existing multipath situations in practice. The applications for the procedure would be to obtain information about the constituent components of an unknown multipath geometry. This could be in cases where radio links suffer from the effects multipath propagation. It could also be used conducting signal strength measurements under multipath conditions where the signal level of individual components could normally not be determined.

A experimental programme was to be set up to demonstrate the practical usefulness of the procedure. This would test the results gained using the computer simulation and the validity of the use the square of the amplitude envelope.

To be able to assess the results obtained from the resolution procedure multipath situations were needed where the individual components of the multipath field could be determined concerning their individual amplitudes and angles of arrival. These values could then be compared to the results obtained by applying the resolution procedure to the amplitude envelope measured in the multipath field at the same location.

During the experimental program three different kinds of measurements were carried out, which can be categorized as:

(i) Experiments carried out at the University of Glamorgan playing fields.

The aim of these experiments was to create several multipath geometries which can be altered and repeated. The large open playing field area was chosen as location for this set. The multipath geometries were created using reflector boards. This allowed the creation of several different geometries at the same location.

(ii) Experiments in multipath situations involving real buildings.

In this set of experiments, existing buildings were utilized to create multipath geometries rather than reflector boards. This set was carried out to assess some example situations where existing buildings give rise to the multipath rather than artificially created path geometries with reflector boards.

(iii) Anechoic chamber measurements.

During the course of the research programme anechoic chamber facilities became available. These provided a controlled environment where similar experiments to those on the playing field could be conducted but without having to allow for conditions typically found in outdoor experiments.

The outdoor experiments were carried out at a frequency of 11.2 GHz, whereas the anechoic chamber measurements were conducted at 20 GHz.

Section 6.2 describes the different measurement systems used in the various sets of experiments.

6.2 Description of the measurement systems

Two different measurement systems were used during the experiments. A mobile 11.2 GHz system (section 6.2.2) used for outdoor measurements and a 20 GHz laboratory system (section 6.2.3) for the anechoic chamber measurements. A mobile receiver trolley (section 6.2.1) was constructed and used to carry the complete receiver unit for the 11.2 GHz experiments and provide a means of antenna displacement for all experiments.

6.2.1 Mobile receiver trolley unit

This unit was designed and constructed to carry the complete receiver unit required for the experiments. It was designed as a mobile unit so that the outdoor measurements at 11.2 GHz could be carried out in any given receiver location independent from. The mobile receiver

trolley was equipped with an independent power supply unit capable of providing the mains power for the equipment used. For the 20 GHz indoor measurements available laboratory facilities were used. Common to all experiments was the need to displace the receiving antenna linearly in small equidistant steps within the multipath field to record the interference pattern. The unit was designed to provide this antenna displacement.

The trolley carries all the necessary components for the mobile power supply unit as well as the measuring device in the form of a spectrum analyzer for the 11.2 GHz system, see section 6.2.2.

To record the interference pattern or amplitude envelope the receiving antenna was displaced linearly and incrementally over distance of a few wavelength. The system enabled the recording of the signal strength of the amplitude envelope at closely spaced equidistant points over the whole length of the antenna displacement. In these measurements the antenna was mounted rigidly and carefully, so that its orientation and straight line movement were maintained during the experiment.

The displacement and rigid support is realized by means of a slider to which antenna mounts are connected. The slider moves along a straight steel rail, mounted on top of the measurement trolley. Inside the steel rail running along its whole length is a threaded stud carrying a metric M10 thread. Along the threaded stud rides a nut which is connected to the slider. The stud is held by two mounts at either end of the steel rail, so it remains in position when turned. Rotation of the stud using the hand crank connected to one end of the stud will move the nut along its thread. With the nut moving the slider connected to it provides displacement of the receiving antenna mounted onto the slider. The pitch of the standard M10 thread used is 1.5 mm, so that with each turn of the hand crank the antenna is displaced by exactly 1.5 mm.

An overall displacement of 880 mm of the antenna is possible on the steel rail, which at 11.2 GHz equals about 33 wavelengths or 59 wavelengths at 20 GHz. Figure 6.1 shows a sketch of this trolley including the spectrum analyzer and the mobile power supply unit, which were used for the 11.2 GHz experiments only.

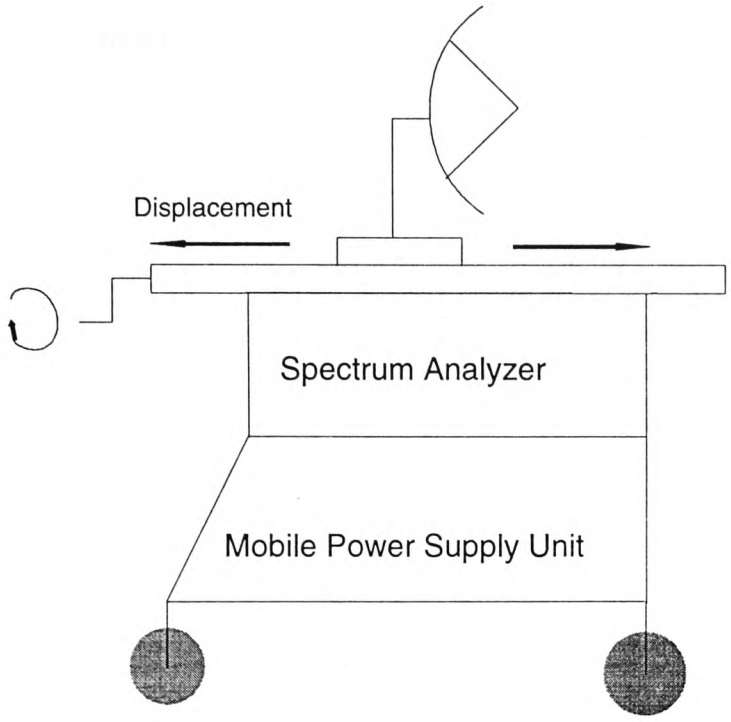

Figure 6.1 *Sketch of mobile measurement trolley for amplitude envelope measurements*

6.2.2 The 11.2 GHz system

Figure 6.2 shows the main components of the 11 GHz measurement system in the form of a block diagram. The different components will be described in more detail below.

6.2.2.1 Transmitter

The source used was a dielectric oscillator of a frequency of 11.2 GHz at a power of measured at 14 dBm. To this oscillator a range of different horn antennas could be connected. Horns of gains 10, 15 and 20 dBi were available. During the measurements on the university playing fields the distance between transmitter and receiver was typically around 50 m. Because of this short distance the received signal would overdrive the sensitive LNB in the receiver. To prevent this the transmitted signal was attenuated by a waveguide attenuator situated between

the oscillator and the horn antenna. A photograph of a typical transmitter assembly is shown in figure 6.3.

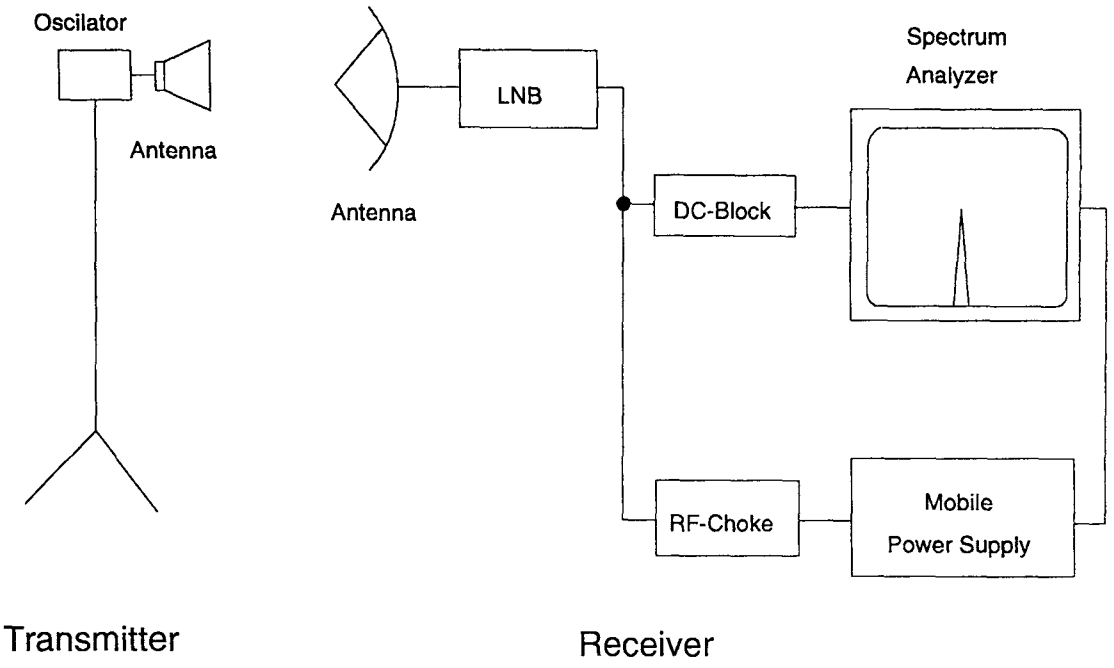

Figure 6.2 *Measurement system for the 11.2 GHz experiments*

6.2.2.2 Receiver

The complete receiver system was mounted on the measurement trolley described above (see figure 6.1). A photograph of this measurement trolley as it was equipped during the measurements is shown in figure 6.3. The receiver system components are seen in the block diagram in figure 6.2. The receiver comprises of:

(i) Antenna:

A 60 cm dish antenna with a gain of 33 dBi

(ii) Low Noise Block (LNB):

The LNB is commonly used in commercial satellite TV systems. The internal amplifier has a specified gain of 50 dB. The 11.2 GHz input signal is mixed down with a 10 GHz internal oscillator yielding a 1.2 GHz output. The noise figure of the LNB is typically 1 dB. The

maximum input signal for the LNB was measured to be -50 dBm. Above this input level the amplifier starts to saturate and becomes non-linear.

(iii) Spectrum analyzer:

A mobile HP8950 1.5 GHz spectrum analyzer was used to display the 1.2 GHz signal level observed at the output of the LNB.

(iv) DC-Block:

The LNB requires to be supplied with a DC voltage of 20 V via the RF-cable. To protect the spectrum analyzer input from this DC supply and prevent damage, a DC-Block which blocks the DC from getting to the instrument is used.

(v) RF-Choke:

This prevents RF from getting into the power supply.

(vi) Mobile power supply:

This unit provides 240 VAC to power the spectrum analyzer and 20 VDC to supply the LNB. The mains voltage is supplied from 12 V heavy duty lead acid batteries via an inverter. The 20 VDC is provided from a common DC power supply driven by 240 VAC generated by the inverter.

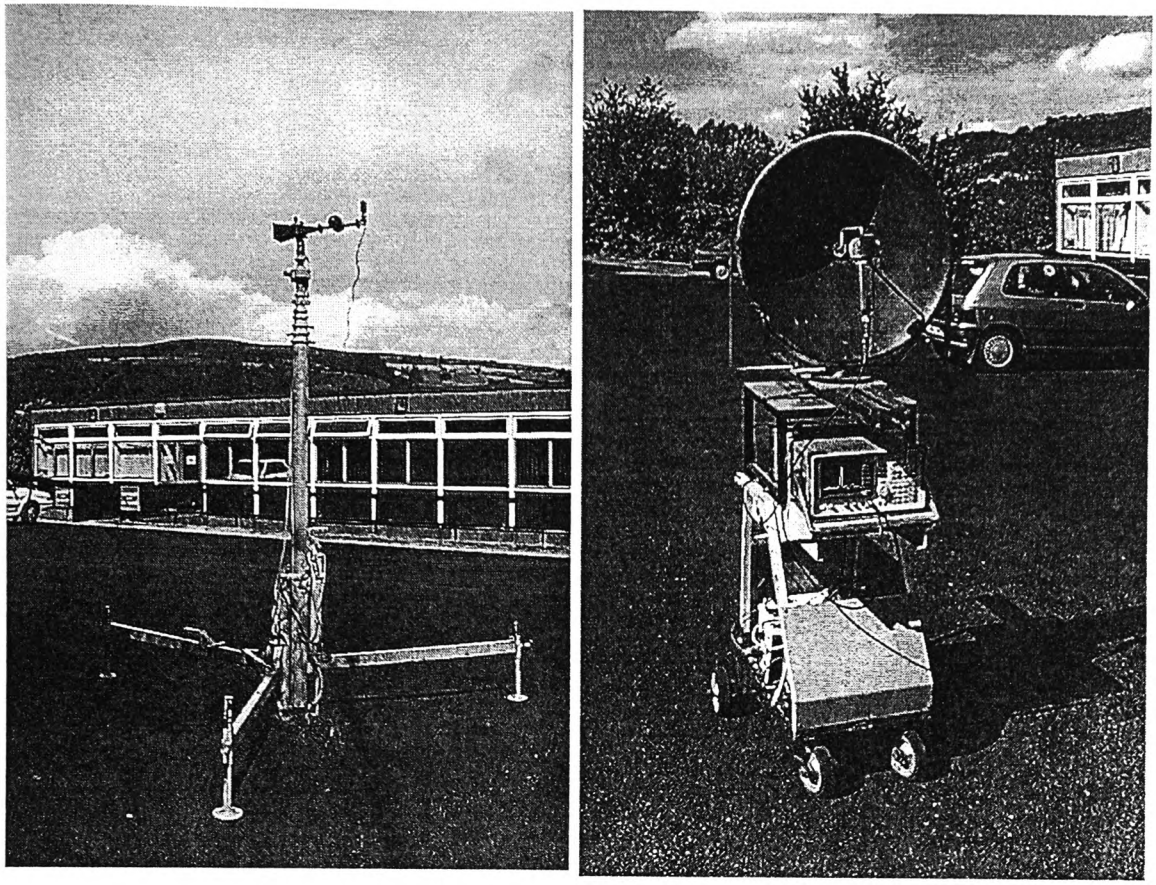

Figure 6.3 *Transmitter mast (left) and mobile measurement trolley (right) as used at 11.2 GHz*

6.2.3 The 20 GHz system

The measurements at 20 GHz were carried out indoors inside an anechoic chamber, the system used differs from the mobile unit used for the 11.2 GHz set up. Although the measurement trolley (fig. 6.1 and 6.3) was also used to displace the receiving antenna, the receiver configuration is significantly different. The 20 GHz system is shown in the block diagram in figure 6.4.

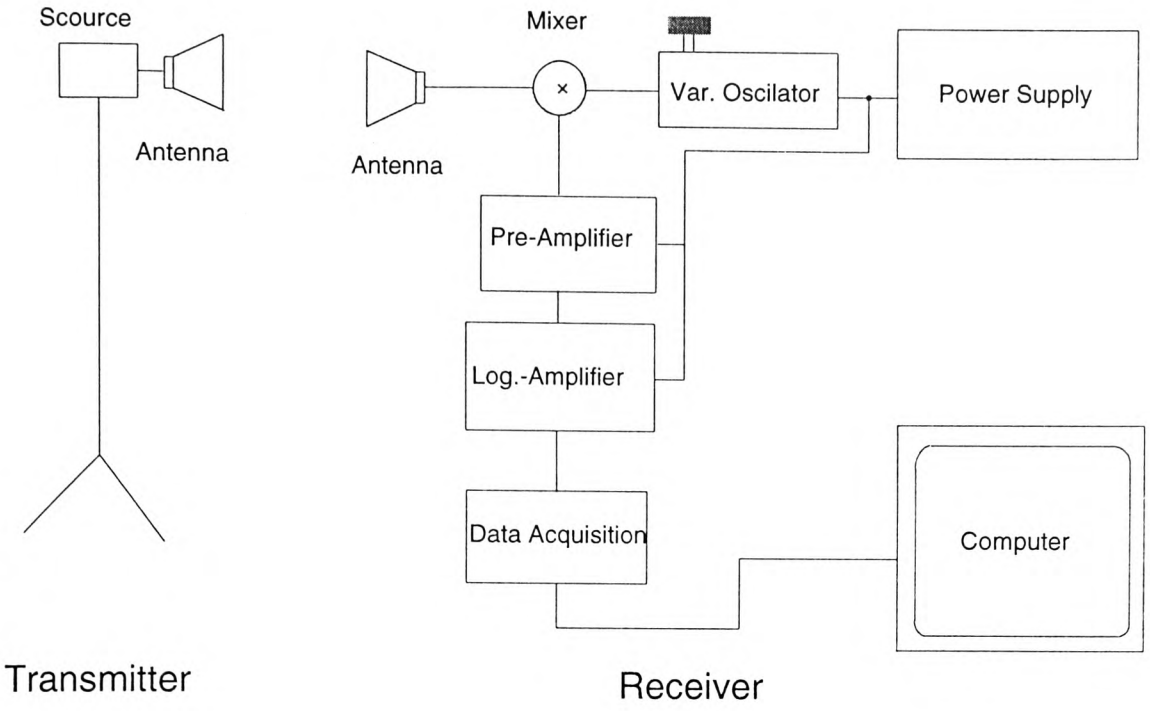

Figure 6.4 *Block diagram of the 20 GHz measurement system*

6.2.3.1 Transmitter

The transmitter again is an oscillator as source, emitting a carrier-wave signal at 20 GHz and a power of 20 dBm. Transmit antennas available were 10, 15 and 20 dBi horn antennas. Compared to the 11.2 GHz experiments the distance between transmitter and receiver was much shorter (about 5 m). Because of this short distance attenuators were used to limit the level of the transmitted signal, thus preventing the log. amp. from being saturated.

6.2.3.2 Receiver

The experiments at 20 GHz were carried out indoors inside an anechoic chamber. The receiver system used in this case was a fixed (as opposed to the mobile 11.2 GHz unit) laboratory assembly. The signal strength was measured via a logarithmic amplifier and a data acquisition board to be displayed and stored directly onto a PC.

The measurement trolley described in section 6.2.1 was used to carry and displace the receiving antenna.

The receiver system subassemblies in fig. 6.4 are detailed below:

(i) Antenna:

For the 20 GHz receiver a range of horn antennas were used with gains of 10, 15 and 20 dBi.

(ii) Mixer:

The output signal of the antenna is mixed with the signal emitted by a variable oscillator, so that the signal resulting from the difference term can be fed into the logarithmic amplifier at an IF of 220 MHz.

(iii) Variable oscillator:

The oscillator provides the frequency for the mixing process with the received microwave signal to mix down to the log. amp. input frequency. The oscillator is variable so that the resultant signal after the mixing can be adjusted to accord with the centre frequency of the logarithmic amplifier.

(iv) Pre-amplifier:

Low noise amplifier providing a gain of 30 dB

(v) Logarithmic amplifier:

The logarithmic amplifier provides a DC output signal that is equivalent to the common logarithm of the power of the input signal. The DC output signal is therefore directly proportional to the input signal level expressed in dBm. The centre frequency of the amplifier is 220 MHz at a bandwidth of 50 MHz. It has a rated dynamic range from +15 to -85 dBm.

(vi) Data acquisition:

A data acquisition board is used to sample the output signal of the log. amp. so it can then be presented to and recorded by the PC.

(vii) Computer (PC):

A personal computer is used to record, display and store the sampled data.

6.3 Measurements

All experiments in the different environments outlined above were conducted following the same principal procedure. The receiving antenna was placed inside the multipath field and aligned by pointing it in the direction of one of the multipath components. This corresponded a signal component that could easily be identified as a single component using the antenna directivity. The receiving antenna was then displaced over a certain distance using the displacement mechanism on the receiver trolley described in section 6.2.1. After each displacement step readings of the signal strength were taken. This formed the record of the amplitude envelope or interference pattern in that particular multipath environment. After taking this record the individual signal components were measured using the directivity of the receiving antenna and assisted further by placing reflective boards to shield out contributions from other signal components.

In order to compare the two measurements the radiation pattern of the receiving antenna needed to be known. When measuring the multipath signal components individually these would be received in the main lobe of the receiving antenna. Whereas during the recording of the interference pattern signal components arriving at an angle of arrival not equal to 0 with respect to the principal axis of the receiving antenna would be received through side lobes. They would hence be attenuated compared to the signal arriving in the main lobe and the signal level measured individually. All signal levels stated in chapter 7 will be signal levels as they were received by the receiving antenna in the position during then amplitude envelope measurement displayed on the spectrum analyzer or PC respectively. This means system gains and losses as well as receiving antenna radiation patterns will be considered for these figures. Therefore it was necessary to establish the radiation patterns of the receiving antennas and the measurement system parameters.

The measured antenna radiation patterns are shown in section 6.3.1.

The measured system parameters are:

6.3.1 Link Budgets and measured system parameters

6.3.1.1 Link budget for 11.2 GHz experiments

Component	Associated Loss/Gain	Link Budget
Power level of microwave source	14 dBm	14 dBm
Loss in feed and adaptor	-4 dB	10 dBm
Gain of transmitting antenna	20 dBi	30 dBm
Free space loss (50 metres)	-87 dB	-57 dBm
Gain of receiving antenna	33 dBi	-24 dBm
Gain of LNB	50 dB	26 dBm
Loss in cable and connectors	-3 dB	23 dBm

Table 6.1 *Link budget for 11.2 GHz experiments*

The overall system gain for the 11.2 GHz system results from the LNB gain minus losses in the connectors and cables plus the antenna gain. The antenna gain in the main direction was 33 dBi for the parabolic antenna. The link budget shows that attenuators had to be used to avoid saturating the LNB. The maximum input signal level at the LNB input is -50 dBm, whereas the link budget shows a signal level of -24 dBm. To complete the system parameters the angular gain function (antenna radiation pattern) had to be determined. It is an important influence on any signal component not arriving in the direction of the principal axis of the

antenna on the recorded amplitude envelope. The radiation patterns of the antennas used are shown in section 6.3.2.

The rated LNB gain was confirmed by measurements at 50 dB, system losses in cables and connectors were 3 dB. The spectrum analyzer hence displayed signal levels 47 dB above the antenna output level. The system was identical for all measurements, including radiation pattern, amplitude envelope and individual multipath component measurements.

6.3.1.2 Link budget for 20 GHz experiments

Component	Associated Loss/Gain	Link Budget
Power level of microwave source	20 dBm	20 dBm
Loss in feed and adaptor	-3 dB	17 dBm
Gain of transmitting antenna	20 dBi	37 dBm
Free space loss (5 metres)	-72 dB	-35 dBm
Gain of receiving antenna	20 dBi	-15 dBm
Gain of pre-amplifier	30 dB	15 dBm
Loss in cable and connectors and mixer	-5 dB	10 dBm

Table 6.1 *Link budget for 20 GHz experiments*

The link budget shows that when using 20 dBi horns the maximum signal input value for the log. amp. was not reached, but to an add extra safety margin for the constructive addition of signal components during the experiments the transmitted signal was attenuated. The values displayed by the computer were calibrated to represent dBm values at the output of the receiving antenna considering the losses and the characteristic of the logarithmic amplifier. Again the system set up was identical for all measurements.

6.3.2 Antenna radiation patterns

6.3.2.1 The 11.2 GHz antennas

For the 11.2 GHz experiments the radiation patterns of the 20 dBi microwave horn and the 60 cm parabolic dish antenna were measured in field experiments. The test site was located on the hill side near the university campus overlooking an open area to one side, see section 6.4.1.1. The resulting antenna patterns are shown in figures 6.5 and 6.6. Although only the 60 cm parabolic dish antenna was used as a receiving antenna during the experiments, it was useful to know the radiation pattern of the 20 dBi horn antenna when used as transmit antenna.

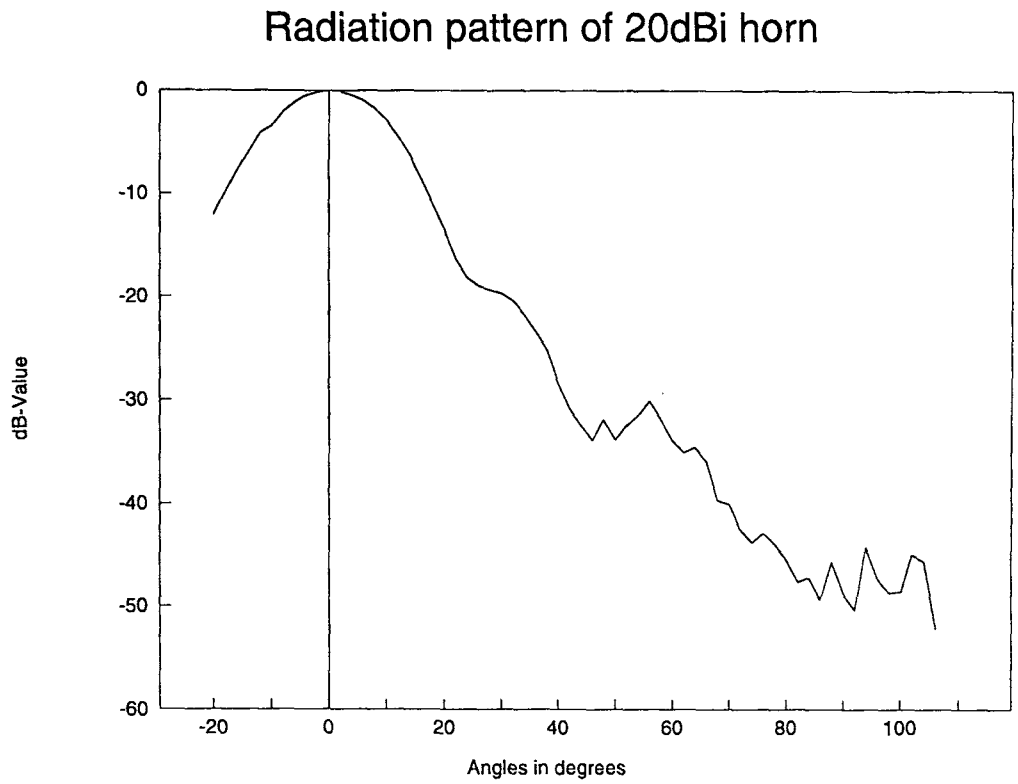

Figure 6.5 *Measured radiation pattern of 20 dBi microwave horn (11.2 GHz)*

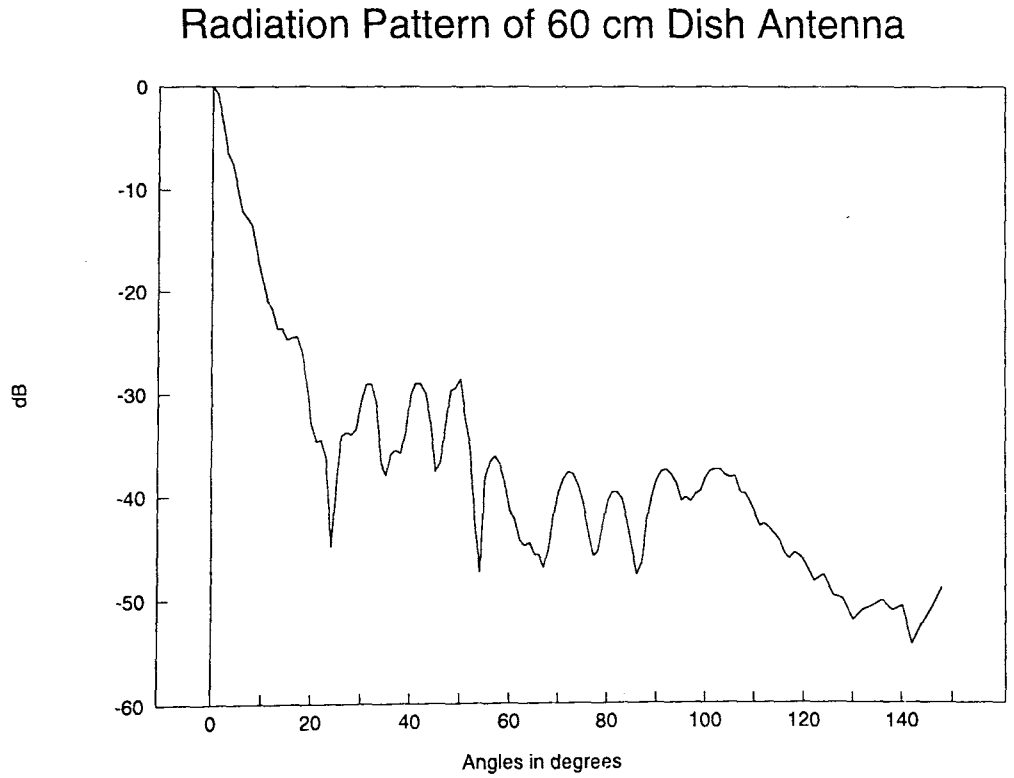

Figure 6.6 *Measured radiation pattern of 60 cm parabolic dish antenna (11.2 GHz)*

6.3.2.2 The 20 GHz antennas

For the 20 GHz experiments the radiation patterns of all three available microwave horn antennas were measured in the anechoic chamber, the measured patterns are shown in figure 6.7.

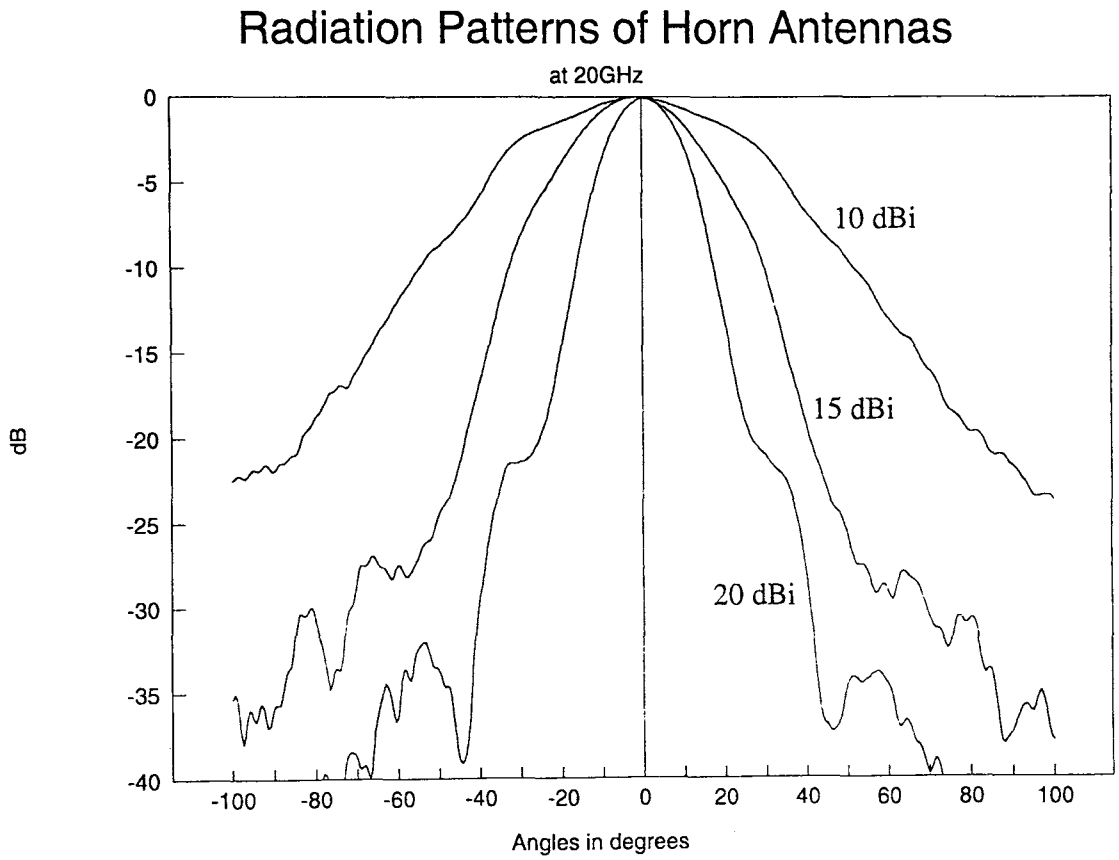

Figure 6.7 *Measured radiation patterns of 3 microwave horns at 20 GHz*

6.3.3 Experiments at university playing fields using reflector boards

The playing field experiments were designed to provide a set of different experiments conducted in different multipath geometries. Wooden reflectors coated with aluminium foil were used to provide the reflecting surfaces to create the multipath field. With these arrangements it was possible to obtain controlled and repeatable conditions could be created.

The chosen experiment site:

The experiments were conducted at the university playing fields, since they provide an ideal site for these measurements. An area of approximately 300 m x 350 m of virtually unobstructed environment surrounded by low vegetation was found here. The unobstructed grass covered smooth surface meant that scatter from a rough ground surface was minimised as was scatter from man-made structures such as fences, lamp or goal posts or banisters. The fields were sufficiently large to conduct the experiments well away from the surrounding vegetation. This tended to be very low in height and consisted mainly at the time of the experiments of shrubs and very young small trees. No other large structures were in the vicinity to influence the measurements.

Other experimental requirements:

It was important that for these first initial measurements controlled conditions existed, so that the amplitude envelope measurements could be conducted without distortions by unknown influences. This would lead to a reliable comparison between results obtained from the application of the resolution procedure to the measured envelope and the individually measured components.

To provide reflected signal components for the generation of a multipath field, reflector boards of the size 1.2 m x 1.2 m were built. These boards had to be light enough to be easily manoeuvred, so they could be aligned accurately. The alignment proved to be an important factor in these experiments in order to achieve reliable results. The region of specular reflection had to be utilized for the experiments to provide strong enough reflected signals. It was critical that the boards were aligned so that the reflected signals and the original signal met at the receiver location. The boards had to be strong enough remain in position even in breezy conditions. This led to the construction of wooden boards coated with thick aluminium foil. The size used was found to be the best compromise between manoeuvrability and

providing a sufficiently large reflective surface. The boards were mounted onto triangular supports, so that their centres were the same height as the receiving antenna.

In order to asses any results found by the resolution procedure, the signal amplitudes of the constituent multipath components were measured individually at the receiver location. These values were subsequently compared with the results of the resolution procedure applied to the amplitude envelope.

While it was easy to determine any direct signal component between the transmitter and receiver, by measuring it before the reflector boards were in place or after they had been removed, this was not the case for any reflected component. Even in the case of only two components there was always a compound field of those two components. In this two component case the measurement of the reflected component could be conducted by pointing the receiving antenna, a 60 cm parabolic dish antenna towards the reflector. An additional metal foil coated reflector board was used to block off the signal arriving directly from the transmitter at the receiver.

This measure plus the high directivity of the antenna allowed reasonably accurate measurements of the signal amplitudes. In the case of a three component measurement which needs two reflector boards the signal originating from the board nearest to the receiver was measured first. Again the receiving antenna was pointed in the direction of origin (reflector board) of this component. The other two components which were the direct signal and the reflection from the other board were blocked using the additional reflector. After this measurement the reflecting board causing this signal was taken down, so the procedure could be repeated for the next reflected signal without having to block off two signals from two almost opposite directions. Taking down reflector boards one by one and re-erecting them was not an option, because it could not have been guaranteed, that the boards re-aligned exactly the same way as they were positioned during the envelope measurement.

In all the playing field experiments there was a direct line of sight between transmitter and receiver, so this direct LOS signal accounts for one component. Two principal measurement set ups were used. The first one was a set up using one reflector board to create a two

component multipath geometry, caused by the interference of the direct and the reflected signal. A number of different three component measurements were carried out sharing the same basic set up. Different angles of arrival were achieved by different positions of the reflectors. This set up used two reflector boards creating a three component geometry. The principal set ups are shown in figures 6.8 and 6.9. Figure 6.10 shows a photograph of an early experiment on the playing fields. Although this scene shows a microwave horn used as receiving antenna (mounted to the mobile measurement trolley) instead of the parabolic dish it gives a good indication of the set up. The two reflector boards are clearly visible to the right of the trolley. The transmitter mast can be seen in the background on the left of the picture just above the middle of the photograph. The shiny rectangular object on the left of the trolley is the foil coated board used to block unwanted signal components.

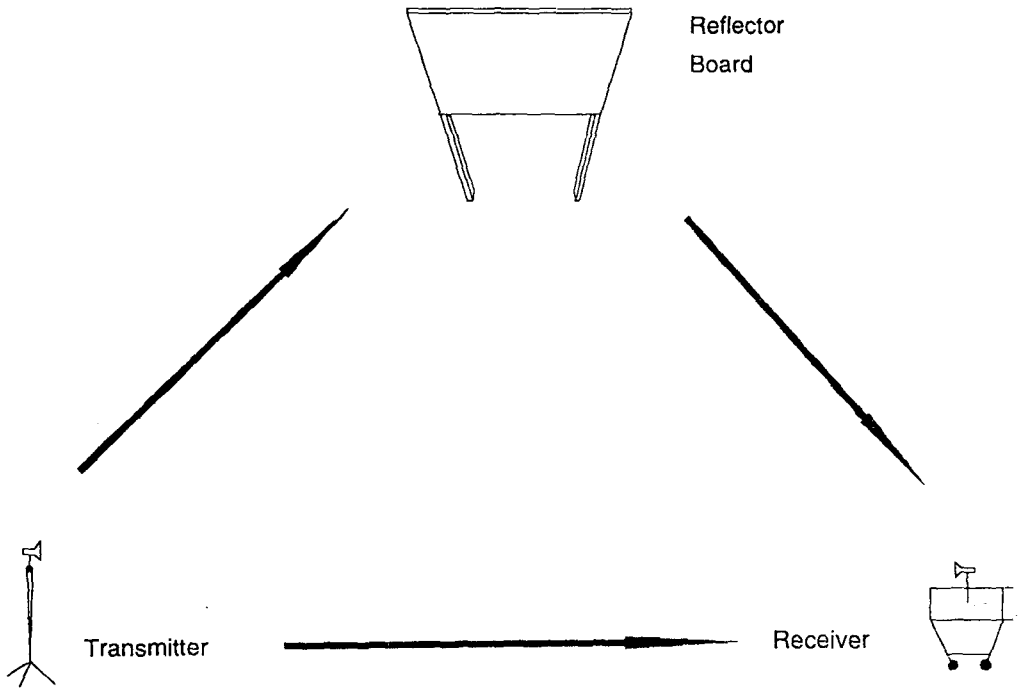

Figure 6.8 *Principal experimental set up for a two component measurement*

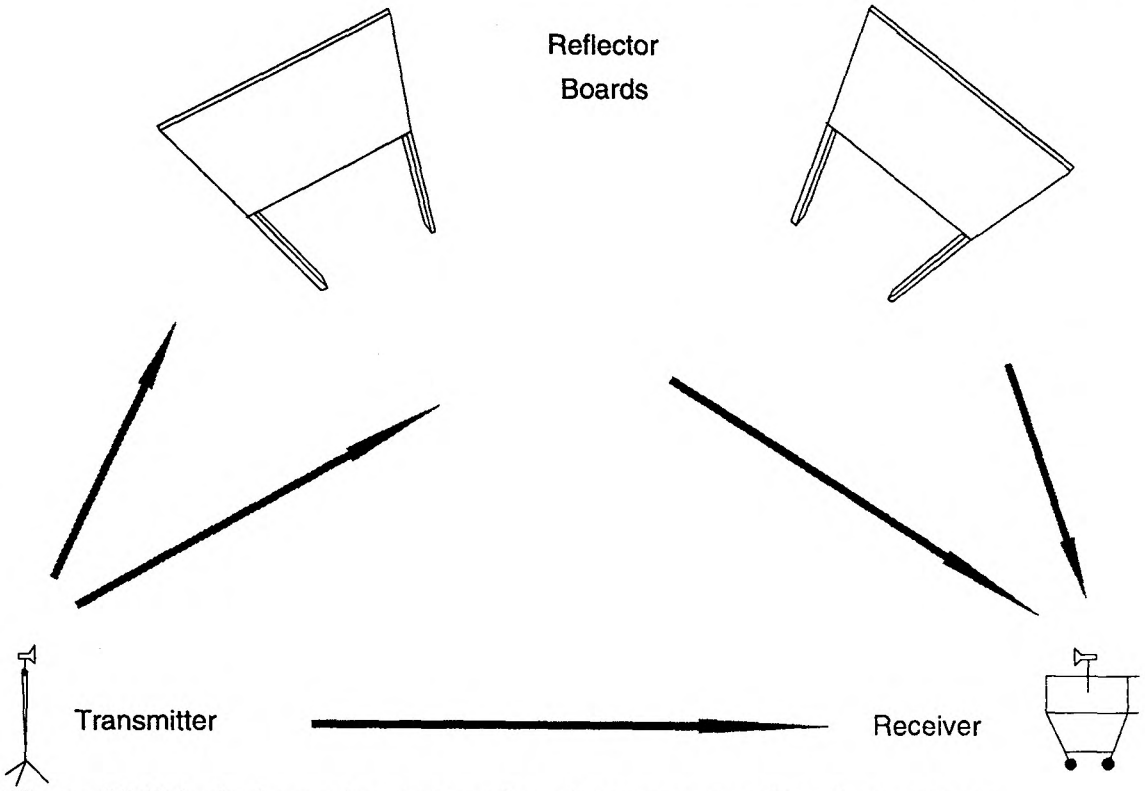

Figure 6.9 *Principal experiment set up for a 3 component multipath experiment*

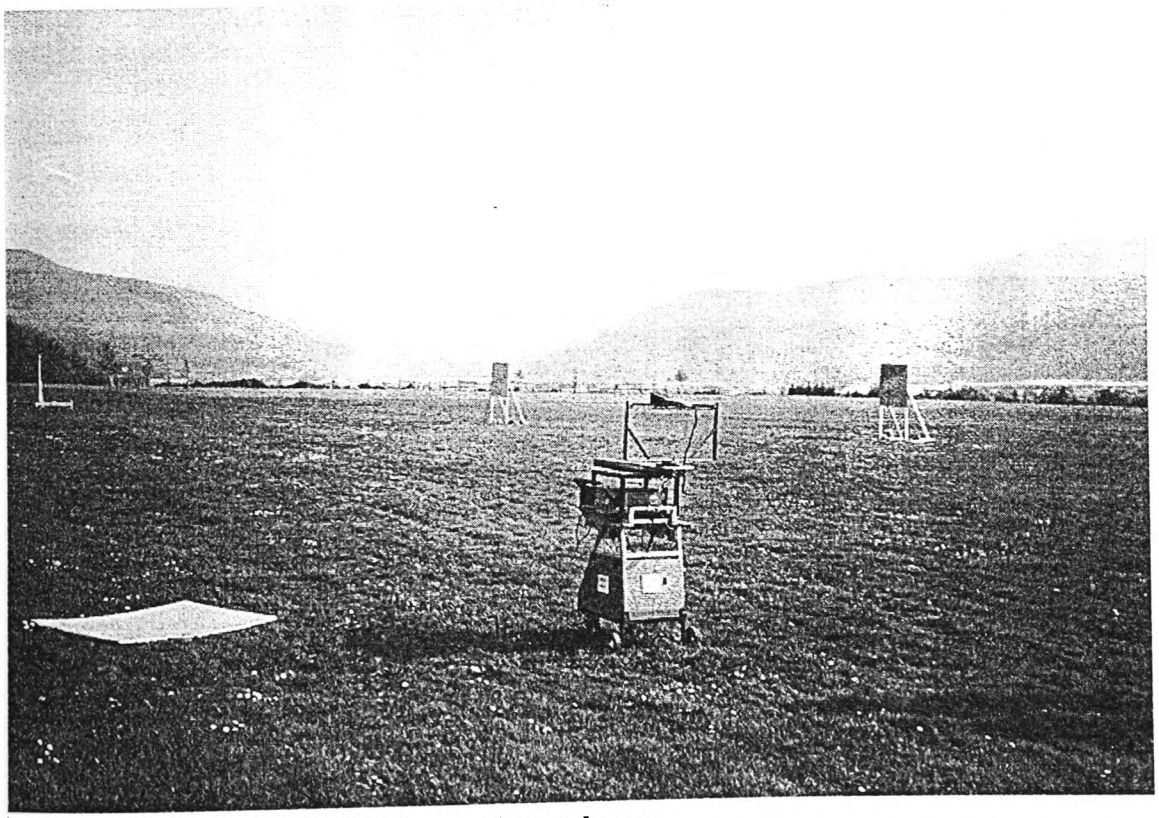

Figure 6.10 *Photograph of early experimental scene*

The geometries and experiment results of the playing field measurements are presented in section 7.1.

The reflector boards were positioned to achieve the wanted multipath geometry using a theodolite. The theodolite was placed at the receiver location and used to mark the position of the centre of the reflector boards. The distance between transmitter and receiver was set to 50 m, the distance between reflectors and receiver was between set to 30 and 50 m, depending on the angle of the boards with respect to the transmitter receiver line.

6.3.3.1 Summary of the measurement set up

The university playing fields provided an ideal site with a large area of virtually unobstructed ground. The level of background scatter was very small due to the lack of scattering sources. Surrounding vegetation was of low density and hight and at sufficient distance from the measurement sites. It was possible to create multipath geometries with the constructed reflector boards and conduct measurements within the resulting multipath field. However the reflector boards used were far smaller than any building surface in a real multipath situation would have been. Therefore care had to be taken during the alignment of the reflector boards because of their relatively small area of specular reflection. Although the supports for the boards were firmly pinned to the ground the influence of wind is evident in the measurements (see section 7.1). Even small movements of the reflectors due to wind are noticeable in the record of the amplitude envelope. The fluctuations caused are evident in the recorded pattern and can be interpreted as noise added to the envelope record.

6.3.4 Multipath generated by existing buildings

In this section two experiments are documented where existing buildings rather than reflector boards simulating buildings gave rise to a multipath geometry. These experiments were conducted to demonstrate that the resolution developed procedure could be applied to

practical multipath situations. Surfaces of existing buildings give rise to a multipath environment rather than a geometry being set up with reflectors. This would create a realistic multipath geometry of realistic dimensions. If the resolution of the multipath components was achieved in these realistic environments this would further validate the usefulness of the procedure in practice.

Again in order to evaluate the results obtained by using the resolution procedure a well defined and easily modelled environment was needed. It required to be possible to identify possible sources of signal components leading to the interference and these could be individually measured in amplitude and angle of arrival thus providing data to compare and validate the results of the resolution procedure.

The motivation for this research leading to the development of a multipath component resolution procedure was that multipath situations are often too complex to be determined easily or resolved by directional discrimination of the antenna alone. In order to predict the resulting multipath field, sites had to be located where a relatively simple geometry can be found. To achieve this the experiment site required to be lacking in structures like fences, lamp posts, banisters and vegetation, which would give rise to unpredictable multipath components.

To be able to measure the signal strength of individual components the structures, e.g. buildings, giving rise to these components were required to be sufficiently spatially separated. Otherwise contribution from one component through side lobes, or even a part of the main lobe would make an individual measurement impossible.
In addition to this requirement the building surfaces needed to be orientated so that spectral reflections of the transmitted signal could recombine at one location.

An detailed site survey revealed the difficulty of location sites that feature all the above mentioned requirements. The survey found two suitable locations for possible experiments. One site was located in the Sandwell area, north of Birmingham and another suitable site was found on the university campus behind a tall building, referred to as G-block.

6.3.4.1 The Birmingham site experiment

Figure 6.11 shows a section of the Ordnance and Survey map for the Sandwell area, where the experiment site is marked. The map shows a playing field area around which several rows of blocks of flats could be found and a number of tower blocks at the southern edge of the field. This site is shown in more detail on a section extracted from a larger scale map in Figure 6.12. The transmitter at this site was placed on the playing field in front of the several blocks of flats and tower blocks. In doing so it was possible to utilize the face of one of the blocks of flats and one tower block in reflecting the signal directly from the transmitter so that they and the transmitted signal would recombine at the chosen receiver location also situated on the playing field. The signal components arriving at the receiver location in this way are labelled 'comp. 1' to 'comp. 3' on the map. The blocks of flats were 3 storey high buildings and therefore much smaller than the multistorey tower blocks.

The receiving antenna was pointed towards the smaller building (component 1), so that both the stronger signal from the transmitter and the stronger reflected signal from the large tower block (Cheviot House) would arrive through the side-lobe of the dish antenna. This was set up in this way so that in comparison much weaker reflection from the small building would be received through the main lobe of the antenna. Otherwise the contribution from the small building would have been too insignificant to have any measurable influence.

The dashed line indicates a fourth component which was not considered during the experiment. The orientation of the second tower block (Chiltern House) was such that no specular reflection was expected at the receiver location (see map). However the results of the component resolution procedure of this experiment (see section 7.2) produced clear evidence of a fourth component arriving at an angle in the direction of this tower block.

This site offered a relatively simple geometry where individual signal component measurements were possible. Although interestingly it had to be discovered that a 4th previously not considered signal component was presenting of the multipath field. Results and the discussion of this experiment are given in section 7.2.

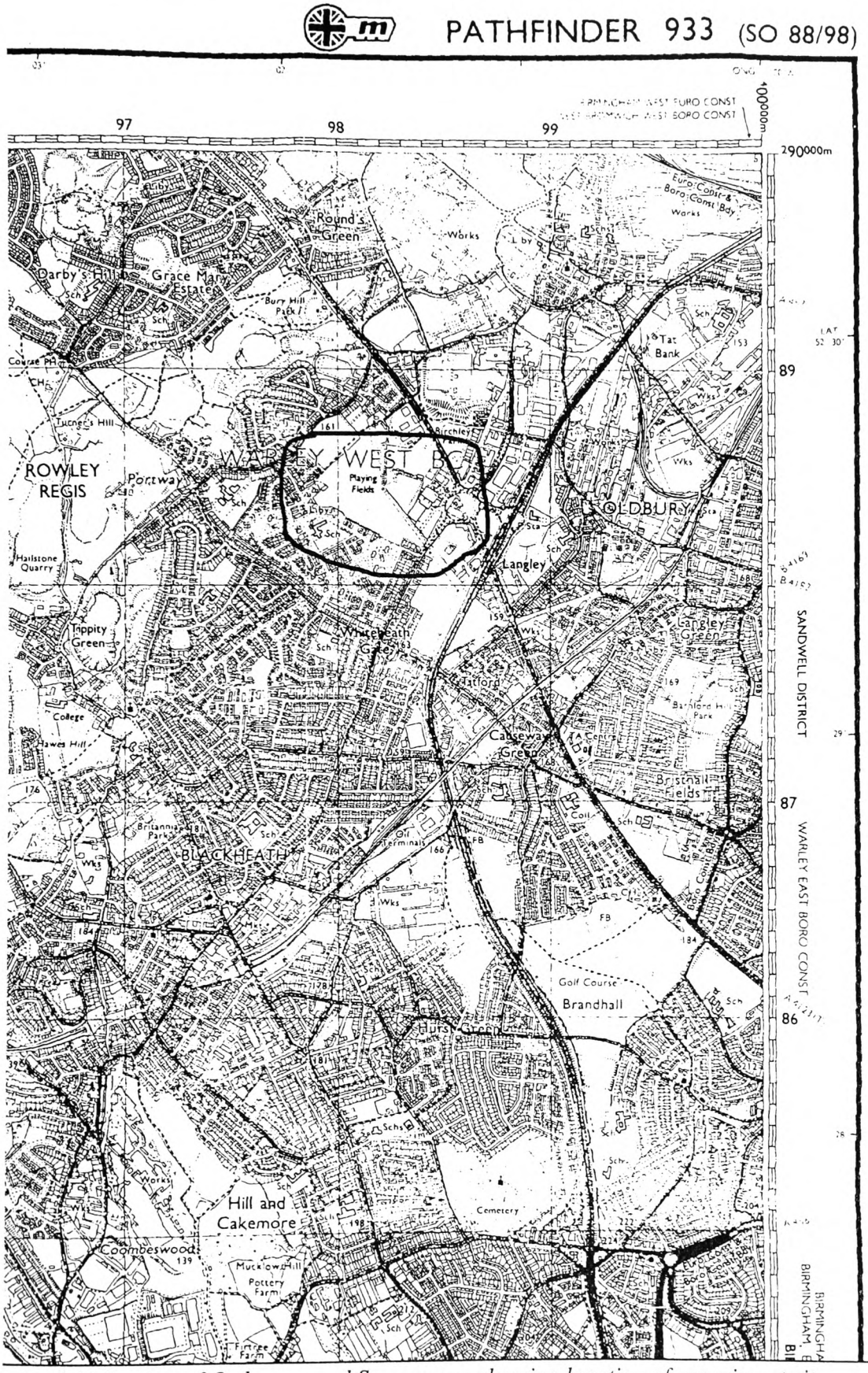

Figure 6.11 *Section of Ordnance and Survey map showing location of experiment site*

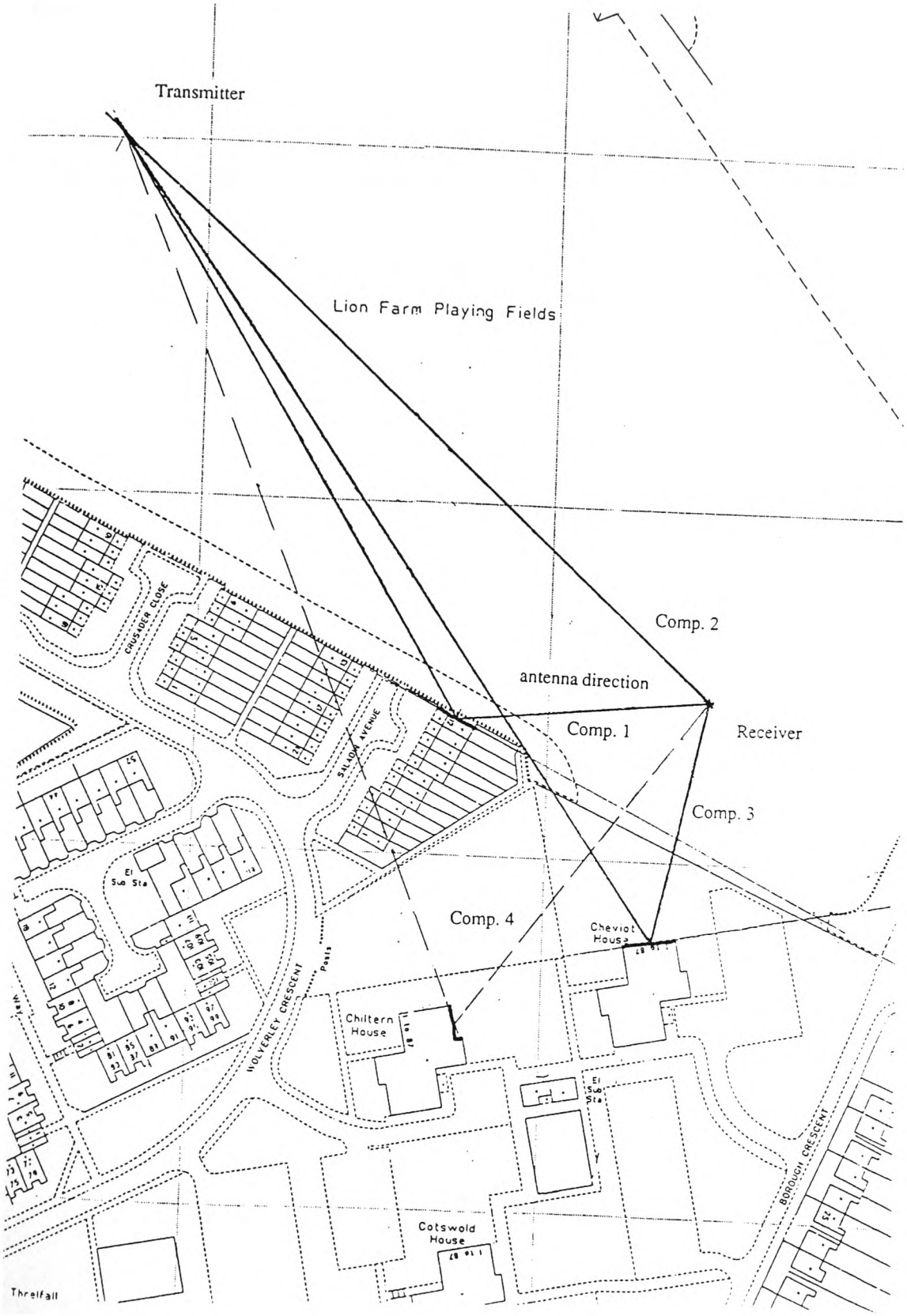

Figure 6.12 *Experiment set up in detail*

6.3.4.2 The campus site experiment

The second site was located on the university campus behind the tallest building on campus. The building was blocking the line of sight path from a distant transmitter. The multipath field resulted from the interference of a signal component penetrating through the building, received at the face of G-block, a reflection from an adjacent building and a third component arising from diffraction signal over a lower section of the tall building. The transmitter was located at a distance of around 2 km on a hill-side seen from the campus. This location was chosen because it offered a multipath geometry that was more complex than at the Birmingham site as far as the signal paths are concerned. Nevertheless it was still possible to identify the structures giving rise to the signal components causing the interference. Figure 6.14 shows a map of the experiment site. The tall building causing the obstruction is labelled 'G1'. The lower wing of this building is 'G2'. The third signal component is a reflection of the 'refectory'. Figure 6.13 shows a photograph of the tall building (G1). The camera was looking at this building from the receiver location.

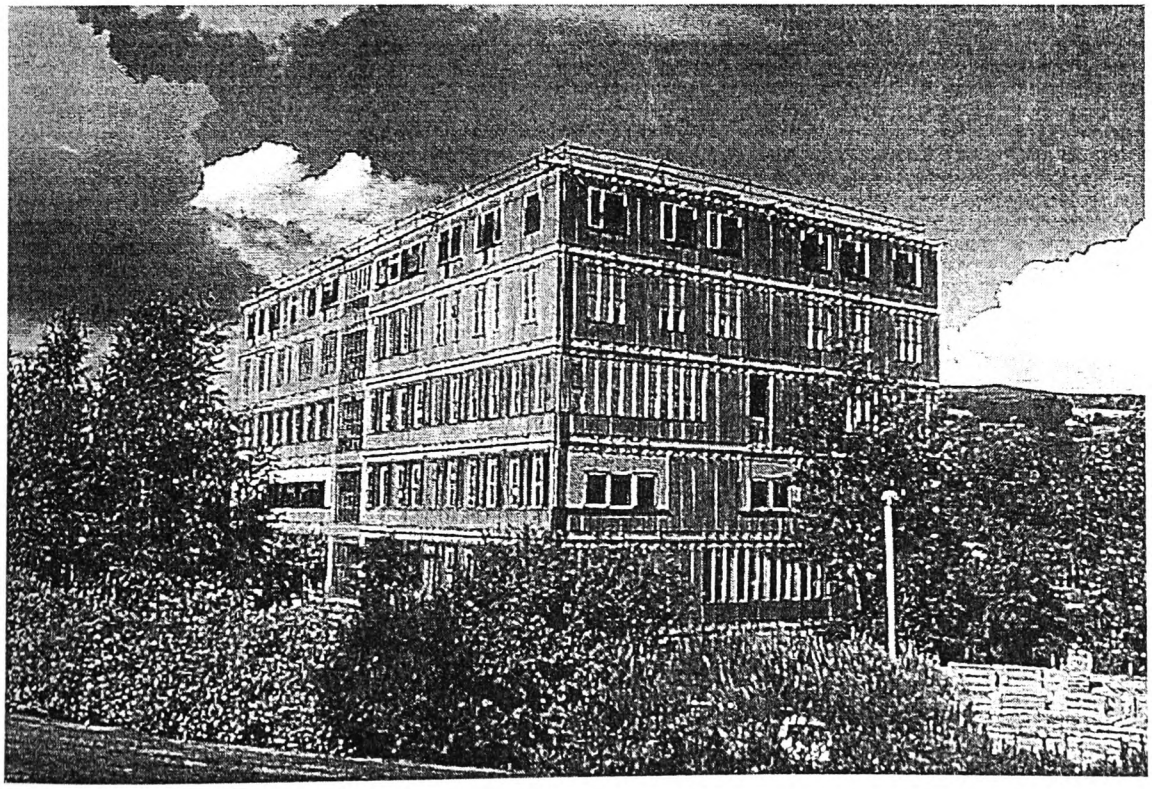

Figure 6.13 *Photograph of higher part of G-block (G1) as seen at the receiver location*

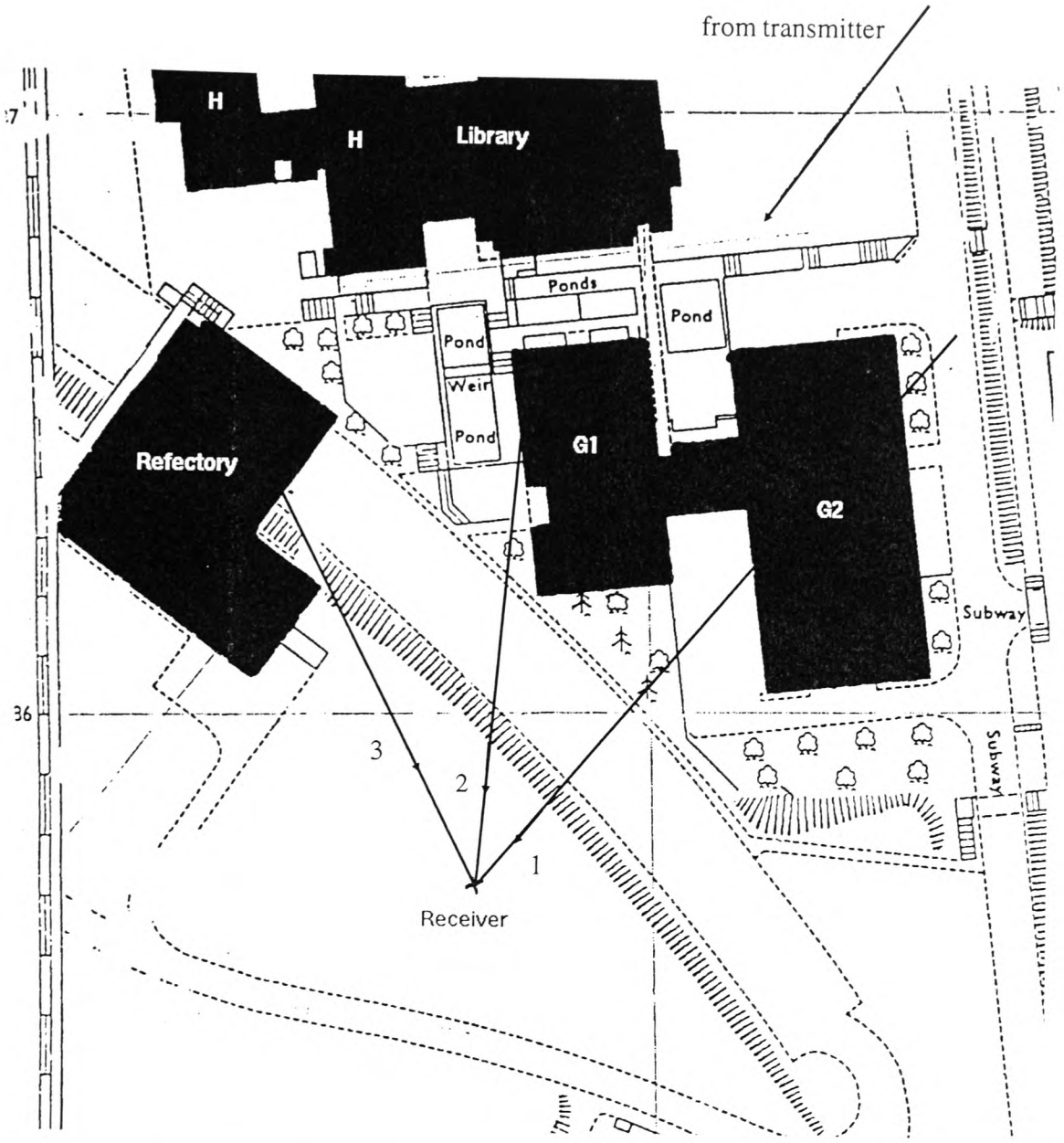

Figure 6.14 *Experiment location of campus measurement*

On the map in fig. 6.14 the signal components giving rise to the multipath field at the receiver location are labelled as:

1) The diffracted signal over the lower wing of G-block (G2).

2) The signal penetrating through G-block (G1), the receiving antenna was pointed in the direction from where this component arrived.

3) The reflection caused by the refectory.

This site was of great interest for the investigation because of the nature of the paths over which the signal components arrived at the receiver location. The lack of a LOS path was mentioned above, all other experimental sites had one component arriving on an LOS path. Furthermore none of the components followed a simple path which only included one reflection as in the other experiments. Component 1 originated from a diffracted signal over building G2. Component 3 reflected by the refectory can only have reached the refectory wall by means of either reflection from other adjacent buildings or penetration through building G1. The most likely origin for component 2 is transmission through building G1 and a subsequent diffraction to reach the receiver location. This appears to be the most likely explanation since the library building is much lower in height and is obscured from the view at the receiver. Reflection from this building is therefore unlikely. The part of building H that could have contributed which is immediately adjacent to the library was considered unlikely to reflect any signal onto the face of building G1 because of the orientation of its front wall. Additionally the photograph and the map give an indication of vegetation that is present in the vicinity of the receiver location. This site was capable of demonstrating that exact knowledge about the individual signal paths is not necessary when using the resolution procedure. It further demonstrated that component resolution is possible when signal components arrive on more complex paths than those represented by LOS and a single reflection propagation modes.

The results of this experiment are presented and discussed in section 7.2.

6.3.5 20 GHz measurements in the anechoic chamber

With anechoic chamber facilities becoming available during the project, it was considered useful to conduct experiments on controlled multipath geometries indoors. The anechoic chamber measurements utilized reflector boards to create the multipath geometries. The experiments in the chamber were carried out at the higher frequency of 20 GHz. The measurements were undertaken using a different measurements system to that used in the 11.2 GHz experiments. The different frequency and measurement system can be useful in

demonstrating that experimental results can validate the resolution procedure which is independent of the actual frequency, equipment and path geometries used. In addition to this the anechoic chamber offered an indoor environment independent of environmental changes which may occur during the outdoor experiments. Fluctuations in the microwave signal arising due to movement of the reflectors in the wind in the playing field experiments are eliminated in the indoor measurements. The chamber furthermore offers an environment with very little back-scatter or reflections. Thus well controlled experimental conditions can be set up.

The major disadvantage in these experiments were the relatively small dimensions of the chamber. Compared to the playing field experiments the frequency had nearly been doubled, but only a one tenth of the physical dimensions were available. The displacement of the receiving antenna was between 400 and 800 mm in the experiments conducted in the chamber. Considering the distances of the reflector boards from the receiver, the angles of arrival of the components arising from these reflectors varied a little in moving over the whole length of antenna displacement as stated in section 7.3.1.

Trials were undertaken whereby the DFT was applied to simulated interference patterns of geometries with varying angles of arrival. The variations would only be in the order of a view degrees during the antenna travel. It was found that the DFT procedure produced angles of arrival equivalent to the mean value of the minimum and maximum angle encountered. This meant that as long as the orientation of the reflector board was measured at the half way point of the antenna displacement in every experiment the angle of arrival would be resolved with reasonable accuracy by the procedure.

Figure 6.15 indicates the physical dimensions of the available space within the chamber. The figure shows a principal measurement set up for a three component experiment inside the anechoic chamber. For a two component experiment only one reflector board would be needed (similar to playing field experiments, section 6.3.1.)

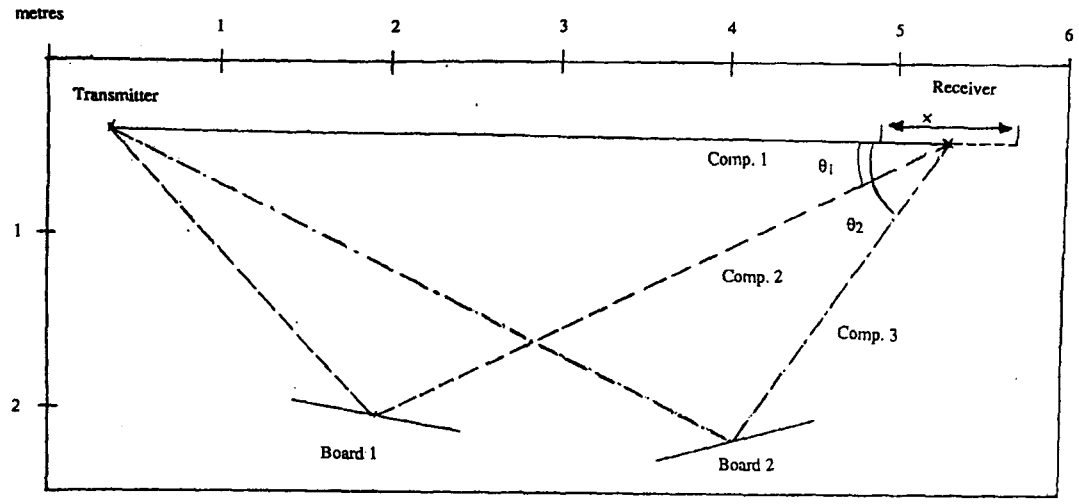

Figure 6.15 *Principal experiment set up for 20 GHz experiments inside the anechoic chamber (three components)*

The reflector boards shown in figure 6.15 are drawn to scale. Solid aluminium sheets of dimension 1 m x 1 m mounted on supporting tripods were used. When setting up a three component experiment care had to be taken that the boards did not obstruct signal paths from and to the other reflector board. It was found that aluminium sheets of this dimension had to be used, because of the relatively long travel of the antenna in comparison to the other distances. Smaller boards would have resulted in smaller areas of specular reflection, outside which the reflected signal level reduces significantly. If the antenna moves outside the specular reflection region of a certain board this will lead to a reducing amplitude of that signal component for certain antenna displacements and lead to a distortion of the amplitude envelope. The theory in chapter 3 considers the individual component amplitudes to be constant over the whole length of antenna displacement.

One experiment with a multipath field arising from two signal components and two experiments involving three component multipath geometries were carried out. The results are presented and discussed in section 7.3

6.4 Assessment of experimental errors

This section presents an assessment of the accuracy obtained in carrying out the described experiments. The assessment considers the factors influencing the system accuracy as well as random and systematic errors that could have arisen during the measurements.

6.4.1 11.2 GHz experiment errors

6.4.1.1 Accuracy of the 11.2 GHz system

The central measuring device in the 11.2 GHz was the spectrum analyzer. The random errors of the signal amplitude measurements are mainly those of the spectrum analyzer. For amplitude measurements at this frequency the manufactures specifications are an accuracy of ± 1 dB.

The gain function of the LNB was measured linearly from the LNB's noise floor to the maximum input, when the LNB saturates and the gain function becomes non-linear. The maximum input level for the LNB was measured at -50 dBm. It was ensured during all 11.2 GHz experiments that this maximum input signal was not exceeded. The small rated noise figure of 1 dB meant little extra noise being introduced by the LNB and a large dynamic range for the experiments from 0 dBm to -85 dBm was available. All the measured amplitude levels during the experiments were well above the LNB noise level, so that random errors from the LNB can be excluded.

All signal amplitude levels stated in the experimental results in section 7.1 are referred to as those obtained at the analyzer input. Both the measurements of the individual signal components of the multipath field and the interference pattern were carried out with the same measurement system. Therefore systematic errors arising from the estimation of the system link budget considering the LNB gain and combined cable and connector losses would be identical in both measurements. Errors arising here will therefore tend to cancel out.
Systematic errors can arise from errors in the measurements of the patterns of the antennas

used in the measurements.

Measurements of the antenna radiation pattern were conducted placing a transmit antenna and the antenna under test on two relatively open elevated locations respectively. A 180 degree radiation pattern measurement was conducted rotating the antenna under test so that its principal axis was turned in the direction of an open valley. The elevated positions of the antennas as well as the open valley contributing to the minimisation of scatter signal reaching the main lobe while measuring the signal received by any side lobe. The accuracy achieved under these conditions can be considered to be around ± 2 dB.

The resulting random error for the amplitude measurements including consideration of the antenna radiation pattern was therefore estimated at ± 3 dB.

6.4.1.2 11.2 GHz Experiments

Signal amplitudes:

A difficult task of the experiment was the measurement of the individual signal components. The playing field experiments had the advantage that after measuring the signal component closest to the receiving antenna the reflector board giving rise to this component could be removed. Then the other reflected signal component could be measured while only the LOS signal from the transmitter had to be blocked off by means of a reflective board. During the experiments on buildings it was of course impossible to remove the sources of the signal components. Here shielding the receiver antenna from other signal components while measuring the component of interest was the only alternative. The error for the measurements of individual signal component was greatest when measuring weak signal components in the presence of stronger components in the compound field. The high directivity and careful shielding of the antenna from unwanted signals allowed measurements of the component of interest with reasonable accuracy. The geometries had been chosen and set up, so that in comparison to the beamwidth of the receiving antenna there was a sufficient spatial separation of the angles of arrival thus aiding the measurement of individual components.

For weaker signal components an additional error is very likely. Here because a stronger component through a side-lobe of the measuring antenna could result in a comparable contribution it will be difficult give a precise figure assessment.

Accuracy of measured angles:

The angles of arrival of the signal components were determined in both the playing field and the building measurements using a theodolite. The theodolite itself is a very accurate instrument and allows angle measurements as a accurate as ± 20". During the experiment the location of the centre of the reflector boards was marked using the theodolite. After the boards had been placed at this marked location they were then adjusted so that the receiver obtained a maximum signal from the reflection of the board. This ensured that the specular reflection of the transmitted signal was directed towards the receiver. Considering this the measurement of the angles of arrival cannot be assumed any more accurate than ± 1°.

This figure must also be considered reasonable for the building experiments. The theodolite was used to determine the angles under which the sources giving rise to the signal components could be seen from the receiver location. Nevertheless it was in many cases difficult to determine from which exact point of the structure (e.g. large wall) the signal component originated from.

An additional random error for the angles of arrival arises from the alignment of the direction of displacement of the receiving antenna with the direct propagation of one of the signal components. During the experiment the steel rail on which the antenna is displaced was aligned with the source of one of the signal components. The alignment of the steel rail is possible to an accuracy of around ± 1°.

The resulting random error for the angle measurements is thus estimated at ± 2°.

6.4.2 20 GHz system experimental errors

Signal amplitudes:

The 20 GHz used a logarithmic amplifier, data acquisition board and a PC to measure the signal amplitude level. This system was calibrated so that this system including the mixing stage used in converting the 20 GHz RF signal down to an IF signal of 220 MHz. The log. amplifier together with the data acquisition are scaled so that dBm values representing the output signal from the antenna. The calibration insured an accuracy of the system around ± 1 dB.

The antenna radiation patterns of the 20 GHz antennas were measured in the anechoic chamber and can be considered more accurate than the outdoor measurement used in the 11.2 GHz system. The radiation patterns can be considered to have an error of ± 1 dB.

Similarly to the 11.2 GHz experiments the same system was used for the measurement of both the individual components and the amplitude envelopes. Systematic errors concerning the equipment would arise in both measurements and would cancel each other out. Again the antenna radiation pattern can be a source of systematic errors.

As in the 11.2 GHz experiments an additional source of errors was caused by the measurement of the individual signal components. Similar considerations thus arise here. Great care was taken when measuring the individual components, by utilizing the directivity of the receiving antenna and the use of metal sheets to shield off unwanted contributions for each particular measurement. As in the 11.2 GHz experiments an additional error in the estimation of weaker components must be considered.

Accuracy of measured angles:

The dimensions of the anechoic chamber allowed the geometry for each experiment to be determined. Distances were measured between transmitter, reflector boards and the receiver, plus relative distances of reflector boards with respect to the transmitter receiver line. From

these all the resulting angles were calculated. The angles of arrival at the half way point of displacement of the receiving antenna determined in this way were considered to be accurate within ± 1°. The direction of antenna displacement as in the 11.2 GHz experiments was estimated to be in error of ± 1°.

The resulting random error for the angle measurements of the 20 GHz experiments was estimated at ± 1°.

6.5 Interim conclusion of chapter 6

Descriptions of a range of different experiments conducted during the experimental program were presented. The university playing field offered a useful environment for the measurements of different multipath geometries created using reflector boards. Largely controlled and repeatable experiments were possible on these fields.

Predictable multipath environments in which controlled measurements could be conducted were difficult to find. A survey revealed two locations at which experiments were carried out in multipath geometries created by effects of existing buildings. These experiments were conducted to validate the developed resolution procedure and demonstrate its practical usefulness.

Anechoic chamber experiments were carried out at a different frequency using a different receiver and measurement system. This was considered of value in demonstrating the validity of the resolution procedure at different operating frequencies.

The results of the experimental measurements are presented in chapter 7, where their implications are discussed.

CHAPTER 7 RESULTS OF EXPERIMENTS AND THEIR ASSESSMENT

In this section the results of the various experiments described in chapter 6 are presented and are discussed for each set of experiments. For presentation and discussion of the results the different sets of experiments are divided into the same categories used in chapter 6.

In all sets of the experiments the multipath geometry will be described by stating the angles of arrival of the signal components giving rise to the multipath field. These angles of arrival refer to the direction along which the signal component originates with respect to the direction of receiver antenna displacement. The measured amplitudes stated for the individual signal components are the result of the signal magnitude measured considering the effect of the radiation pattern of the receiving antenna. The received interference pattern (amplitude envelope) is the result of the interaction of the signal components considering the angular gain function of the receiving antenna. The component resolution procedure results are derived from the received amplitude envelope. In order to compare the individually measured component amplitudes with those produced from the application of the procedure their amplitudes must be adjusted to the level the receiving antenna receives at the given angle. This means that the individually measured amplitude since it was obtained through the main lobe of the measuring antenna must be reduced by the appropriate value at a given angle of arrival due to the antenna radiation pattern.

7.1 Results of playing field experiments

The set of experiments carried out on the university playing fields consists of four different experiments. Four different multipath geometries were created using the reflector boards. The transmitter signal was received as line of sight signal. The receiving antenna was directed towards this signal and also displaced in the propagation direction of this signal. The first experiment was carried with one reflector board, which results in a multipath geometry of two constituent components. In the remaining three experiments two reflector boards were used, resulting in multipath geometries of three constituent components in each case.

Table 7.1 shows the geometries chosen in each experiment. The measured geometry (angles of arrival) and individual amplitudes under consideration of the antenna radiation pattern are listed as individual measurements in the three left hand columns of the table. The results of the resolution procedure applied to the measured interference pattern are listed in the three right hand columns.

Figures 7.1 to 7.4 show the received amplitude envelopes in each experiment.

	Individual measurements			Resolution procedure results		
	Comp. 1	Comp. 2	Comp. 3	Comp. 1	Comp. 2	Comp. 3
Experiment 1 **Amplit. [dBm]** (2 components) **Angle θ**	-10.9	-14.1	---	-10.3	-15.1	---
	0°	45°	---	0°	43°	---
Experiment 2 **Amplit. [dBm]** (3 components) **Angle θ**	-3.6	-32.0	-16.3	-4.4	-27.4	-16.4
	0°	22°	45°	0°	27°	44°
Experiment 3 **Amplit. [dBm]** (3 components) **Angle θ**	-8.9	-26.3	-20.9	-9.0	-26.6	-21.0
	0°	22°	43°	0°	23°	42°
Experiment 4 **Amplit. [dBm]** (3 components) **Angle θ**	-13.2	-22.3	-21.0	-13.3	-21.9	-25.5
	0°	22°	32°	0°	22°	33°

Table 7.1 *Results of playing field measurements*

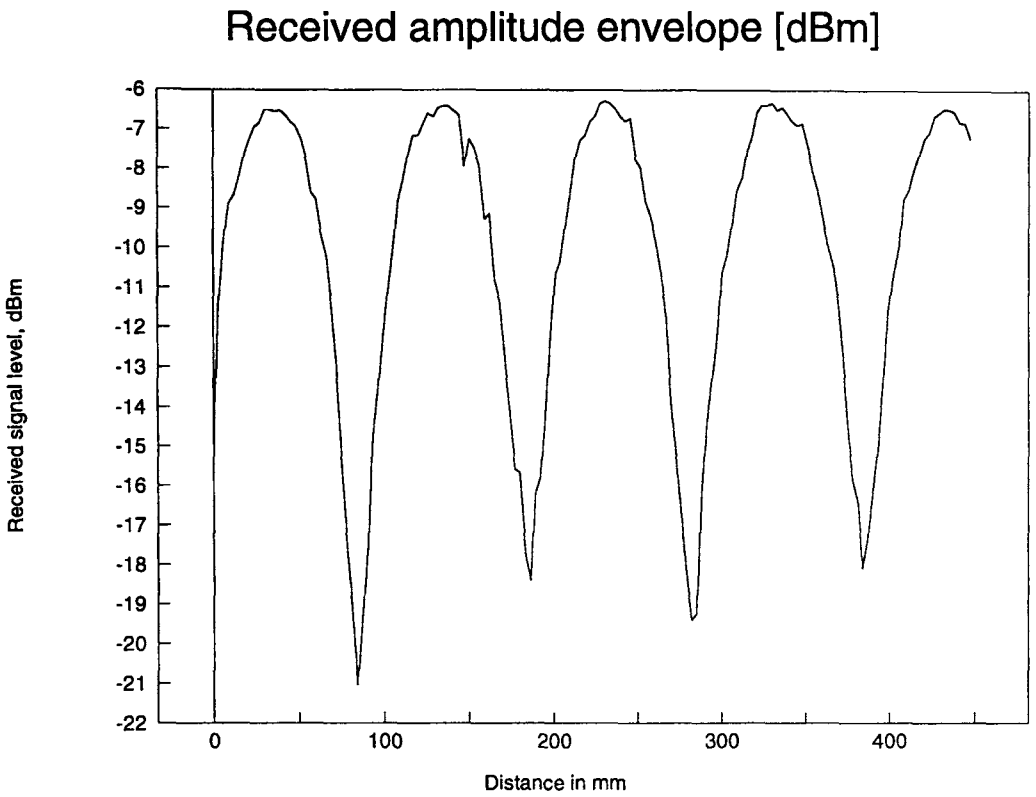

Figure 7.1 *Received amplitude envelope in 1. playing field experiment (two components)*

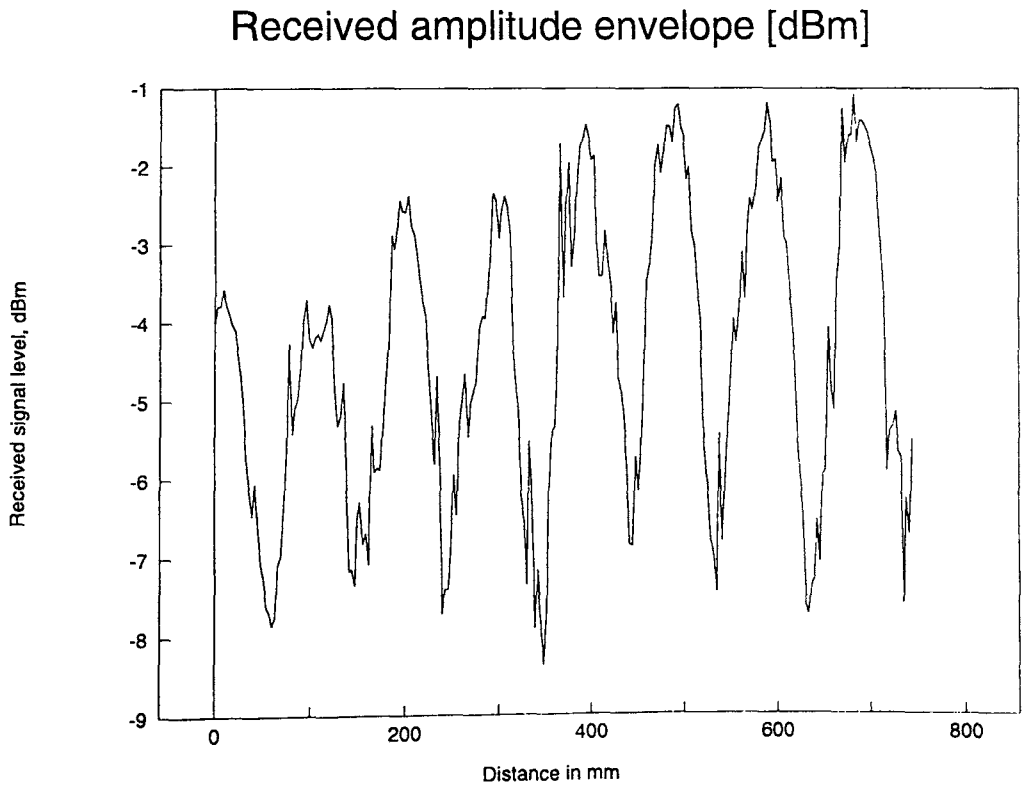

Figure 7.2 *Received amplitude envelope in 2. playing field experiment (three components)*

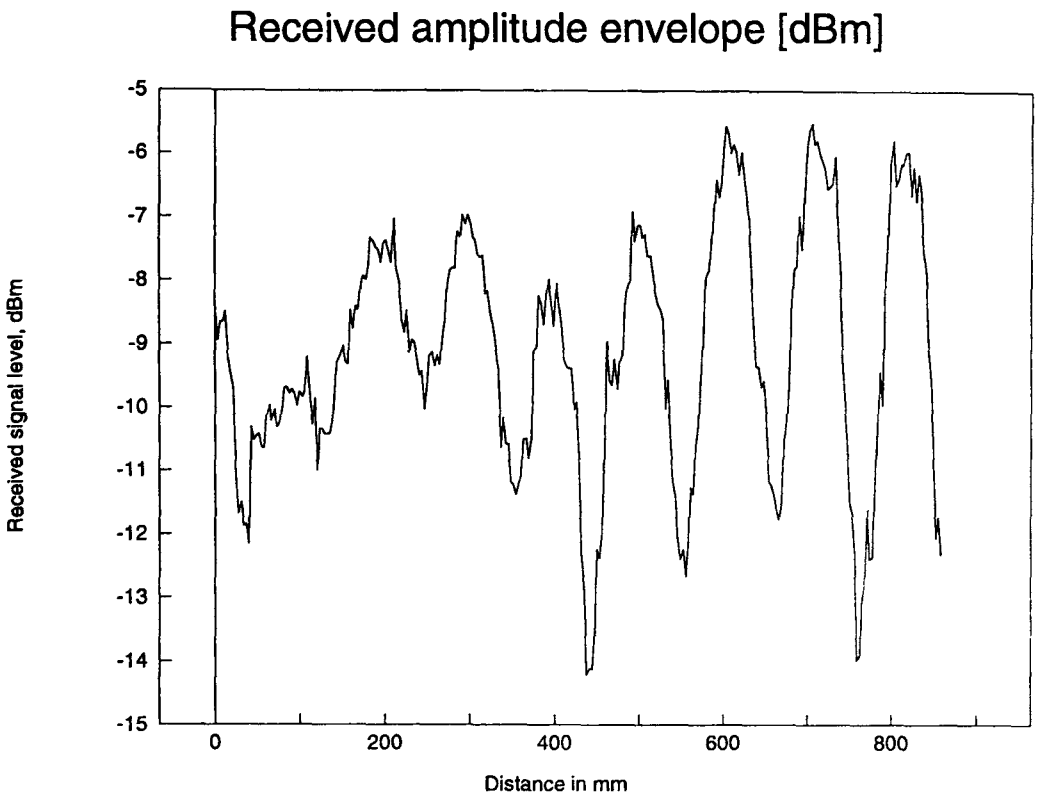

Figure 7.3 *Received amplitude envelope in 3. playing field experiment (three components)*

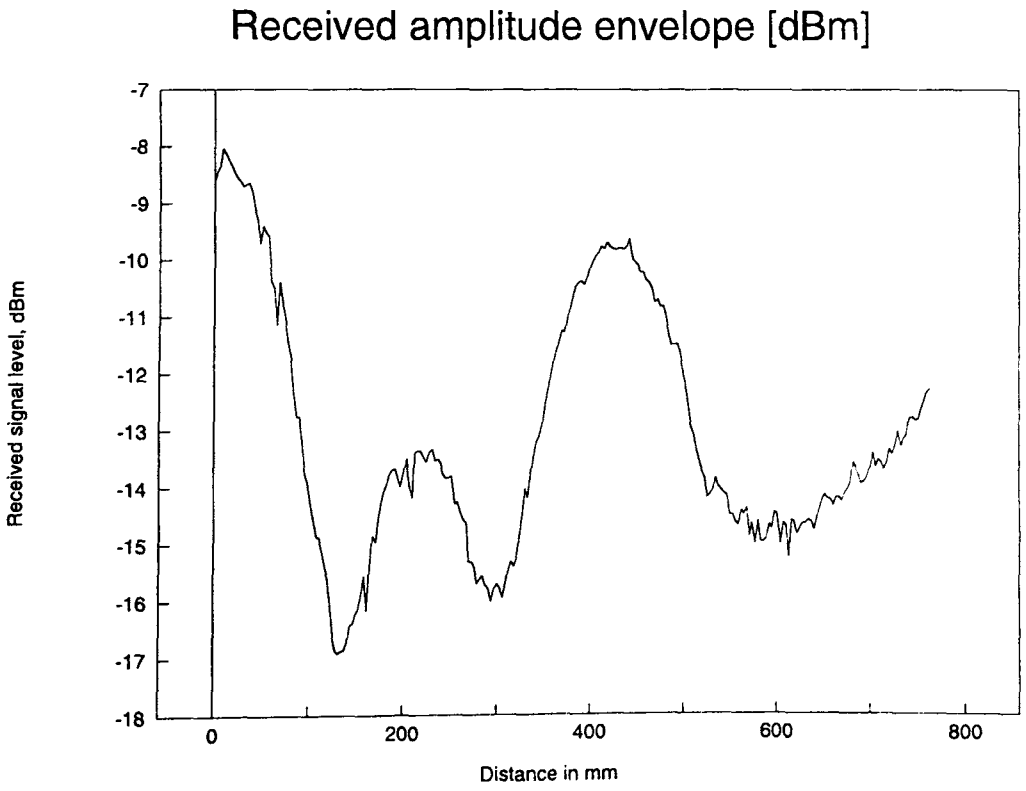

Figure 7.4 *Received amplitude envelope in 4. playing field experiment (three components)*

7.1.1 Discussion of playing field results

The received amplitude envelopes in the playing field experiments show that it was possible to set up multipath geometries. The arising interference pattern, recorded over distance, by displacing the receiving antenna clearly demonstrated the occurrence of a multipath field. Amplitudes and angles of arrival of the signal components giving rise to the interference pattern were derived using the developed component resolution procedure. The comparison in table 7.1 between the individually measured multipath components and results of the component resolution procedure show good agreement. The amplitudes listed under 'individual measurements' are derived from measurement of individual component levels and measured radiation pattern. The resulting random error for the two combination of the two measurements as shown in section 3.4.1 is ± 3 dB. The same section states random error for the angles of arrival of $\pm 2°$. Nearly all figures for the individual component measurements compare with the resolution procedure results within these errors. As stated in section 3.4.1 an additional error for the individual component amplitudes is possible due to the interference from the other signal components during the individual component measurement.

The results are within the random error determining the accuracy of the measurements. This suggests that this individual component measurements were in most cases sufficiently accurate.

One exception can however is the second component in the second experiment. It is significant that both the amplitude and the angle of arrival in this case differ between the two measurements. The resolution procedure gives an angle of arrival that exceeds the one in the individual measurement by 5°, and an amplitude for this component that is nearly 5 dB more than the individually measured. The combination of these two factors indicate an error in positioning the reflector board with respect to the location marked by the theodolite, leading to a larger angle of arrival than indicated. This is supported when considering the shape of the function of the antenna radiation pattern at these angles.

The slope of the antenna radiation pattern is very steep at the angles in question. An increased angle of 5° results in an increase in gain of the order of the difference between the two

measurements. The antenna radiation pattern is used to calculate the signal components strength with the effect it has on the interference pattern as received by the antenna. Had the gain been underestimated due to using the wrong angle of arrival the amplitude for this component as seen by the receiving antenna would also have been underestimated. This makes an error in the positioning of the reflector board the most likely explanation for the discrepancy.

7.2 Results of building measurements

As in the playing field experiments the existence of multipath field was observed by the presence of an interference pattern. Component signal levels could be derived from the measurement of the interference pattern using the resolution procedure. The results of the resolution procedure in comparison to individual measurements are summarized in table 7.2. The received amplitude envelopes are shown in figures 7.5 (Birmingham) and 7.6 (campus).

	Individual measurements			Resolution procedure results			
	Comp. 1	Comp. 2	Comp. 3	Comp. 1	Comp. 2	Comp. 3	Comp. 4
Experiment 1 **Amplit. [dBm]** (Birmingham)	-7.5	-19.7	-44.3	-6.9	-21.0	-36.7	-33.5
Angle θ	0°	47°	73°	0°	47°	75°	57°
Experiment 2 **Amplit. [dBm]** (Campus of UoG)	-34.0	-47.6	-60.4	-34.9	-47.8	-56.7	--
Angle θ	0°	29°	41°	0°	30°	42°	--

Table 7.2 *Results of building experiments*

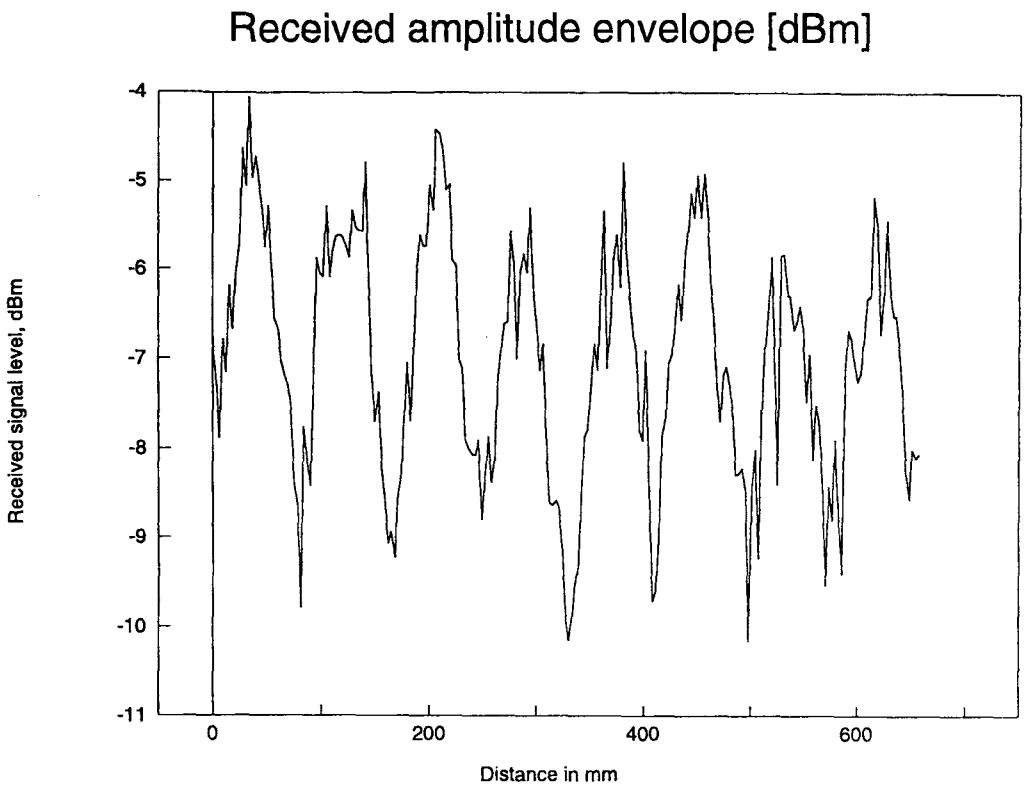

Figure 7.5 *Received amplitude envelope of Birmingham experiment*

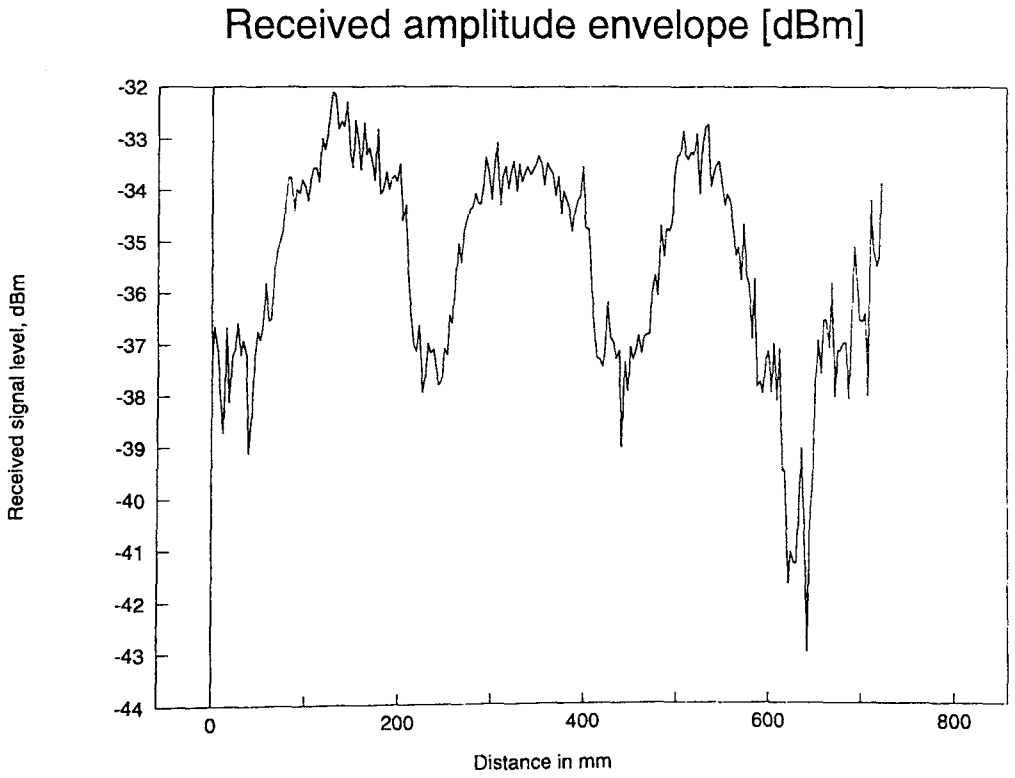

Figure 7.6 *Received amplitude envelope of campus experiment*

7.2.1 Discussion of results of building measurements

Birmingham experiment:

The experiment at the site near Birmingham produced one very interesting result, that is also indicated in section 6.3.3.1. The resolution procedure revealed an additional signal component to those considered when setting up the experiment. A fourth component was clearly evident from the result of the resolution procedure. The resolved angle of arrival of this component is in direction of the second tower block. This fourth component was resolved as:

Amplitude: -33.5 dBm

Angle of arrival: 57°

Since the contribution from the second tower block had not be regarded significant when setting up the experiment the signal amplitude of this signal had not been measured. Therefore the resolved amplitude level cannot be compared to any individual measurement. It is encouraging however that it was possible using the procedure to identify a source of a multipath signal component not considered from a preliminary examination of the path geometry.

Both experiment sites:

Using a similar experimental method and the same measurement system as in the playing filed experiments random errors from these experiments can be considered to be the same as in the previous set of experiments.

The angles of arrival in both experiments are resolved within the random error band of $\pm 2°$. The agreement between individually measured component amplitudes and values resulting from the resolution procedure is very good for the two stronger signal components in both experiments. Significantly in both experiments the weakest component has been overestimated. In the Birmingham experiment the weakest component is overestimated by nearly 8 dB by the resolution procedure. In the campus experiment it is nearly 4 dB. In both experiments these components were very weak in comparison to the strongest received one.

In the Birmingham experiment the difference considering the antenna radiation pattern between the strongest and the weakest component is nearly 37 dB. The weaker components are the ones likely to be measured incorrectly during the individual amplitude measurements in the presence of stronger components, although in both cases the difference is very significant. Also both components have been measured as of weaker level in the individual measurements compared to the resolution procedure results. Therefore in both cases a stronger component would have had to interfere destructively with the signal of the weaker component to lead to a smaller value being measured. The spatial separation between the direction of the weaker component and the direction of arrival of the stronger ones is relatively large in both cases (see maps in section 6.3.3), and all the stronger signal components originate from one side looking in direction of the weaker component. Both these factors combined should have made it possible to measure the weaker component more accurately than the figures suggest.

A more likely explanation for the differences between the figures is discussed in section 8.3.2. It is the influence of noise on the DFT. Both received amplitude envelopes show some fluctuation resembling noise rather than a regular pattern of component interference. In both cases the amplitudes of the weak signal components will be close to the experienced noise level of the spectra. As shown in section 8.3.2 and documented by Prewit (1978) signal levels of signals with a low signal to noise ratio will be overestimated by the DFT. This indicates one explanation why only the weak signal components are overestimated by the resolution procedure. On the other hand as stated before in practical multipath situations it is strictly speaking impossible to measure component amplitudes individually. The interaction of other components arriving at the measuring antenna through a side lobe with the main lobe signal may have introduced additional errors in the measurements of the weaker components.

7.3 Results of anechoic chamber experiments

At the higher frequency of 20 GHz interference patterns were recorded in multipath geometries set up using reflectors. Multipath signal components were derived from the

interference patterns. Table 7.3 lists a comparison of the results from the resolution procedure and individual signal component amplitude measurements. As in the case of the 11.2 GHz experiments the individual component amplitudes listed have been calculated considering the antenna radiation patterns of the receiving antenna. The receiving antennas in the 20 GHz measurements were microwave horn antennas as opposed to the parabolic dish reflectors in the 11.2 GHz experiments. A 10 dBi horn was used for the first and second experiment and a 20 dBi horn for the third one. The different geometries used are listed in table 7.3. The recorded amplitude envelopes are shown in figures 7.7 to 7.9.

	Individual measurements			Resolution procedure results		
	Comp. 1	Comp. 2	Comp. 3	Comp. 1	Comp. 2	Comp. 3
Experiment 1 **Amplit. [dBm]** (2 components)	-39.9	-48.9	--	-39.6	-49.8	--
Angle θ	0°	37°	--	0°	38°	--
Experiment 2 **Amplit. [dBm]** (3 components)	-8.4	-13.2	-17.3	-8.0	-14.4	-20.5
Angle θ	0°	26°	48°	0°	26°	46°
Experiment 3 **Amplit. [dBm]** (3 components)	-19.0	-28.0	-34.5	-18.3	-28.6	-37.8
Angle θ	0°	30°	51°	0°	32°	53°

Table 7.3 *Results of anechoic chamber experiments*

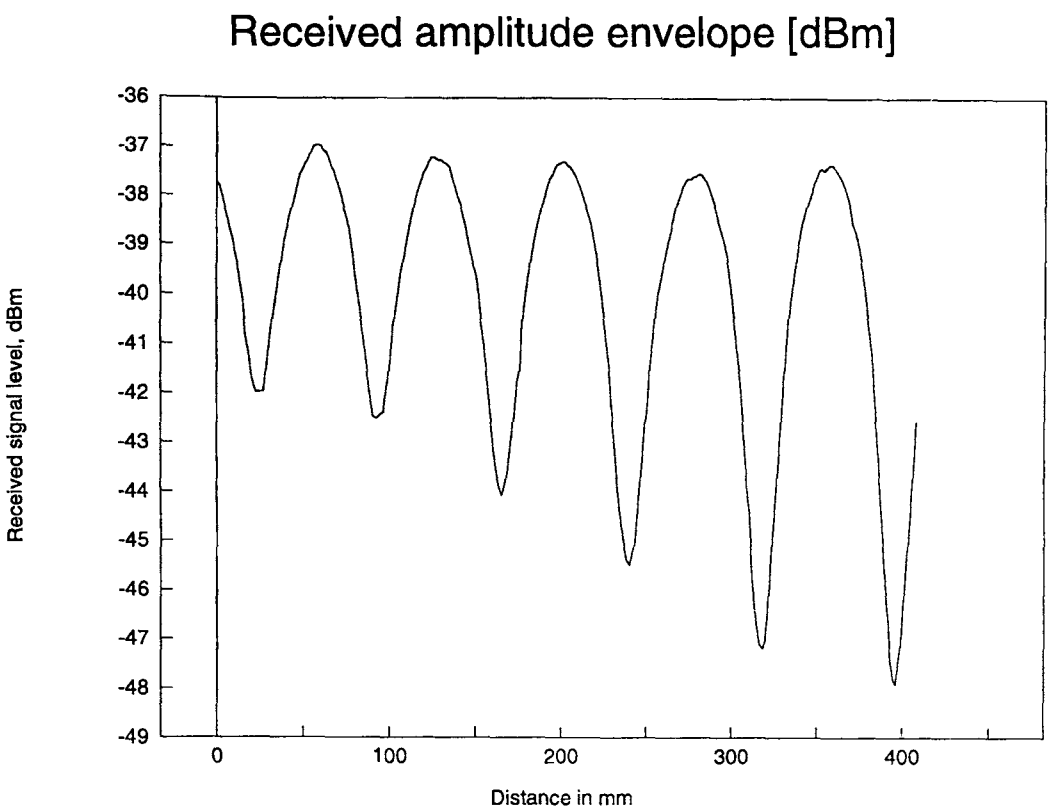

Figure 7.7 *Received amplitude envelope in first anechoic chamber experiment*

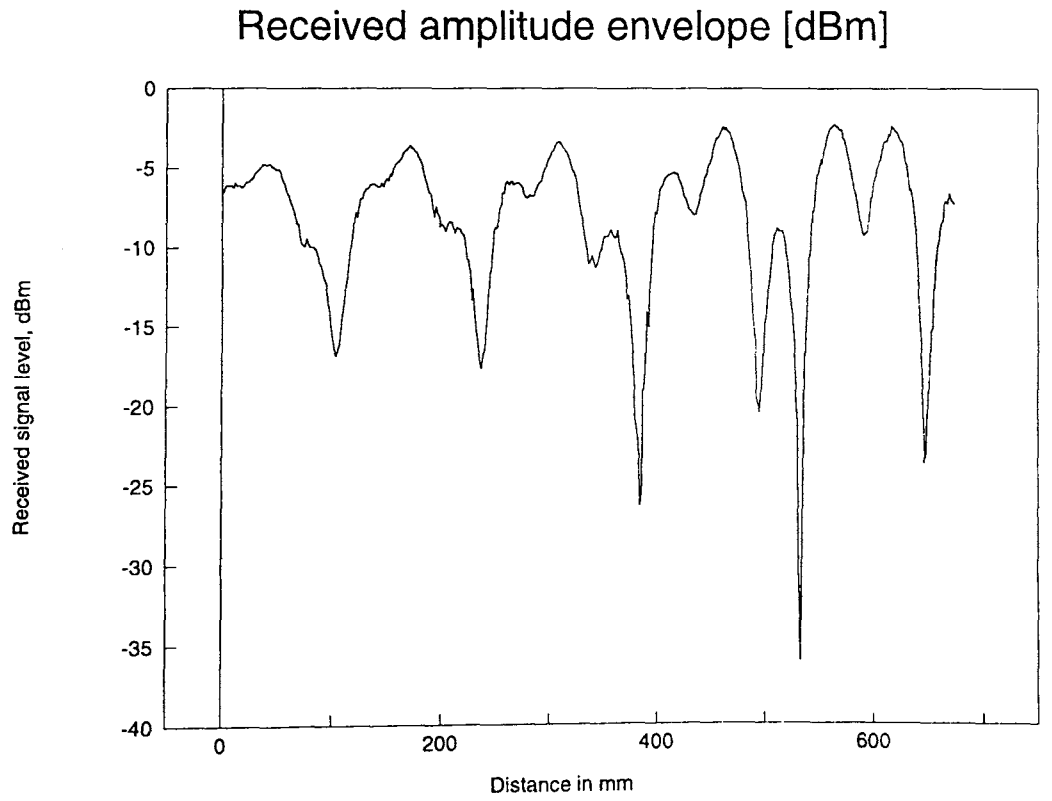

Figure 7.8 *Received amplitude envelope in second anechoic chamber experiment*

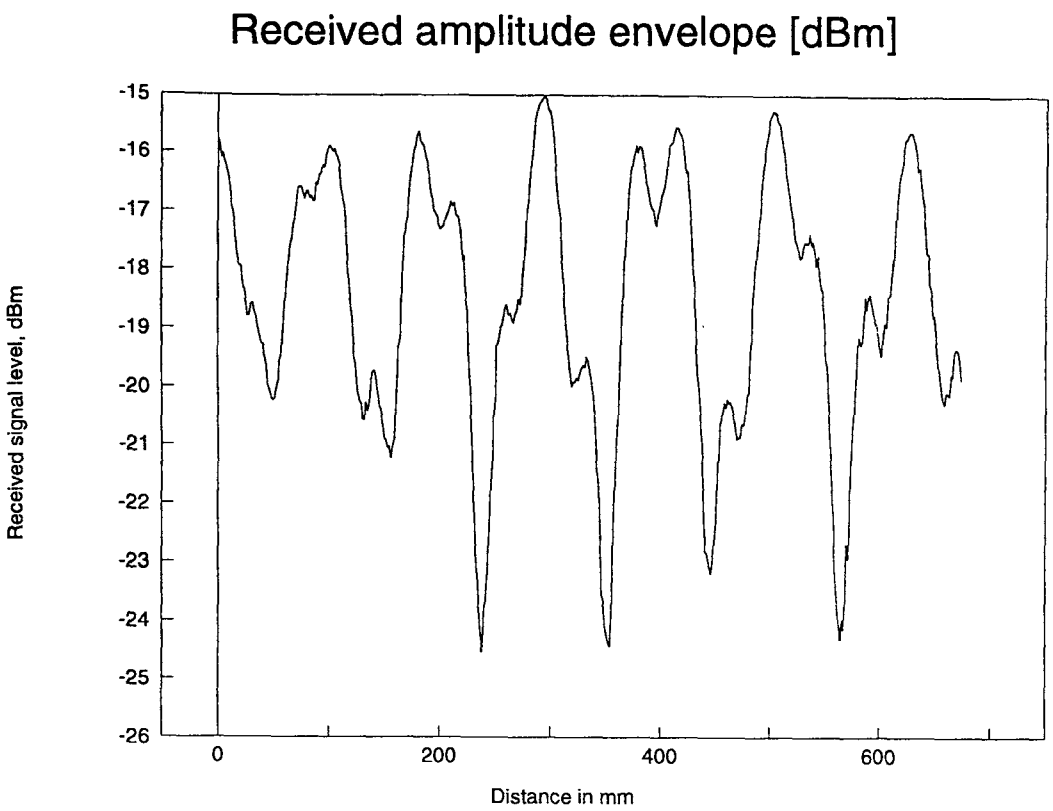

Figure 7.9 *Received amplitude envelope in third anechoic chamber experiment*

7.3.1 Discussion of anechoic chamber measurements

Comparing the graphs of the received amplitude envelopes above with those recorded on the playing fields at 11.2 GHz in section 7.1 the curves appear much smoother. This confirms that the signal fluctuations due to e.g. reflector board movement were successfully eliminated in the indoor experiments. The angles of arrival were resolved by the resolution procedure with the expected $\pm 2°$. This represents a very good result considering that angles of arrival change by a few degrees during the displacement of the receiving antenna, being comparable to other path geometry dimensions.

The agreement between the amplitude values resulting from individual measurements and from the resolution procedure is generally good. The amplitude of the 0° component and smaller angle of arrival in the three components experiment as well as both components in the two component experiment agree very well in the two measurements. There is a

difference of around 3 dB in the component amplitude levels of the larger angle components between individual measurement and resolution procedure result. This is somewhat disappointing as it exceeds the random error of ± 2 dB of the experiments. A possible explanation can be due to the size of the displacement distance of the receiving antenna in comparison to the overall dimensions of the anechoic chamber. The receiving antenna was moved out of the area of specular reflection of the larger angle reflector board. This meant that the reflected signal decreased in amplitude during the displacement.

According to Ding (1994) the width w of the specular reflection area in azimuth direction of a near perfect conductor is:

$$w = a \cos\theta_0 \tag{7.1}$$

where: a is the length of the reflecting surface

θ_0 is the angle of incidence (or reflection) of the signal arriving at the board with respect to the normal.

For the larger angle signal components in the three component experiments the angle θ_0 was around 50°. For a 1 m reflector board this results in a specular region of 64 cm at the location of the receiver antenna displacement. This is approximately the length of the antenna displacement so that any slight misalignment of the reflector board with respect to the area of displacement of the receiver antenna would affect the measurement of the amplitude envelope. The alignment of the reflector board at such oblique angles of incidence for the signal is relatively difficult and a misalignment was likely.

If in the third anechoic chamber measurement the last half of the recorded amplitude envelope are used to resolve the multipath geometry, the resulting amplitudes are:

A_1 = -18.4 dBm, A_2 = -27.9 dBm, A_3 = -33.9 dBm,

which only differ from the individual component amplitude measurements by less than 1 dB and are hence well within the expected measurement accuracy.

In the second chamber experiment the figure for A_3 varied even more through the travel of

the receiving antenna. If only the latter part of the received pattern is considered the following amplitudes are recorded:

A_1 = -8.6 dBm, A_2 = -13.3 dBm, A_3 = -15.8 dBm.

The individually measured value for A_3 lies between this result and the one given in table 7.3.

The third anechoic chamber measurement is used in the following as an example for demonstrating the validity of the achieved results.

The results of the resolution procedure will be used for a simulation of the interference pattern for this example using the computer simulation described in section 3.1.2. The simulated interference pattern is shown in figure 7.10. For easier comparison the measured record is shown again in figure 7.11. The simulation used the results obtained from latter half of the amplitude envelope to avoid the area of non-specular reflection for the third component, as explained above. The simulation did not consider the changing angle of arrival, which increases in the measurement towards the end of the record. Therefore a lower rate of variation can be observed towards the end of the recorded pattern. Otherwise simulated and actual recorded amplitude envelope are very similar.

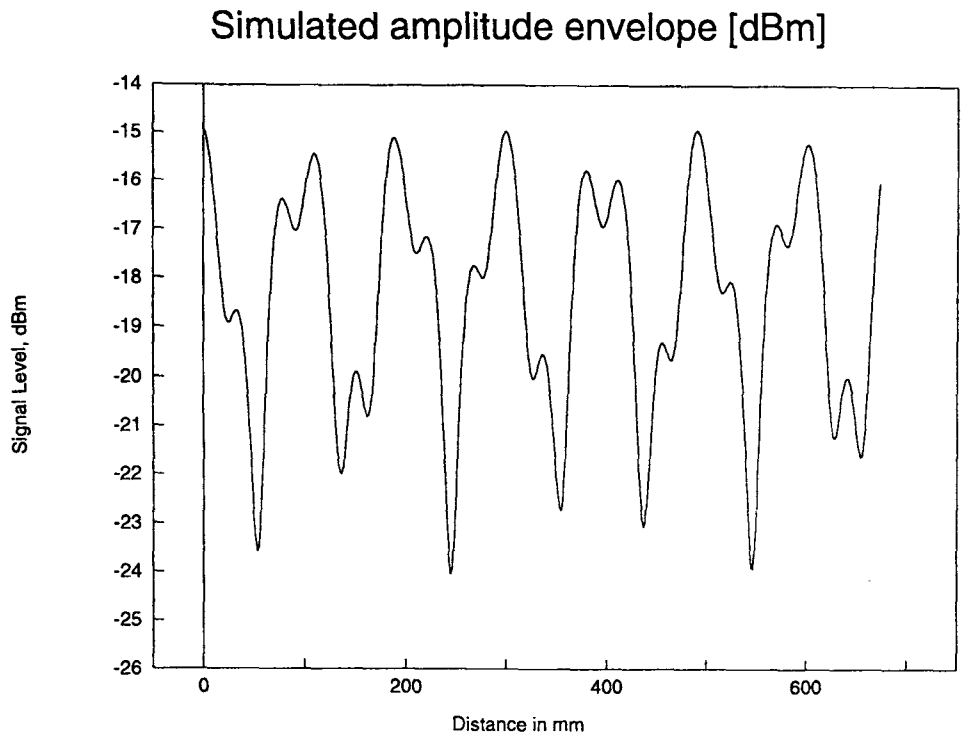

Figure 7.10 *Simulated amplitude envelope using results of third chamber experiment for the simulation*

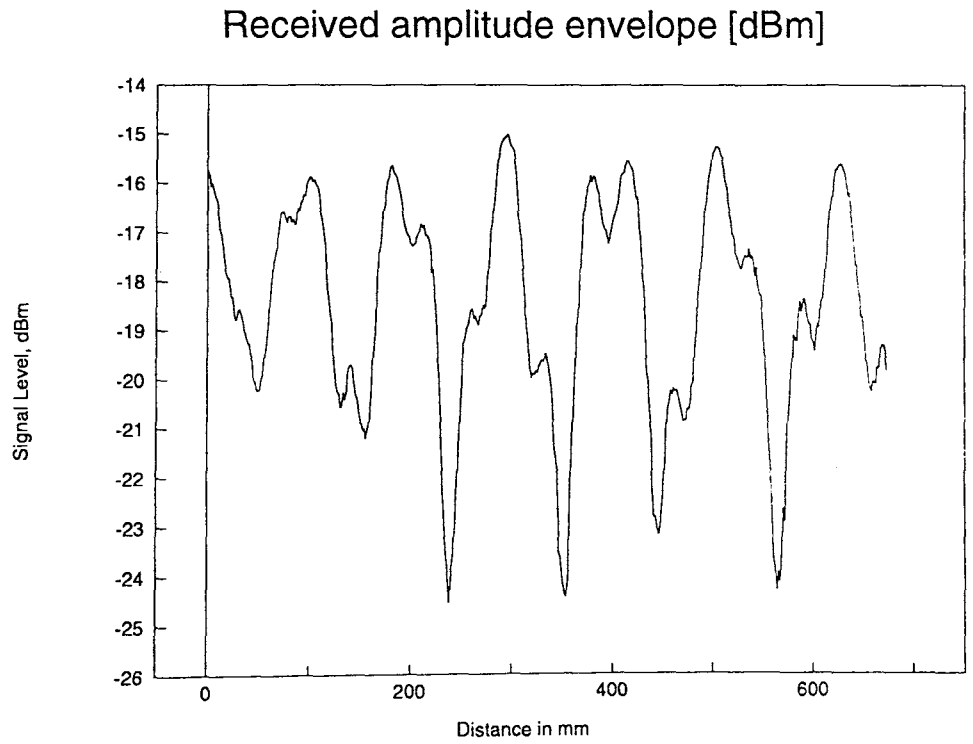

Figure 7.11 Measured amplitude envelope for comparison with figure 7.10

7.4 Interim conclusion of chapter 7

The results of the experiments presented in this chapter show that the multipath signal components can be resolved from a recorded amplitude envelope. Experiments were conducted in three different environments and at two different frequencies. The environments were outdoor experiments using reflector boards, outdoor experiments in multipath geometries caused by buildings and indoor experiments inside an anechoic chamber using reflector boards. The outdoor experiments were conducted at 11.2 GHz and the indoor ones at 20 GHz. It was possible to resolve the multipath components of the multipath geometries in the experiments in all these cases. The majority of the experimental results comparing amplitudes and angles of arrival of individually measured multipath components with those resolved using the developed procedure give good agreement and fall within errors estimated. Exceptions in both the playing field and the anechoic experiments can be explained by systematic errors during the experiments. The exception in the playing field experiment is the result of an error when aligning one of the reflector boards. In the anechoic chamber the differences are caused by moving the receiving antenna out of the region of specular reflection of one of the reflector boards, due to the small dimensions of the chamber.

The building experiments showed that the resolution procedure revealed a signal component thought to be insignificant when setting up the experiment. It appears that relatively weak signal components will be overestimated by the DFT procedure. This can be related to noise, which will be discussed in section 8.3.

Overall the results of the experiments validate the developed resolution procedure. Overall the procedure can be implemented in real multipath scenarios with relatively inexpensive means and yield accurate information about the constituent components of a multipath field.

CHAPTER 8 ACCURACY, RESOLUTION AND LIMITATIONS OF RESOLUTION PROCEDURE

8.1 Introduction

This chapter investigates the factors influencing the accuracy of the developed resolution procedure. Factors have an influence on the resolution and limitations of the procedure are discussed. The first part focuses on angles of arrival results, whereas the second part discusses factors influencing the resolution of component amplitudes including the influence of noise.

8.2 Angular resolution of the procedure

The angles of arrival result from the spatial frequencies using equation 4.4 derived in section 4.1:

$$\theta_j = arcos(1 - f_{sp1j}) \qquad \text{with j = 2,3, ... , n} \tag{4.4}$$

The sampling interval in the spectrum of the DFT is the reciprocal of the record length in the spatial domain. If T is the record length in the spatial domain expressed in units of wavelength λ the sampling interval in the spatial frequency domain is:

$$\Delta f_{sp} = \frac{1}{T} \tag{8.1}$$

θ_j is measured with respect to θ_1 equating to 0

In the sampled spatial frequency domain the error in the resolved spatial frequencies will be $\pm\Delta f_{sp}$. The *arcos* function is a non-linear function so that negative and positive errors have to be considered separately. Using the equations above and plotting positive and negative errors in two separate graphs produces curves as shown in figures 8.1 and 8.2. They show the percentage error in the calculation of angles of arrival depending on the value of the angle.

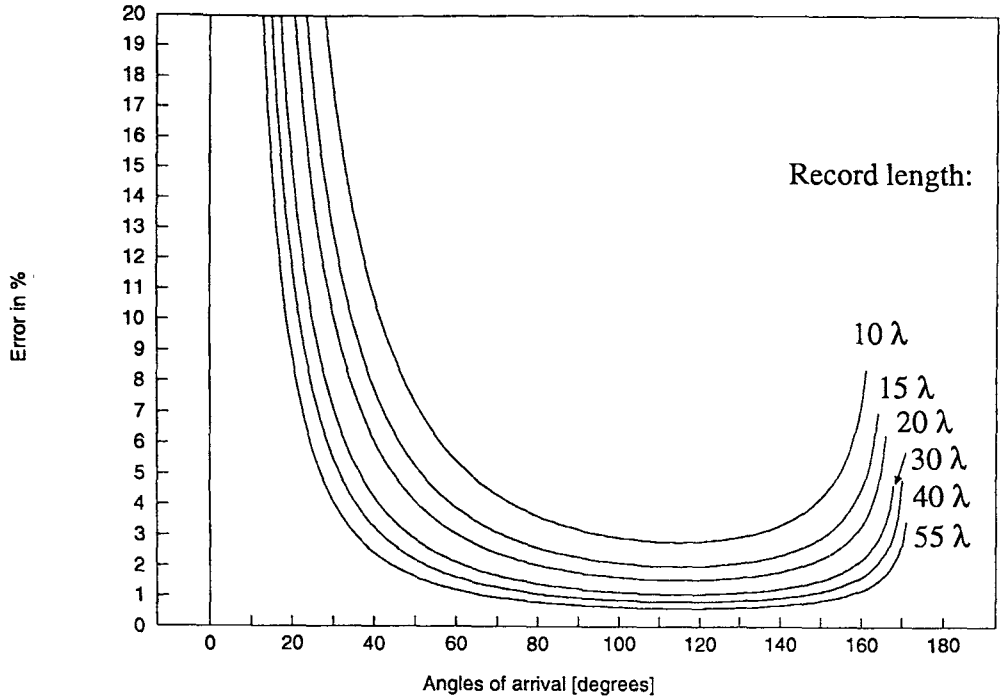

Figure 8.1 *Positive errors of angles of arrival, depending on spacial domain record length when using a single DFT*

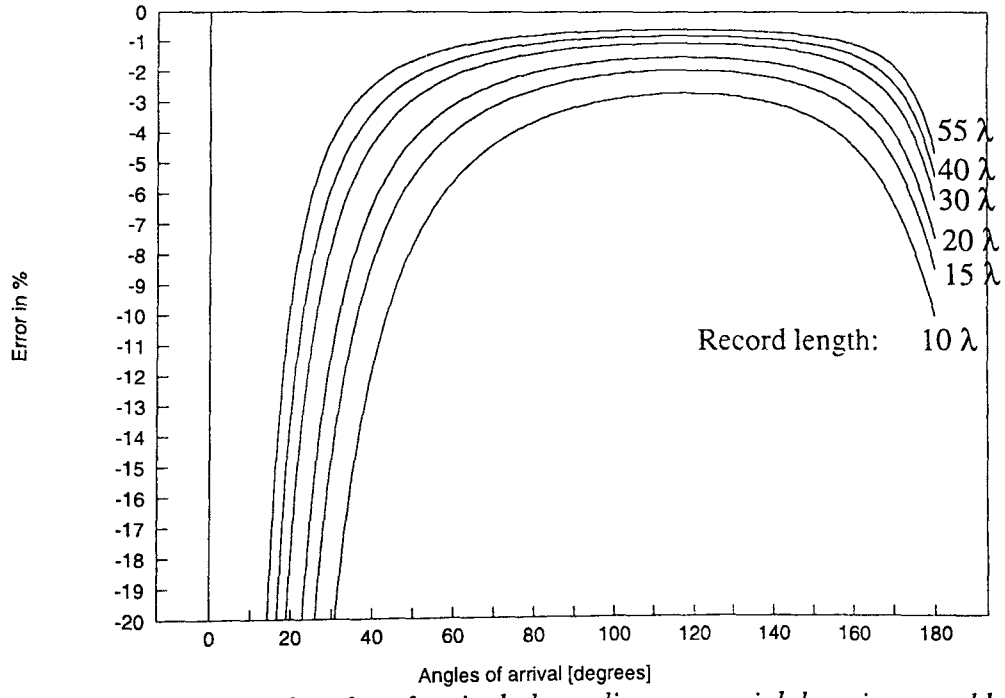

Figure 8.2 *Negative errors of angles of arrival, depending on spacial domain record length when using a single DFT*

The different curves have the record length in the spatial domain as a parameter. The record length is expressed in units of wavelength λ.

The graphs shown in figures 8.1 and 8.2 represent the theoretical error for angles of arrival resulting from using one DFT on the square of the amplitude envelope and using its spectrum to resolve the multipath components. However the results shown in section 5.3 where the developed resolution procedure was applied to simulated amplitude envelopes show much smaller errors that those indicated in figures 8.1 and 8.2.

The record lengths used for the simulations were between 14 and 22 λ. Yet the errors experienced are below 2% and often much smaller than that depending on the multipath geometry simulated. These small errors are achieved by using the adaptive window size method described in section 5.2.2. This method will always attempt to find a record length in the spatial domain that is an integer multiple of cycle length of the spatial frequency component in question. Because of the integer relationship between cycle length and record length the spatial frequency line should ideally coincide with a sampling point in the spatial frequency domain. Inaccuracies can however arise from the fact that the record in the spatial domain is also sampled. The record length as integer multiple of a cycle record can only be achieved within the sampling interval in the spatial domain.

The sampling interval is determined by the number of samples the record comprises. The simulations were carried out on records of 512 sampling points and the measured amplitude envelopes were recorded using length between 200 and 450 sampling points. Applying the adaptive window size procedure gradually reduces the record length to a chosen minimum of half the original length. Nevertheless the sampling intervals are relatively small and the errors of fitting a window whose size is an integer multiple of the cycle length to each spatial frequency component will be small. This explains the increased accuracy when using the adaptable window size, as shown in section 5.3.

8.2.1 Minimum resolvable angle difference

The size of the sampling interval Δf_{sp} determines how closely spaced adjacent angles of arrival can be, for them to be distinguishable. The sampling interval in the spatial frequency domain is the reciprocal of the record length in the spatial domain, therefore this record length determines the resolvable angle difference. Because of the non-linear nature of the *arcos* function a different angle difference can be expected for $f_{sp} + \Delta f_{sp}$ and $f_{sp} - \Delta f_{sp}$. Figures 8.3 and 8.4 show for each angle of arrival how closely spaced the nearest angle of arrival can be depending on the spatial domain record length. Figure 8.3 shows the minimum angular resolution in the case of $f_{sp} + \Delta f_{sp}$. Figure 8.4 shows the minimum angular resolution in the case of $f_{sp} - \Delta f_{sp}$. The angle difference in the latter case leads to smaller angles compared to the one at f_{sp}, therefore the angle difference is displayed as negative.

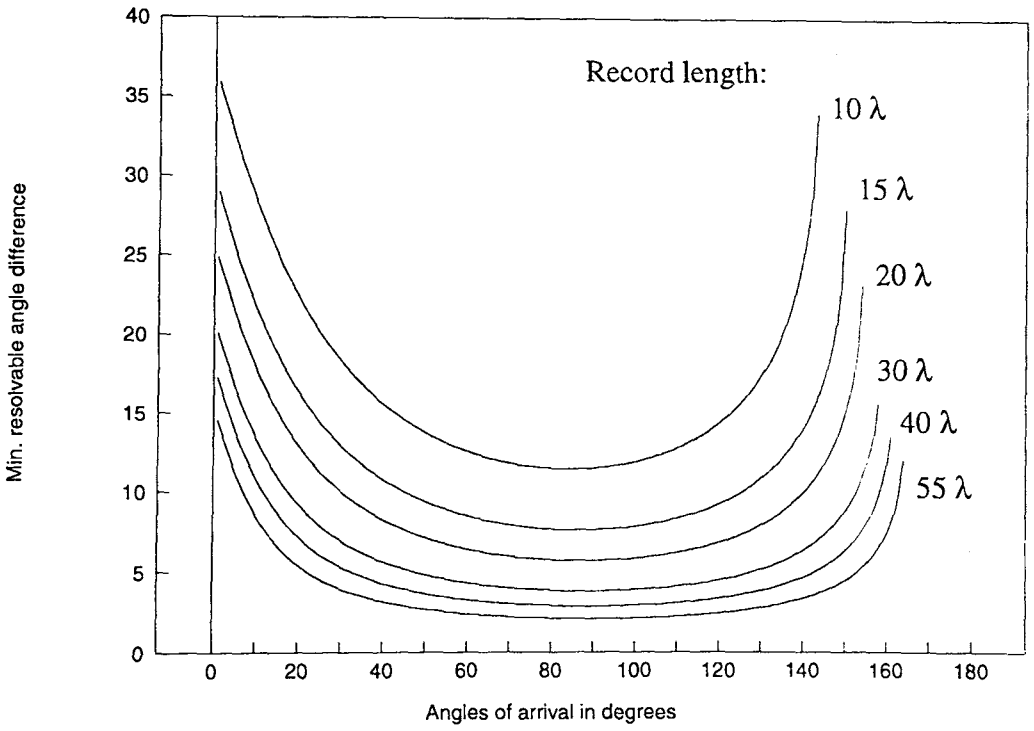

Figure 8.3 *Minimum resolvable angle difference (positive direction) depending on spatial domain record length*

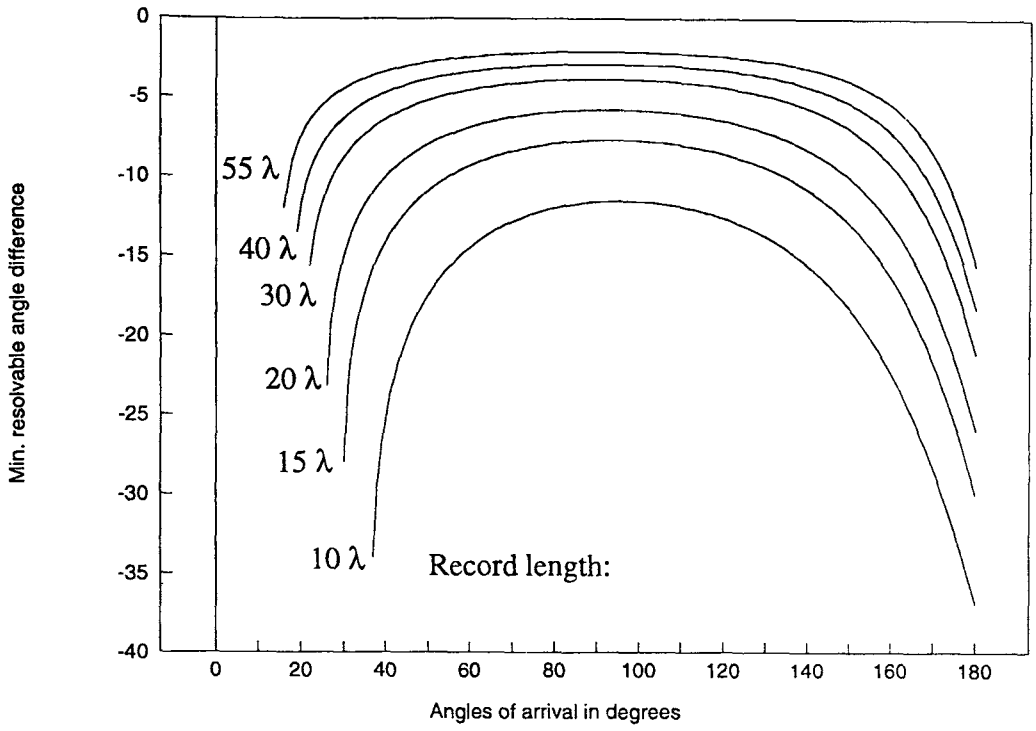

Figure 8.4 *Minimum resolvable angle difference (negative direction) depending on spatial domain record length*

As detailed in section 5.2.2 the resolution procedure applies several DFTs to the amplitude envelope. The window size is reduced by one step before the application of the next DFT until a minimum window length is reached. This method yields very accurate results as demonstrated the above mentioned section. However to assess the minimum resolvable angle the final shortest record length has to be used.

8.2.2 Smallest resolvable angle of arrival

The smallest resolvable angle of arrival will be represented by the first spatial frequency line. To be distinguishable this line will have to be at a distance of $2\Delta f_{sp}$. Figure 8.5 shows the minimum resolvable angle of the procedure depending on the record length in the spatial

domain. Using the adaptive window procedure again this applies to the smallest record length used during the window size adaptation.

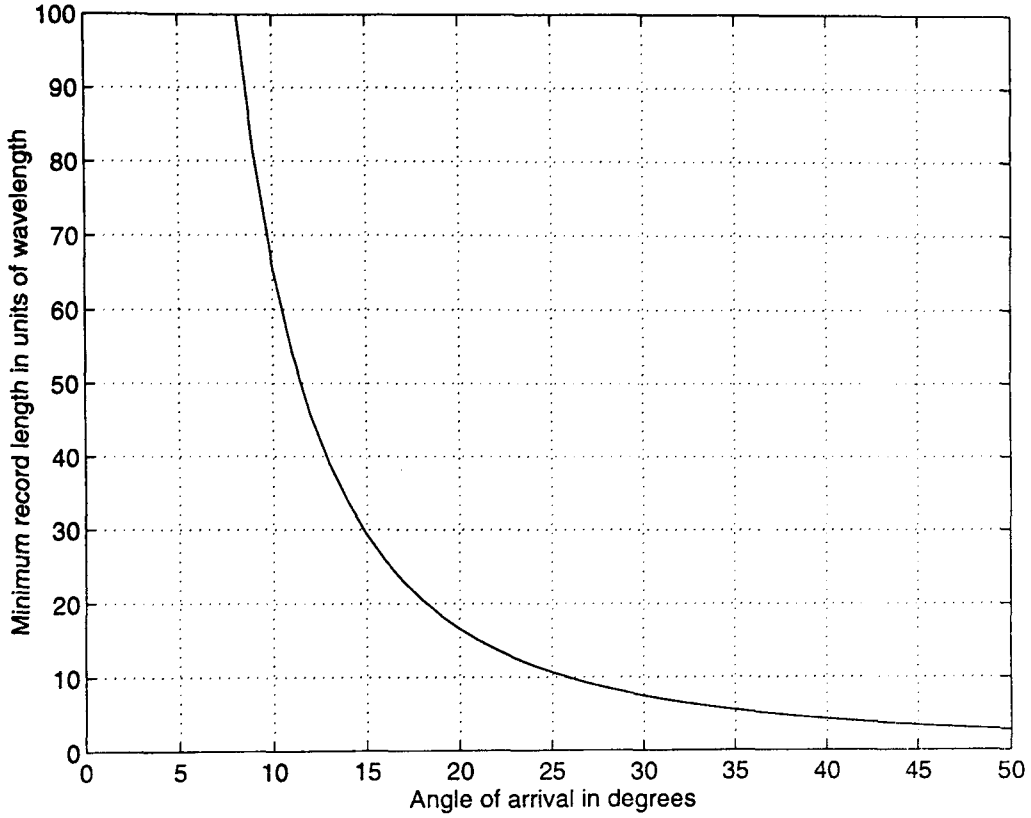

Figure 8.5 *Minimum resolvable angle of arrival depending on spatial domain record length*

8.3 Factors influencing the accuracy of resolved amplitudes

The main factors influencing the amplitude resolution of the DFT are discussed in chapter 5. It is shown in this chapter that the truncation interval in the spatial domain has a very significant influence on the accuracy of signal amplitudes by causing errors due to spectral leakage. It is shown how using the adaptive window size procedure the errors can be minimized very effectively. However some errors when applying the DFT still arise when using this method.

8.3.1 Increased error of adjacent spectral lines

Discussing the leakage problem of the DFT relevant papers (Bergland, 1968; Brigham, 1988; Harris, 1978; Kay and Marple, 1981) often concentrate on the obscuring of smaller adjacent spectral lines by larger ones through leakage. The effect that a small signal component gets completely obscured by the leakage of a much larger adjacent component is virtually eliminated using the adaptive window size method.

Investigating the accuracy of the component amplitudes resolved by the developed procedure an increased error was found in some cases. The investigation showed that these errors were caused by a different leakage related phenomenon which is not well documented.
This phenomenon also arises with closely spaced spectral lines. It was found that in cases where a large signal component shows a large amount of leakage the adjacent (smaller) component can increase in amplitude, appearing as if the leakage of the larger component 'lifts' up the smaller one. The effect bears similarities to the effect of noise on the signal (Prewitt, 1978), which is discussed in section 8.3.2.

This effect can be demonstrated on the spectrum of a simulated squared amplitude envelope using the simulation described in section 3.1.2. The simulated multipath geometry is:

$A_1 = 1, \theta_1 = 0°; A_2 = 0.7, \theta_2 = 60°; A_3 = 0.3, \theta_3 = 70°.$

The initial record length in this simulation was spanned a distance of 27.7 λ with 512 sampling points. The spectral lines of interest are Val_{12} and Val_{13}. Using equations 4.38 and 4.40 in chapter 4, they can be calculated from the geometry given above as $Val_{12} = 1.4$ and $Val_{13} = 0.6$. Figures 8.6 and 8.7 show the results of two different DFTs carried out on the simulated amplitude envelope of this multipath geometry. The original record length of 512 sample points has been reduced to 481 in figure 8.6 and to 504 in figure 8.7. Figure 8.6 shows that Val_{12} has been windowed so that hardly any leakage is present for this line and its amplitude is virtually 1.4 as calculated. Val_{13} shows some leakage and its amplitude is just below the calculated value of 0.6. In figure 8.7 the record length in the spatial domain was such, that Val_{12} shows a large amount of leakage and its amplitude is reduced to a value

around 1.1. It also clearly shows that this leads to Val_{13} exceeding the theoretical value of 0.6, while hardly showing any leakage of its own.

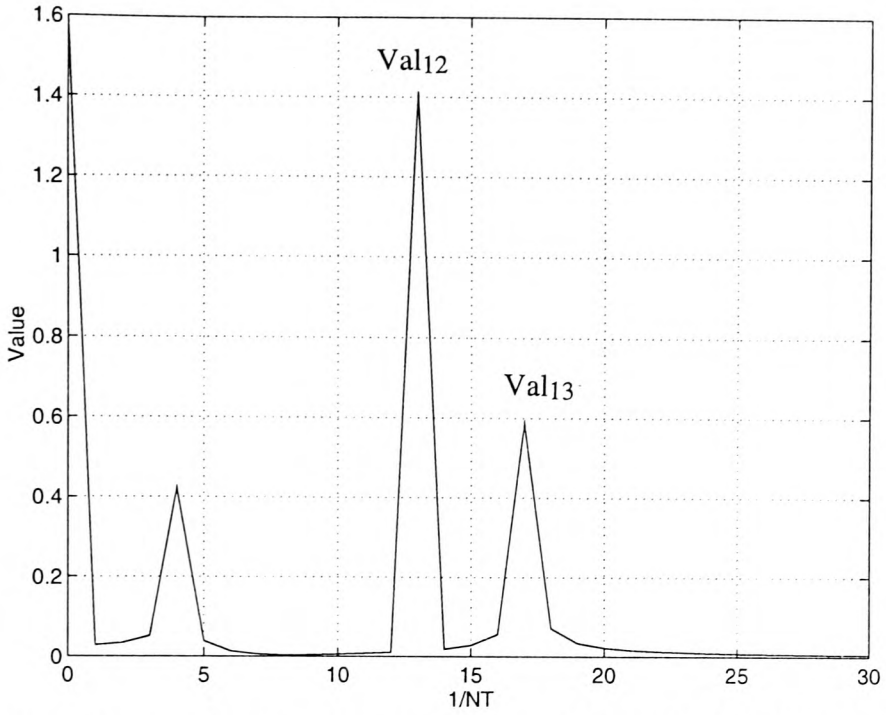

Figure 8.6 *DFT of a simulated interference pattern with record length 418 sampling points*

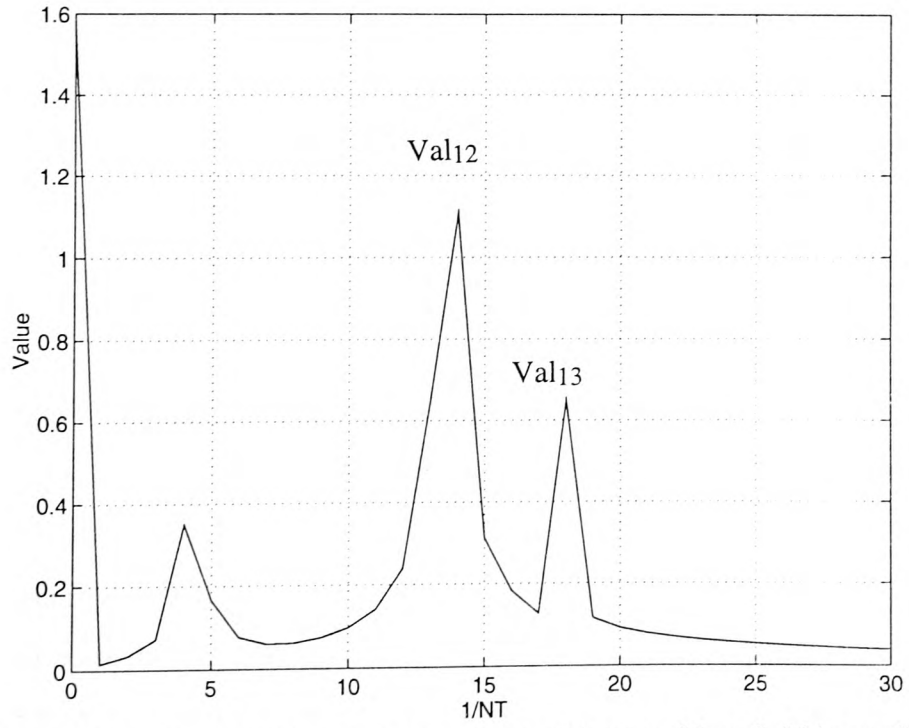

Figure 8.7 *DFT of a simulated interference pattern with record length 504 sampling points*

This (constructed) example demonstrates the effect that leads to additional errors. The adaptive window procedure will by using the minimum leakage test described in section 5.2.2.1 minimize the effect to some extent. A certain record length will be chosen when the amplitudes of the two sample points either side of the spectral line of interest are minimal. However an decrease in accuracy will remain for cases of one strong and one weak signal component with closely spaced angles of arrival. The effect can be minimised by increasing the resolution in the spatial frequency domain, i.e. increasing the number of spatial frequency samples between the spectral lines corresponding with the angles of arrival. An increase in spatial frequency domain resolution can be achieved by increasing the initial record length of measure amplitude envelope data.

8.3.2 The influence of noise on the amplitude envelope

The influence of noise of on the result of the DFT is discussed by Prewitt (1978). He states that an amplitude bias on the DFT output spectrum will result from presence of noise on the signal. In a practical measurement situation it is very likely to find noise present in the recorded amplitude envelope data. This noise will be of the order of the normal signal fluctuations due to outdoor factors. The outdoor experiments described in section 6.3.2 and 6.3.3 were affected by fluctuation noise as can be seen from their results in sections 7.1 and 7.2.

Noise on any of the signal components that give rise to the multipath field in which the amplitude envelope is recorded will influence the resulting interference pattern. This will affect the smaller signal components more than the larger ones. Random errors of the measurement system will also generate a small amount of noise on the measured pattern. A reduction of noise during the measurement can be achieved by averaging over a number of records taken at each step of the antenna displacement. This will average out some of the random fluctuations in the signal and minimize the effect of noise on the signal.

Analysing the experiments of multipath geometries caused by buildings (section 6.3.3 and 7.2) it was found that the weaker signal components were significantly overestimated. These signal components were received at a significantly lower signal level than the dominant component. In both measurements the signal level difference between strongest and weakest component was around 26 and 37 dB respectively. In the experiment with the larger difference in the two signal levels a greater overestimation of the weakest signal level was obtained. The effect of noise on the amplitude envelope is demonstrated here using a simulated amplitude envelope and adding random white noise to this. Table 8.1 shows the result of the resolution procedure applied to a simulated amplitude envelope. Three different cases are shown. The first one is a simulation without noise whereas in the second and third example random white noise has been added to the amplitude envelope. The amount of noise added is $\pm$ 1 dB in the second example and $\pm$ 3 dB in the third.

These examples demonstrate that noise on the recorded amplitude envelope will lead to an overestimation of some amplitude levels. Most significantly affected are the weakest signal components as expected. A slightly increased error on the resolved angles of arrival is also evident, but is insignificant, since the accuracy they are resolved with is still very good. An identification of signal components is still possible in the presence of noise. Very noisy amplitude envelopes will still yield the signal components, although weaker contribution will be overestimated.

In many practical applications signal components where this overestimation is significant will most likely be regarded as insignificant. In practical situations the underlying back scatter in an urban area can be as high as -30 dB (Al-Nuaimi and Ding, 1994), so that measurements will rarely extend to very low signal components. If however more accurate information on their amplitude levels is required the noise-level will have to be reduced (e.g. by averaging over a larger number of measurement samples or by applying a low pass filter to the resulting amplitude envelope).

	Procedure result **no** noise		Procedure result **1 dB** noise		Procedure result **3 dB** noise	
Simulated geometry	Resolution result	Error	Resolution result	Error	Resolution result	Error
$A_1 = 1.0$	0.9995	0.05 %	0.9960	-0.39 %	0.9991	0.09 %
$A_2 = 0.7$	0.6999	-0.001%	0.7048	0.69 %	0.7038	0.54 %
$A_3 = 0.05$	0.0497	-0.45 %	0.0644	28.8 %	0.0705	41 %
$\theta_2 = 45°$	45.06°	0.13 %	45.06°	0.13 %	45.11°	0.24 %
$\theta_3 = 150°$	149.9°	-0.08 %	154.1°	2.7 %	154.1°	2.7 %

Table 8.1 *Effect of noise on the resolution procedure*

The experimental measurement strongly affected by the influence of noise was the one carried out at the Birmingham site. The effect of noise can be demonstrated using the computer simulation for the amplitude envelope to simulate an envelope with the individually measured signal levels of the components. Similarly to the examples given in table 8.1 a certain amount of noise can be added to this simulation. Adding white noise of 2 dB to the simulation of this amplitude envelope the resolution procedure yields the following amplitude levels:

Component 1: -7.5 dBm
Component 2: -19.7 dBm
Component 3: -36.2 dBm

Comparing these figures with table 7.2 the amplitudes for components 1 and 2 are equal to the measurements because no tolerance for the measurements was assumed. The simulation used exactly the measured values for those components, therefore the procedure result equals the measurements. However it is significant that using a simulated amplitude envelope with an added noise of a realistic level the amplitude value for component 3 equals that of the procedure result using the measured envelope. The fact that the component amplitudes obtained by applying the resolution procedure to simulated data with an added noise match the ones gained from the measured amplitude envelope indicate that noise present in this measurement was a contributing factor to the errors observed.

8.4 Limitations of the developed procedure

Some limitations have already been discussed in sections 8.2.1 and 8.2.2. The minimum resolvable angle of arrival and the minimum angle difference both depend on the record length of the recorded amplitude envelope. The procedure cannot yield results for angles of arrival below the smallest value given for a certain record length.

Another limitation results from the symmetry of the cosine function. The cosine function produces duplicate answers for angles greater than 180°. The discussed resolution procedure produces angle of arrival values between 0° and 180°, with respect to the direction of antenna displacement. In a practical environment once angles of arrival are established for certain signal components it will often be possible to identify structures from which they arise. Therefore it will often be possible to identify whether the signal component travelled from the left or right hand side with respect to the direction of displacement of the receiving antenna.

8.4.1 Resolution of ambiguity for angles larger than 180°

In situations where it is not possible to identify from which half circle either side of the line of antenna displacement the multipath components arise, a method will be useful to provide that information. The symmetry of the cosine function leading to duplicate results for angles larger than 180° makes it necessary to acquire extra information to resolve this ambiguity. The additional information needed can be obtained by measuring a second amplitude envelope at the same location in the same multipath field. The direction of displacement will have to be at an angle (ψ) with reference to the direction of the first displacement. The angle ψcan be chosen as a convenient value, as explained below, see figure 8.8.

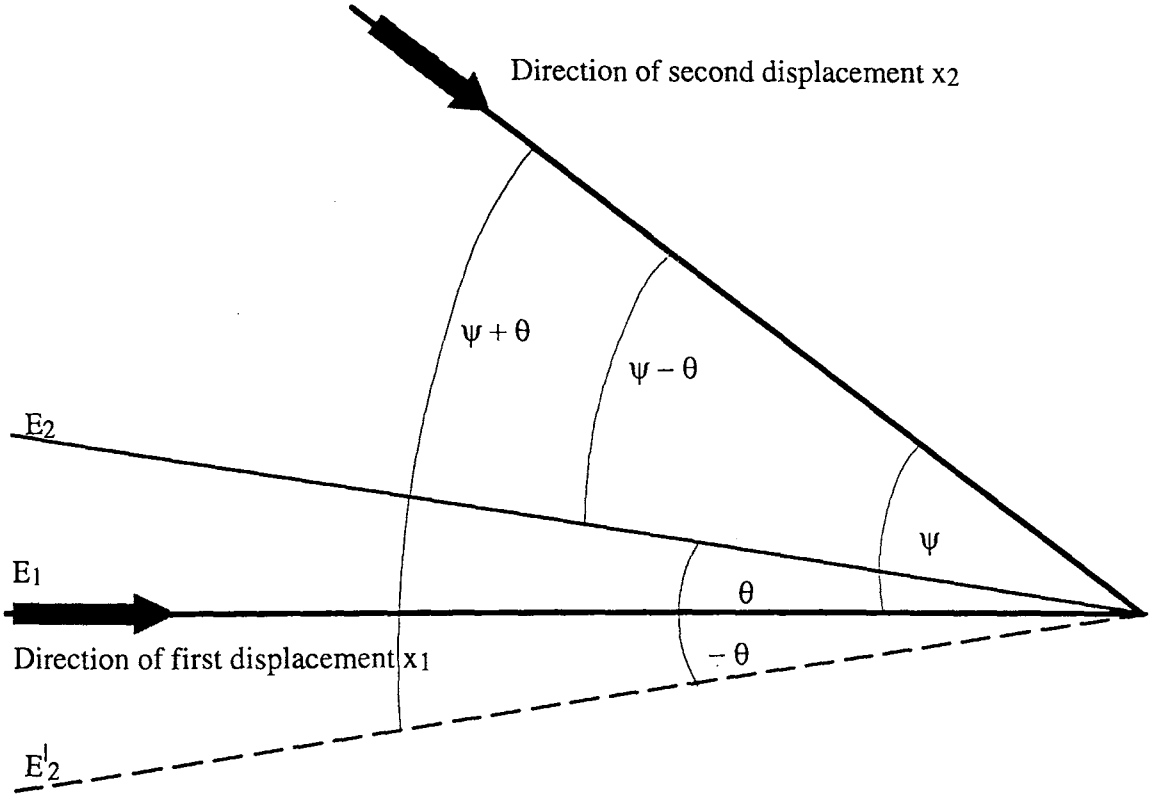

Figure 8.8 *Measurement set up to resolve angle ambiguity*

Using one displacement (x_1) of the antenna it is not possible to distinguish whether the second signal component in figure 8.8 is E_2 arriving from direction (θ) or whether it is E'_2 arriving at $-\theta$. By displacing the antenna along a second direction (x_2) which is of angle ψ, an amplitude envelope pattern will be recorded caused by the same two signal components E_1

and E_2 (or E'_2) as during the first measurement. With respect to the direction of the second displacement signal component E_1 arrives at angle ψ. But the second component will either arrive at angle $\psi + \theta$ or $\psi - \theta$. The cosine function is non-linear and therefore yields a different result for both angles. Using equation 3.27 the two different spatial frequencies f_{sp12} and f'_{sp12} can be calculated with known angle ψ:

$$f_{sp12} = | \cos(\psi - \theta) - \cos(\psi) | \tag{8.2}$$

$$f'_{sp12} = | \cos(\psi + \theta) - \cos(\psi) | \tag{8.3}$$

The spatial spectrum will yield the different spatial frequencies f_{sp12} or f'_{sp12} for the two different angles θ and $-\theta$. The values for either are different, the ambiguity is thus resolved. The angle ψ can be chosen as a convenient value in the first quadrant (0° to 90°). But it cannot be chosen to be 90°, since cos 90° = 0. This would lead to $\cos(\psi) = 0$ in eqns. 8.2 and 8.3. Therefore the terms $\psi + \theta$ and $\psi - \theta$ would result in the same absolute value and only differ in their sign. The information about the sign is lost in eqns. 8.2 and 8.3 and therefore does not lead to any additional information about the angles of arrival. In cases of more than 2 components (n > 2) eqns 8.2 and 8.3 can be generalized as:

$$f_{sp1j} = | \cos(\psi - \theta_j) - \cos(\psi) | \tag{8.4}$$

$$f'_{sp1j} = | \cos(\psi + \theta_j) - \cos(\psi) | \tag{8.5}$$

with j = 2,3,.....n

Comparing of the two resulting spatial spectra of the amplitude envelopes obtained by two antenna displacements it will possible to resolve the ambiguities using the chosen angle ψ.

8.5 Summary and interim conclusion of chapter 8

The accuracy of the spatial frequencies is mainly determined by the length of the record in the spatial domain, meaning the length of the amplitude envelope in wavelength λ. It is shown how the record length influences the accuracy in the spatial frequency domain using one DFT on a given amplitude envelope data set.

Comparing the figures given here with the results given in chapter 5 using the resolution procedure which utilizes the adaptive window method it can be seen that the accuracy of the latter is significantly greater.

For closely spaced signal components, especially in the case of one strong and one weak component problems will arise for the amplitude accuracy, because leakage from the strong component leads to an over-estimation of the weaker component. Improvements can be achieved by increasing the displacement distance of the receiving antenna and hence the record length.

Displacing the antenna in one direction through the multipath field will lead to ambiguities of angles of arrival greater than 180°. If this ambiguity can not be resolved in a practical situation with the knowledge of the geometrical features on the paths a second amplitude envelope can be recorded. Conducting this measurement at a direction of displacement of angle ψ with respect to the first displacement will after applying the DFT lead to a second spatial spectrum. Comparing the different spatial frequencies and the knowledge of angle ψ can be utilised to resolve the ambiguity in the angle of arrival.

CHAPTER 9 SUMMARY, CONCLUSIONS AND FURTHER STUDIES

9.1 Summary of studies and results

The ever increasing demand for radiowave communication systems has led to a growing number of users in the available frequency bands. This makes it desirable to utilize previously unused frequencies and to share existing frequency allocations. Chapter 1 highlights the relationship between large numbers of users of the same frequency bands and the increase in the risk of co-channel interference. Furthermore the move from long overland radio links to shorter local services with many services operating in and extending into urban areas gives rise to the need to assess the effects of buildings on the propagation channel in order to obtain a more efficient system planning.

Radio communication systems in built up areas are in many cases affected by multipath propagation. The concentration of buildings makes it very likely that a receiver will be subjected to a number signal components caused by reflections, scatter, diffraction etc from adjacent buildings. For efficient system planning as well as improving existing links it is important to gain an understanding of the multipath field geometry resulting from the interaction of signal components.

Usually a multipath field is complex and not easily resolved into its individual components. It is desirable to develop a technique that can identify the number of constituent signal components present and to quantify relatively the individual amplitudes as well as their angles of arrival at the receiving antenna. Such technique can also be used to yield valuable results for assessing the shielding properties of particular buildings. The amount of protection gained from a building in urban areas is reduced greatly by signal components being reflected, diffracted and scattered by adjacent obstacles. To assess the site-shielding properties of a building a complete understanding of the multipath field geometry therefore needs to be gained. These multipath geometries will often not be predictable because of the

complexity of the physical processes giving rise to them. An analytical tool suitable for the investigation of such geometries would be very helpful.

Chapter 2 gives an overview of the phenomenon of multipath propagation as well as the problems associated with it. It describes the propagating mechanism leading to the arrival of several signal components at a receiver location. The concept of site-shielding is introduced and the importance of an understanding of the multipath geometries involved in urban site-shielding situations is shown. The project is put into context with previous work undertaken in the field. The adaptation of holographic principles as used in optics for the purpose of angle of arrival estimation on height gain curves is explained. Chapter 2 gives an overview over various previous investigations into direction finding, component identification mainly based on using multiple array antennas for the measurements. The literature shows that data gathered in this way can be processed with a variety of the processing techniques. The choice of the Fourier transform as signal processing technique for this particular application is explained.

The aim of this research programme was to develop a multipath resolution technique utilizing the resulting amplitude envelope which can be recorded when displacing a receiving antenna linearly through a multipath field. Chapter 3 analyses mathematically the interaction of the various constituent multipath components. Functions are derived describing the amplitude envelope pattern measured when displacing the receiving antenna in small steps, each of a fraction of a wavelength through the multipath field. The simple model for the case of a two component multipath is developed and expanded to many components, i.e. $n > 2$.

Chapter 3 also presents a computer simulation which allows us to simulate the amplitude envelope pattern in any arbitrary multipath geometry. This simulation was developed to provide test data for the development and optimisation of a working resolution procedure.

The second part of chapter three investigates a possible method to include multipath contributions originating from continuously distributed sources, i.e scatter.

Information about the number of constituent signal components as well as their amplitudes and angles of arrival can be extracted from the received amplitude envelope described in chapter 3.

This interference pattern exhibits a periodic or quasi-periodic nature. Therefore Fourier transform analysis lends itself for processing the measured pattern. Chapter 4 introduces and investigates the Fourier transform analyses. Spatial spectra of a number of significant simulated amplitude envelopes are presented. It is shown that the use of the recorded amplitude envelope will lead to a spectrum containing a large number of spurious spatial frequency components.

It is shown that the attempt to extract information about the amplitude values of the constituent multipath components will lead to equations which are shown to contain binomial series with slow convergence in cases where signal components become comparable. The resulting large number of terms in the series is an explanation for the numerous spurious spatial frequency components observed in the spatial spectrum. This makes identification of spectral lines linked to angles of arrival very difficult. An alternative was chosen as the method for the resolution procedure. It uses the square of the recorded data set. This leads to spatial frequency spectra with a far smaller number of spectral lines. These lines can be identified and related to the angles of arrival of multipath components. The magnitude of the spectral lines is used to determine the amplitudes of the individual signal components. It is shown, that a multipath component resolution from the spatial spectra of the amplitude envelope is feasible.

The spatial spectra of the received amplitude envelope contains spatial frequencies which in the majority of cases are not harmonically related. Applying the Discrete Fourier transform

to signals of this nature gives rise to a number of problems. Prominent amongst these disadvantage is the problem of spectral leakage. Chapter 5 investigates the problems associated with the DFT and a solution to minimise the effects of these problems is presented. It consists of applying several DFTs with different spatial domain windows sizes to the same measured record which leads to a number of values for each spatial spectral line. It is demonstrated how to identify the correct amplitude and spatial frequency values for a spectral line from each field. The increase in accuracy over applying a single DFT is demonstrated. The different findings are combined and developed into a working multipath component resolution procedure. The accuracy of the final procedure is demonstrated with results gained by applying this procedure to simulated multipath geometries. These results show that high accuracy in resolving the multipath geometry from the simulated amplitude envelope can be achieved.

One of the objectives of this research programme is the establishment of a resolution procedure which can be verified in practical multipath situations. For this purpose an experimental programme was set up to both demonstrate the usefulness and test the performance of the developed resolution procedure which is described in chapter 6.

Three different sets of experiments were conducted. They comprised two different outdoor experimental arrangements and another set of indoor experiments. The outdoor experiments were conducted at 11.2 GHz, whereas the frequency used for the indoor experiments was 20 GHz. The first set of outdoor experiment was set up on a large open area of playing fields. The aim of this set of experiments was to create controlled conditions to assess the validity of the results gained by applying the resolution procedure to the measured data. The open area was chosen because of the small amount of surrounding vegetation and other features, which minimized the level of background scatter and unwanted interference from sources not controlled by the experiment. The geometries creating the multipath field were set up using large reflector boards. This allowed a measurement of the signal contributions individually with reasonable accuracy. The individually measured components could then be compared

with the results of the resolution procedure applied to the measured amplitude envelope in each experiment.

For the second set of outdoor measurements it was decided to use multipath geometries arising between real buildings to validate the results in situations encountered in practice. A site survey was carried out to identify suitable locations. It was essential that the chosen site gave a realistic representation of a multipath situation that might be encountered in urban surroundings. In addition the chosen multipath geometry has to be sufficiently well defined enabling the identification and measurement of the individual signal components with reasonable accuracy. These conditions are required to assess the accuracy of the resolution procedure in these cases. A site was chosen near Birmingham containing a number of high rise as well as smaller buildings.

A second experiment in this set was carried out on the campus of the University of Glamorgan. A location was chosen where the presence of multipath signal components had earlier posed difficulties to the evaluation of the site-shielding of a particular building (Haslett, 1993b).

The third set of experiments was carried out inside an anechoic chamber. The frequency used here was 20 GHz. A higher frequency was chosen partly dictated by the relatively small dimensions of the chamber compared to the outdoor experiments. The measurements were conducted with a different measurement system compared to the 11.2 GHz experiments.

The results of the above experiments are presented and discussed in chapter 7. The first set of outdoor experiments using the reflector boards showed that a multipath field was successfully generated using the boards. It demonstrated that applying the developed resolution procedure to a measured amplitude envelope pattern the multipath geometries could be successfully resolved. It is shown that the accuracy of the experimental results was within the expected limits.

In the second set where buildings have resulted in the creation of a multipath field, resolution of the individual components was achieved. In the Birmingham experiment the results of the resolution procedure led to the discovery of an additional signal component, which had not been thought a significant contribution in the initial planning of the experiment. The multipath components in the campus experiment were again successfully resolved. Common to both experiments was a small over-estimation of the amplitudes of weak multipath components. The reason for this has to be seen in the difficulty of measuring the components individually even with highly directive antennas. Secondly the presence of noise on the measured data could be influential. The subject of noise and its effect in the resolution procedure is discussed in chapter 8.

The anechoic chamber experiments produced sufficiently accurate results despite the relatively small dimensions of the chamber. The indoor experiments demonstrated that the resolution procedure yields accurate results also in cases where a different frequency and measurement system were used.

Chapter 8 addresses the factors affecting the accuracy of the resolution procedure. A comparison is made between the accuracy generally associated with DFT processing and the improvement gained by using several DFTs with adaptable window size, as explained in chapter 5. Still a decrease in the accuracy of the resolved signal components can be observed if any components are of comparable value especially if their angles of arrival are closely spaced together.

Furthermore is the influence of noise on the record of the amplitude envelope discussed. It is shown that high noise levels on the input data for the DFT lead to over-estimation of the amplitudes of very small components.

One limitation found with the resolution procedure is that it only resolves angles between 0 and 180. This is due to the symmetries in the cosine function producing replicated values for angles above 180. The reference direction for angles of arrival is the direction of antenna

displacement. A restriction to 180° therefore means it is not distinguished wether signal components originate from the left or right hand side of that axis. In many practical applications it will be possible to assess from which side with respect to the direction of antenna displacement signal components originate from. However to generalize the procedure a method to extend this to 360° is discussed.

9.2 Conclusions

9.2.1 Contribution to models

The Fourier transform is a well known signal processing technique established for some time and is well documented in literature. It is used in a wide range of applications. Many standard approaches to implement Fourier transform techniques have been developed and are well documented. The DFT is today regarded a standard tool in many data processing applications. Despite the extensive literature on different techniques of implementing the DFT and associated limitations a novel approach had to be developed for the particular application in this research project. The author is confident that the multipath resolution procedure developed, using Fourier transform techniques, presented here is novel and presents an effective solution for a problem which arises in radio communications.

Firstly data containing amplitude values only was used as input for the procedure. Similar work documented in literature generally relies on the provision of complex input data including information about respective phases of received signals measured by the elements of an array of antennas. Furthermore the documented techniques often use several sets of data gathered at different times to increase the amount of input information. An application to follow such procedures would require highly involved measurements and expensive equipment.

Secondly it was possible to extend the procedure to the resolution of multipath field arising from n components. Many earlier reports had concentrated on the more trivial case of two

components only mentioning the expansion to more terms, without actually demonstrating the multi-component case.

Finally and most importantly in order to achieve a high accuracy of the achieved results a method is developed which is novel differing from the classic windowing techniques reported in conjunction with DFT application.

To overcome the inevitable errors caused by spectral leakage when the DFT is applied a novel technique was developed. The effects of spectral leakage were found to be especially apparent because of the relatively short spatial records. These were in some cases no longer than one period for the fundamental spatial frequency of data with non-harmonically related frequency components. Applying several DFTs to the same data but with different window length in the spatial domain leads to a field of amplitude values for each spatial frequency line. It is demonstrated how the correct amplitude value for each line can be identified from this field and that a substantial increase in accuracy is achieved in this way. This made DFT analysis possible where results were not sufficiently accurate, because of the widely accepted shortcomings of the DFT performance on signals with non-harmonically related components.

During the investigations factors influencing the accuracy of the DFT one so far not widely know aspect related to spectral leakage was found and is documented. It is generally reported that spectral leakage of strong frequency components leads to the obscuring of neighbouring small frequency lines. However it was discovered that in some cases at certain window lengths a smaller frequency component is increased in value by the leakage of a strong adjacent spectral line. This 'lifting' effect in the resolution procedure leads to reduced accuracy for multipath signal components if their angles are closely spaced.
The combination of the methods and findings described above is thought to make this approach of DFT application novel and highly useful in problems such as multipath resolution.

9.2.2 Contribution to measurements

An very important aspect of this research programme was to design an experimental set up that could be used to validate in practice the multipath component resolution procedure designed with the help of a computer simulation. It was considered very valuable that a critical assessment of the developed procedure with both a comprehensive number of simulated data and also actual practical measurement data were to be conducted.

Several sets of measured data of amplitude envelopes patterns have been obtained during the course of this research programme. The frequencies at which the experiments have been carried out were 11.2 and 20 GHz. Many previous measurements have concentrated on lower frequencies with the majority of gathered data available in the frequency ranges used for mobile communications, i.e. between 900 MHz and 4 GHz. Although the physical propagation mechanisms involved are similar for those lower frequencies compared to the ones used here, a confirmation based on experiments must be regarded as valuable. The novel aspects of the experiments, as far as the author is aware, is that the dependency of the shape of the amplitude envelope on the different encountered multipath geometries was demonstrated in several different sets of measurements. Equally importantly that the parameters of the multipath geometries are retrievable from a measured amplitude envelope pattern alone without any phase information gathered. The experiments conducted in situations where the multipath field was created by building at existing sites are a valuable addition of practical measurement data at these frequencies. The measurements also show that in practice the number of discrete sources which significantly contribute to the multipath field is relatively small, i.e. $n = 4$.

9.2.3 Contributions to published literature

The author has made the following contributions to published material:

"Results of component resolution of microwave signals received in a multipath field", (Al-Nuaimi, Richter), 8th UK national URSI colloquium, Leicester 1991

Poster presentation: "Method and results of components resolution of microwave signals in a multipath field", (Al-Nuaimi, Richter, 9th UK national URSI colloquium, Bradford 1992

"Resolution of constituent components in a multipath field using DFT", (Richter, Al-Nuaimi), Electronic Letters, 1995

"Characterisation of transhorizon radio paths at microwave frequencies", (Compton, Al-Nuaimi, Richter), submitted to Electronic Letters, 1998

Results of this research have been reported to the management committee of COST project 235, namely working group 3. The committee papers themselves are normally not for publication. But results of this programme have been published in the final report of COST project 235 (COST 235, 1996)

9.2.4 General conclusions

A validated resolution procedure for typical multipath situations encountered especially in urban surroundings has been developed and successfully demonstrated. The intention was to design a procedure that can be relatively easily implemented avoiding the used of complex measurement set ups and expensive equipment. The developed procedure can be implemented with relatively simple means of engineering. Only one movable antenna is used intstead of an array of antennas. The only requirements for the receiver antenna are, that the angular radiation pattern is know and that the antenna small enough to be regarded as a

lumped element in the given measurement environment. Requirements are a displacement mechanism for the receiver system that displaces the receiving antenna in small increments at a time over a distance of a few wavelength. The system used here was a steel guide with a threaded rod and bolt attachment to provide the accurate displacement intervals. A modification for other purposes could be the use of a rail system instead of the guide, if longer displacements are requires. The displacement itself can be automated and computer controlled for easy of data collection. The requirement for the processing of the data is a standard PC.

The method itself is applicable to a wide range of frequencies which makes it useful for many radio communications applications. The measurements in the anechoic chamber demonstrated that meaningful results can be obtained even if the antenna displacement appears to be larger than negligible in comparison to the distances between obstacles and receiver as well as transmitter and receiver. Scaling the 20 GHz anechoic chamber experiments up by a factor 100 for example would lead to an experimental area of 600 by 200 metres at a frequency of 200 MHz. The area described contains the reflecting objects, transmitter and receiver. Judging by the anechoic chamber experiments, meaningful results should be obtainable in the above described scenario at frequencies as low as the upper VHF range. The limiting factor for higher frequency application of the procedure would have to be seen in the possible accuracy of the distance between displacement intervals. The 20 GHz experiments used 1.5 cm intervals. It appears to be reasonable that the mechanics can be engineered at reasonable cost for displacements a factor 10 smaller then those used, making this procedure applicable well into the millimetre wave range.

For an ever increasing number of users of radio frequency bands demands more efficient system planning this procedure should provide a useful tool for the analysis radio wave links over a wide range of frequency applications.

9.3 Further studies

The resolution procedure presented here concentrates on multipath fields created by contributions for discrete sources. These will no doubt be the majority of cases in any urban surrounding. However as shown in the second part of chapter 3 it might be possible to derive methods to extend the resolution of a multipath environment to continuously distributed sources. However further investigation into developing a practical procedure for this purpose would be needed if a general multipath resolution including all possible sources of contributions is desired.

REFERENCES

Allen E.W., "The multipath phenomenom in line-of-sight digital transmission systems", Microwave Journal, pp. 215-225, 1984

Andrews H.C., Caspari K.L., "A generalized technique for spectral analysis", IEEE Trans. Computers, Vol C-19, part 1, pp. 16-25, Jan. 1970

Aoki Y., Boivin A., "Computer reconstruction of images from microwave hologram", IEEE Proc., Vol. 58, pp. 821-822, 1970

Babic H. Temes G.C., "Optimum low-order windows for discrete Fourier transform systems", IEEE proc. acust. speech sign. process., pp 512-517, 1976

Bailey A.E., "Microwave Measurements", 2. edition, IEE Publication, 1989

Bartsch, H.J.,"Mathematische Formeln", VEB Fachbuchverlag Leipzig 1982

Beach M.A., Swales S.C., et al, "A diversity combining antenna array for land mobile satellite communications", 39th IEEE vehicular techn. conf. (IEEE cat no. 89CH2739-1), pp. 749-756, part 2, 1989

Beauchamp K., Yen C., "Digital Methods for Signal Analysis", George Allen & Unwin, London 1979

Bergland G.D., "A guided tour of the fast Fourier transform", IEEE Spectrum, Vol. 6, pp. 41-52, July 1969

Bernyukov A.K., "Microprocessor functional-adaptive signal processing in radio navigation systems in an on-board subsystem", Telecom. and radio eng. vol. 43, part 8, pp. 131-137, 1988

Born M., Wolf E., "Principles of Optics", 6. edition, Pergamon Press, Oxford 1993

Boithias, L. "Screening effect of the terrain for various propagation mechanisms", AGARD Conf. Proc. No. 127, pp. S3/1 - S3/9, Rome, Italy, May 1973

Bratnick, M.,"Shielding earth stations from RF interference (use of barrier walls)", Telecommunications, vol. 17, no. 6, pp 106-110, 1983

Brigham O.E., "The Fast Fourier Transform", Prentice Hall, Engelwood Cliffs, New Jersey 1974

Bronstein ,I.N. Semendjajew, K.A.,"Taschenbuch der Mathematik", 21. edition, BSB B.G. Teubner Verlagsgesellshaft, Leipzig 1979

Brook D., Wynne R. J., "Signal Processing, Principles and Applications", Edward Arnold, London 1988

Brown J., Glazier E.V.D., "Telecomunications", Chapman and Hall Ltd., London 1964

Bryant G.H., "Principles of Microwave Measurements", IEE publications, 1988

Bucker H.P., "Comparison of FFT and Prony algorithms for bearing estimation of narrow-band signals in realistic ocean environment", Jnl. Acoustic Soc. Amer., Vol. 61, pp. 756-762, 1977

Candy J.V., "Signal Processing, the Modern Approach", McGraw-Hill B. Comp., New York 1988

Champeney D.C., "Fourier Transform and their Physical Applications", Academic Press, London, 1973

Cichon D., Kürner T., Wiesbeck W., "Modellierung der Wellenausbreitung in urbanem Gelände", Frequenz, pp. 2-11, Vol. 47, part 1-2, 1993

Chuang C.W., Naffatt D.L., "Natural Resonances via Prony's method and target discrimination", IEEE Trans. Aeropspace Electr. Syst., Vol. AES-12, No. 5, pp. 583-589, Sept. 1976

Cooley J.W., Tukey J.W., "An algorithm for the machine calculation of complex fourier series", Jnl Math. Computation, Vol. 19, No. 90, pp. 297-301, April 1965

Cox, D.C.,"Time- and frequency-domain characterization of multipath propagation at 910MHz in a suburban mobile-radio environment", Radio Science, Vol. 7, pp. 1069-1077, Dec 1972

Ding, M.S.,"Modelling and meassurement of the scatter of microwaves by buildings", PhD thesis, University of Glamorgan, 1994

Duffy T., "Eliminating multipath fading in digital radios", Microwaves + RF, Vol 27, part 6, pp. 127-134, 1988

Eberhard A.," An optimal discrete window for the calculation of power spectra", IEEE Trans. audio electroacuustics, Vol. 21, part 2, pp. 37-43, Feb. 1973

Friedlander, B., "Lattice methods for spectral estimation", IEEE Procs. Vol. 70, No. 9, pp. 990-1017, Sept. 1982

Gabriel W.F., "Spectral analysis and adaptive array superresolution techniques", IEEE Procs. Vol. 68, No. 6, pp. 654-66, June 1980

Gooch, R., Sublett B., Geyer T., "An adaptive nulling system for digital microwave radio," Wescon 189 Conf. Record Meeting: 14-15 Nov 1989, San Fransisco USA, pp. 384-389, 1989

Goodman J.W., "Introduction to Fourier optics", McCraw-Hill B. Comp., New York, 1968

Gould, R.G., Schmitt, C., "Interference reduction tequniques for satellite earth stations", 2nd symposium and technical exhibition of electromagnetic compatibility, pp. 285 - 292, Montreux, Switzerland, June 1977

Hamming R.W.,"Numerical methods for scientists and engineers", McCraw-Hill B. Comp., New York 1973

Hansen, J.C., "Separation of overlapping waveforms having known temporal distributions", Jnl Neuroscience Methods, Vol. 9, pp. 127-139, 1983

Harris J.H., "On the use of windows for harmonic analysis with the discrete Fourier transform", IEEE procs. Vol. 66, No. 1, Jan. 1978

Haslett, C.J., "Multiple path diffraction by rectangular buildings", Electronic Letters, Vol. 29, No. 6, 1993

Haslett C.J., Modelling and measurement of the diffraction of microwaves by buildings", PhD thesis, University of Glamorgan, 1993b

Haykin S., Justice J.H., Owsley, N.L., Yem J.L., Kak A.C., "Array Signal processing", Prentice-Hall Inc. Englewood Cliffs, New Jersey, 1985

Hildebrand F.B., "Introduction to numerical analysis", 2. edition, McCraw-Hill Inc., 1974

Hecht E., Zajac A., "Optics", Addison-Wesley Pub. Comp. Inc., London 1974

Heshmaty-Manesh D., Tam S.C., "Application of Winograd's fast Fourier transform (FFT) to the calculation of diffraction optical transfer function (OTF)", Proc. SPIE Jnl. Soc. opt. eng., Vol. 369, pp. 692-695

Ja, H.Y.,"Measurement of angles of arival of waves by microwave holographic Techniques", IEEE Proc. Antennas and Propagation, Sep. 1975

Ja, H.Y.,"Holographic Reconstruction of source distributions from microwave height-gain curves", IEEE Proc. vol AP-24, pp. 1-5, No. 1, Jan. 1976

Jakes W. C. Jr., "Micowave mobile communications", J.Wiley & Sons, Chichester, 1974

Jensen, O.G., Pandelis, P.P., "Homomorphic deconvolution of potential field data in one and two dimensions", Can. Jnl. Earth Science, Vol. 20, pp. 1260-1281, 1983

Jones N.B., Watson McK.J.D., "Digital Signal Processing, principles, devices and application", IEE publications, 1990

Karl J.H., "An intoduction to digital signal processing", Academic Press Inc., 1989

Kauffman, J.F., Croswell, W.F., "Analysis of the radiation patterns of reflector antennas", IEEE Trans. Ant. and Prop. Vol. AP-24, No. 1, January 1976

Kay, S.M., Marple S.L. jr, " Spectrum analysis - a modern perspective, IEEE Procs., Vol. 69, No. 11, pp. 1380-1419, Nov. 1981

King W.R., "Maximum antropy spectral analysis in the spectral domain", Rome Air Develop. Centre Tech. Report, RADC-TR-78-160, 1978

Kiu-Chuwe N., "On the accuracy of numerical Fourier transforms", Jnl. Comput. Phys., Vol. 16, part 4, pp. 396-400, 1974

Kraus, J.D., "Antennas", McGraw-Hill Book Company, Inc., New York 1950

Kraus J.D., "Electromagnetics", 3. edition, Mc Graw-Hill Book Comp., New York 1984

Kurmaresan, R., Tuffs, D.W. "Estimating angles of arrival of multiple plane wave", IEEE Trans. on Aerospace and Electronic Systems, Vol. AES-19, No 1, Jan 1983

Kürner, T., Wiesbeck, W., "Einfluß der Mehrwegeausbreitung auf die Bitfehlerrate", Frequenz, Vol. 48, part 11-12, pp. 270-278, 1994

Kwon, H.-S., Kim, Y.-H.,"Minimization of bias error due to windows in planar acoustic holography using a minimum error window", J. Acoust. Soc. Amer., vol. 98, No. 4, pp. 2104-2111, 1995

Langewellpott U., "Mehrwegeresistente Datenübertragung mit hohen Raten im Mobilfunk bei 1 GHz", Frequenz, Vol. 36, part 4-5, pp. 105-109, 1982

Levy, M.F., "Diffraction Studies for microcellar application, Proc of 8th Int. Conf. Ant. and Prop. (ICAP), Edinburgh, Vol. 1, pp. 76 - 79, IEE, 1993

Livingston D.C., "The Physics of Microwave Propagation", Prentice Hall Inc, Engelwood Cliffs 1970

Loulay, M.A., Holtzman, J.M. "Multipath fading effects on wide-band DS/CDMA signals: analysis, simulation and measurements", IEEE Trans. Vehic. Techno., Vol. 43, No. 3, pp. 801-807, August 1984

Lucia, E.F.,"Additional measurements on pit shielding for communications satellite earth stations", IEEE Trans. On Aerospace and Electronic Systems, Vol. AES-8, 2, pp. 251 - 253, 1972

Lucia, E.F.,"Artificial site shielding for communications satellite earth stations", IEEE Trans on Aerospace and Electronic Systems, Vol AES-6, pp. 612 - 619, September 1970

Lynn P.A., "An Introduction to the Analysis and Processing of Signals", 3. edition, Mc Millan Education Ltd, London

Lee, Y.W., Cheatham T.P. jr, Wiesner J.B., "Application of correlation analysis to the detection of periodic signals in noise", IRE Procs. Vol. 38 pp. 1165-71, Oct 1950

Markel J.D.. "FFT pruning", IEEE trans. audio and electroacoustics, Vol. AU-19, No. 4 Dec. 1971

Marple S.L., "Spectral line analysis by Pisarenko and Prony methods", IEEE int. conf. on acoustics speech and signal processing, pp. 159-161, 1979

Mattews P.A., Mohebbi B., "Direction of arrival measurements at UHF", Electronic letters, pp1069-70, vol. 25, part 16, 1989

Matthews P.A., Molkdar D., Rashidzadeh B.,"Measurement, description and modelling of the UHF terrestrial mobile radio channel", 3rd int. conf. on land mobile radio, pp. 119-125, Cambridge 1985

Maurice R.D.A., "Convolution and Fourier Transform, for Communications engineers", Pentech Press Ltd 1976

Maynard, J.D., Williams, E.G., Lee, Y.,"Nearfield acoustic holography: I. Theory of generalized holography and the development of NAH", J. Acoust. Soc. Amer., Vol. 78, No. 4, pp 1395-1413, Oct. 1985

Molkdar D., Mathews P.A., "Measurements and charactarization of the UHF mobile radio channel. Part1: Measurements over the band 835-885 MHz", J.IERE, pp. s157-s168 Vol.58 suppl.,1988

Molkdar D., Mathews P.A., "Measurements and charactarization of the UHF mobile radio channel. Part2: Measurements over the band 869-877 MHz", J.IERE, pp. s157-s168 Vol.58 suppl.,1988

Moody, M.P., "Resolution of coherent Sources incident on a circular antenna array", IEEE Procs. Vol. 68 No.2 Feb. 1980

Narayanan R.M., Cox D.D., Ralson J.M.,"Millimitre-wave specular and diffuse multipath components of teerain", IEEE Trans. on Ant. and Prop., Vol. 44, No. 5, May 1996

Neudorfer P.O., "Alternate methods of harmonic analysis", IEEE Procs, Vol. 61, pp. 1661-2, Nov. 1973

Nossek J.A., "Highly bandwidthefficient digital radio systems based on VLSI-signal processing", ITG Fachberichte, Vol. 107, pp. 247-252, 1989

Nuttal A.H., "Spectral estimation by means of overlapped fast Fourier transform processing of windowed data", N.U.S.C. Tech. rep. 4169 - New London CT, AD 739315, 1971

Nuttal A.H., "Some windows with very good sidelobe behaviour", IEEE Trans. Acoust. speech and signal processing, Vol. ASSP-29, No. 1, pp. 84-91, Feb. 1981

Parsons, J.D., "The mobile radio propagation channel", Pentech Press, London, 1992

Peled A., Liu B., "Digital Signal Processing, Theory, Design, and Implementation", John Willey & Sons, New York 1976

Pipes, L.A. Harvill, L.R., "Apllied Mathmetics for Engeneers and Physicists", 3. edition, McGraw-Hill Book Comp. Inc., New York 1958

Pisarenko V.F., "The retrieval of harmonic from a covariance function", Geophysics J. R. Astron. Soc, pp 347-366, 1973

Prewit J.F., "Amplitude bias in the Fourier transform of noisy signal", IEEE Trans. ant. & prop. Vol. AP-26, No. 5, Sept. 1978

Priestley, M.B., "Spectral Analysis and Time Series", Academic Press, London,1981

Rife K.C. Vincent G.A., "Use of discrete Fourier transform in the measurement of frequencies and levels of tones", Bell systems tech. Jnl., Vol 49, pp 197-228, 1970

Sayidmarie, K.H., Khidhir, A.M.,"Holgraphic investigation of multipath interference in line of sight radio links", Proc of ISAP89 (int. conf. on ant. and prop.), pp. 1061-1064, 1989

Sayidmarie, K.H., Khildhir, A.M.,"Holographic prediction of antenna height and ground reflection in LOS radio links", Proc of int. conf. on radar CICR-91, China, 1991

Sayidmarie, K.H., Abbosh A.M., "Holographic prediction of ground multipath parameters from range gain patterns", IEE Proc. part H, Vol. 140, No. 5, pp. 367-372, Oct. 1993

Sheeren, P.M.J., "Interference reduction techniques for earth stations and the specific problem of near field site shielding against terrestrial interference", IEE colloquium digest No. 1988/99, Sept. 1984

Schnorrenberg, W., "Rauschmessung mit dem Spectrumanalysator", Mikrowellen und HF Magazin, p149-155, vol. 16, No. 2, 1990

Schulz U., Höfgen G., "Effective milimeter wave transmission under severe multipath conditions", ARGARO-CP-363, pp 42 1-7, 1984

Schwartz M., "Information Transmission, Modulation, and Noise", 3. edition, Mc Graw-Hill B. Comp, New York 1980

Stefanos, K.D., Christos H.C., "An instrumental approach to minimum-variance seismic deconvolution", IEEE Trans. Geoscience and Remote Sensing, Vol. GE-23, No. 6, November 1985

Stremler F.G., "Introduction to Communication Systems", 2. edition Addison-Wesley Publishing Company, Reading 1982

Tamura, M.,"Spatial fourier transform method of measuring reflection coefficient at oblique incidence. I: Theory and numerical examples", J. Acoust. Soc. Amer., Vol. 88, No. 5, Pp 2259-2264, 1990.

Thomson D.J., Robbins M.F. et al, "Spectral and windowing techniques in power spectral analyses of geomagnetic data", Phys. earth planetary interiors, Vol. 12, pp. 217-231, 1976

Tyras G., "Radiation and propagation of electromagnetic waves", Academic Press, London 1969

van Dooren, G.A.J., "Electromagnetic field strangth prediction model for urban environments", Eindhoven University of Technology, Eindhoven, Netherlands, 1993

van Dooren, G.A.J., Govaerts, H.J.F.G., "Shielding of single-and double-reflector earth station antennas: a near and far-field approach", pp. 309-312, IEE procs. H, Vol. 140, No. 4, 1993

Veronesi, W.A., Maynard, D.J., "Nearfield acoustic holography (NAH) II. Holographic reconstruction algorithms and computer implementation", J. Acoust. Soc. Amer., Vol. 81, No. 5, May 1987

Webb C., "Practical use of the fast Fourier transform (FFT) algorithm in time-series analysis", ARL, Uni of Texas, Austin ARL TR 70 22, part 22, June 1970

Webster, A.R., Scott, A.M.,"Angles-of-arrival and troposheric multipath microwave propagation", IEEE Proc. ant. and prop.,Vol AP-35, No. 1, pp. 94-99, Jan 1987

Webster R.J., "Leakage regulation in the discrete Fourier transform spectrum", IEEE Procs. Vol. 68, pp. 1339-1341, 1980

Welch P.D., "The use of fast Fourier transform for the estimation of power spectra: a method based on time averaging over short, modified periodograms", IEEE Procs. audio and electroacoustics, Vol. AU-15, No. 2, June 1967

William H., Hayt J.R., "Engineering Electromagnetics", Mc Graw-Hill B. Comp, New York 1981

COST 210 Management Committee (Chair: M.P.M. Hall, Editor: Ballabio), COST 210: "Influence of the atmosphere on iterference between radio communications systems at frequencies above 1 GHz", Commission of the European Union, 1991

COST 235 Management Committee (Chair: M.P.M. Hall, Editor: Ballabio), COST 235: "Radiowave propagation effects on the next generation fixed-services terrestrial telecommunictions systems", Commission of the European Union, 1996

Department of Trade and Industry, "Report on the potential for microwave video distribution systems in the UK", HMSO, 1988

World wide web pages (internet):

Dudley-Lab: www.dudleylab.com, May 1998
Phillips: www.phillips.com, May 1998

Appendix

Examples of most commonly used time domain windows and their Fourier transform:

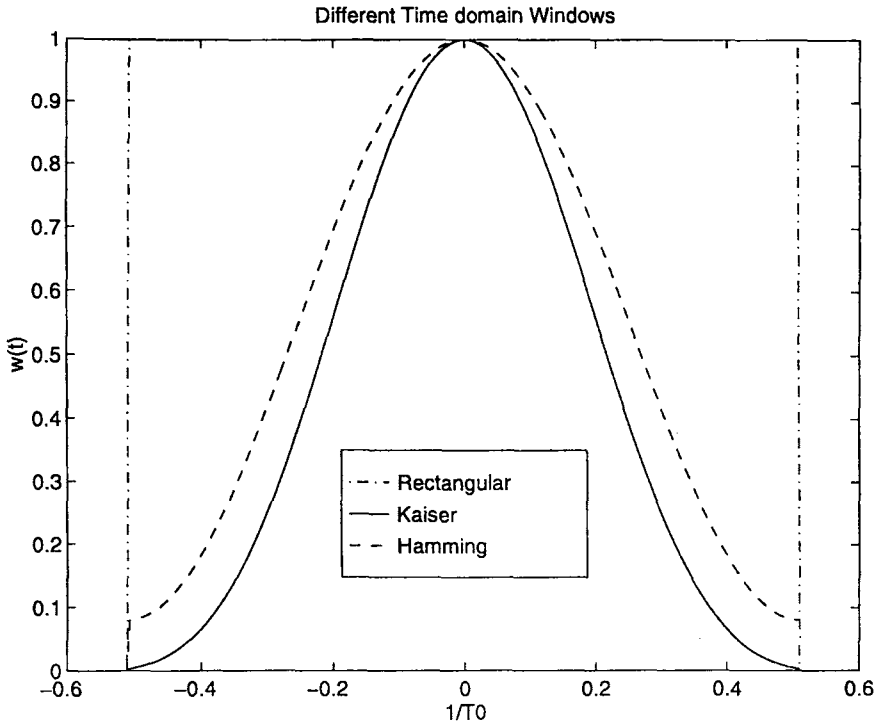

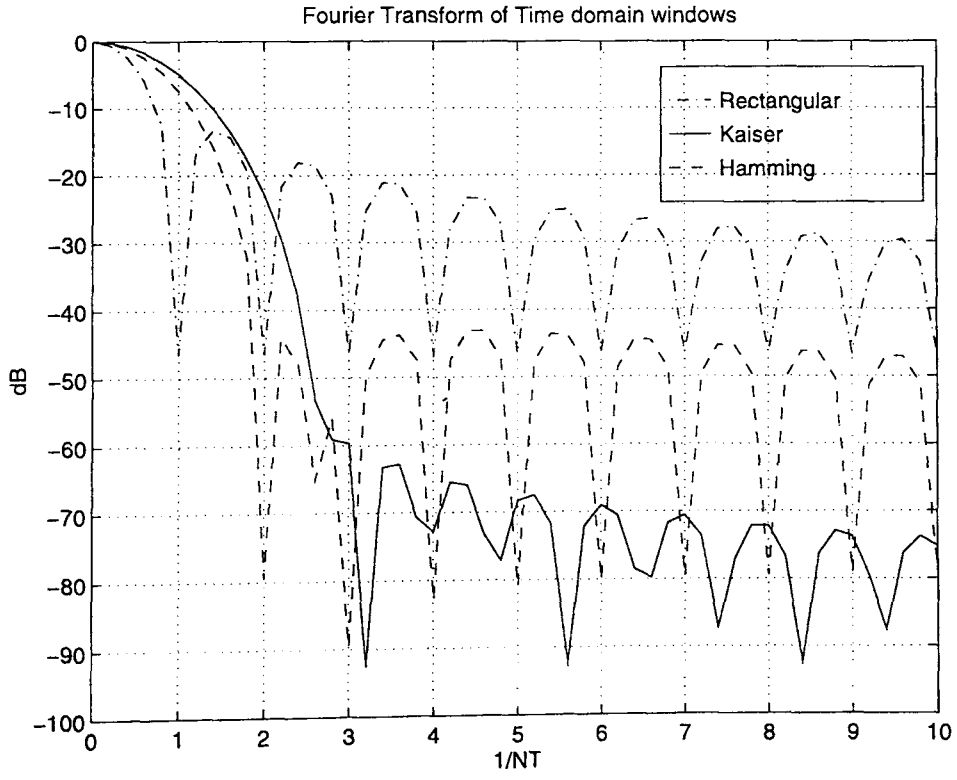

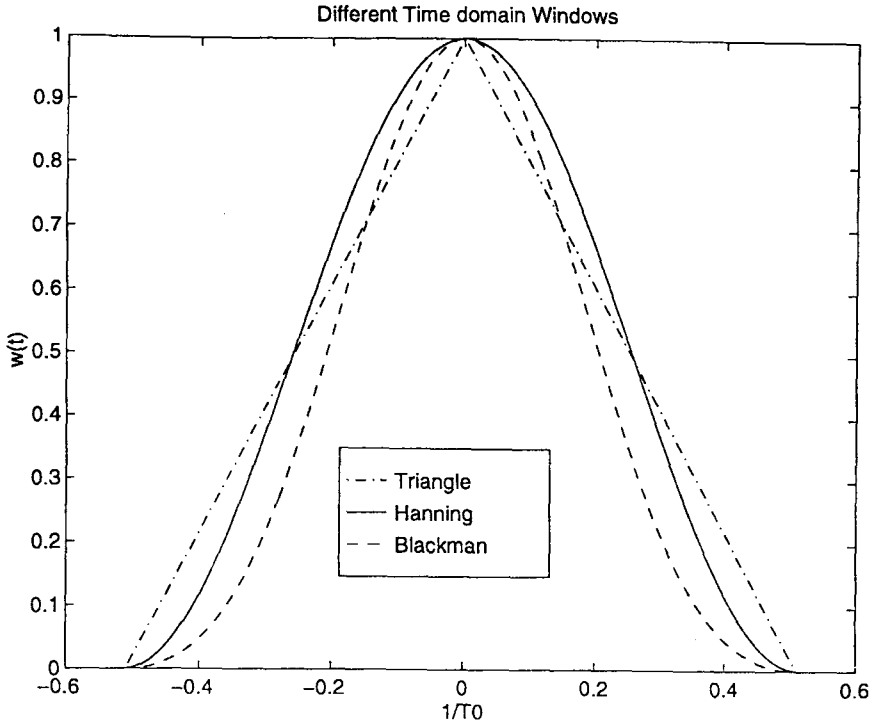
Different Time domain Windows
w(t)
1/T0
Triangle
Hanning
Blackman

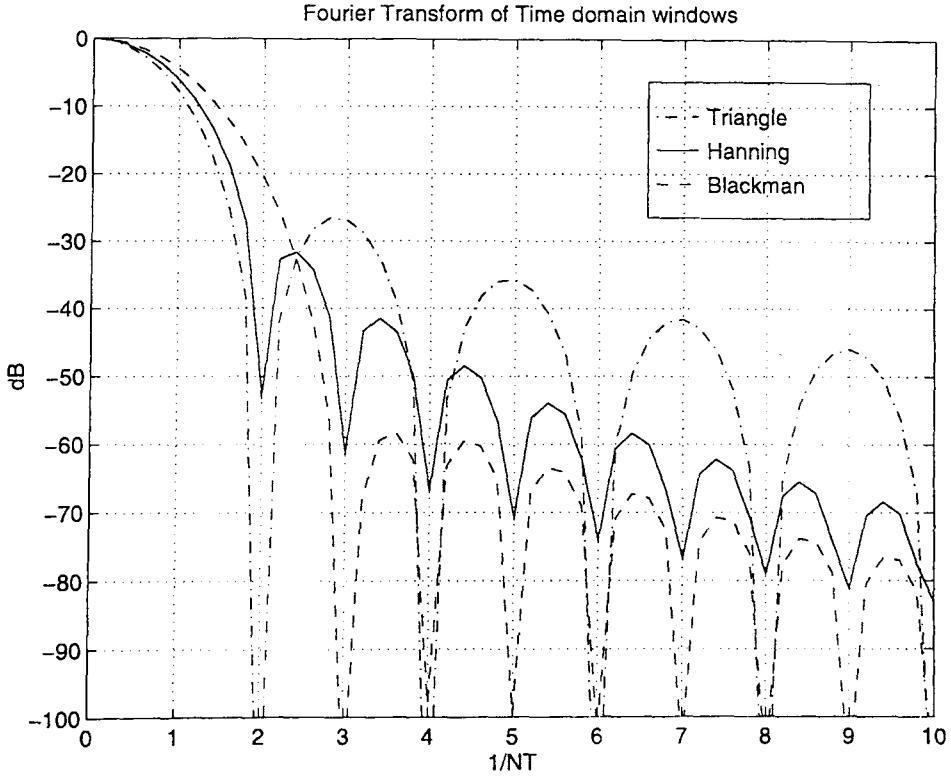
Fourier Transform of Time domain windows
dB
1/NT
Triangle
Hanning
Blackman